



HAL
open science

Interaction of proteins with chemically controlled surfaces for biosensor development

Victor Lebec

► **To cite this version:**

Victor Lebec. Interaction of proteins with chemically controlled surfaces for biosensor development. Chemical Physics [physics.chem-ph]. Université Pierre et Marie Curie - Paris VI; Université catholique de Louvain (1970-..), 2014. English. NNT : 2014PA066095 . tel-01066132

HAL Id: tel-01066132

<https://theses.hal.science/tel-01066132v1>

Submitted on 19 Sep 2014

HAL is a multi-disciplinary open access archive for the deposit and dissemination of scientific research documents, whether they are published or not. The documents may come from teaching and research institutions in France or abroad, or from public or private research centers.

L'archive ouverte pluridisciplinaire **HAL**, est destinée au dépôt et à la diffusion de documents scientifiques de niveau recherche, publiés ou non, émanant des établissements d'enseignement et de recherche français ou étrangers, des laboratoires publics ou privés.



Université catholique de Louvain (UCL)
Institut de la Matière Condensée et des
Nanosciences (IMCN)
Pôle Bio & Soft Matter (BSMA)

Université Pierre et Marie Curie (UPMC)
ED 397
Laboratoire de Réactivité de Surface (LRS)

Interaction of Proteins with Chemically Controlled Surfaces for Biosensor Development

Victor LEBEC

Dissertation soutenue en vue de l'obtention
du grade de Docteur en Sciences de
l'Ingénieur

Thèse de doctorat en Sciences

Promoteurs: Pr. A. DELCORTE (UCL) – Pr. C.-M. PRADIER (UPMC)

Membres du Jury:

Dr. Souhir Boujday (LRS, CNRS – UPMC, Paris, France)

Pr. Giacomo Ceccone (Rapporteur – JRC-IHCP, Ispra, Italy)

Dr. Yann Chevotot (Rapporteur – INL, Lyon, France)

Pr. Valérie Pichon (LSABM, CNRS – ESPCI, Paris, France)

Pr. Sophie Demoustier (IMCN/BSMA, Louvain-La-Neuve, Belgium)

Pr. Jacques Devaux (Président, IMCN/BSMA, Louvain-La-Neuve,
Belgium)

May 2014

Acknowledgments

Les remerciements après plus de 3 années de travail dans deux laboratoires différents sont un exercice difficile, c'est pourquoi je commencerai par remercier généralement toutes les personnes que j'ai pu côtoyer ou qui ont pu aider d'une manière ou d'une autre à la réalisation de ce travail.

Je voudrais d'abord chaleureusement remercier mes deux promoteurs Claire-Marie et Arnaud de m'avoir accueilli dans leurs laboratoires respectifs à Paris et Louvain-la-Neuve et de m'avoir permis de mener à bien cette thèse. Merci de m'avoir donné les moyens de mener mes recherches avec une grande liberté et dans les meilleures conditions. Je veux également remercier ici Souhir pour m'avoir encadré au quotidien dans mes séjours parisiens et pour ses conseils tout au long de ces 3 années.

Je tiens également à dire un grand merci aux membres de mon jury - les Pr. Sophie Demoustier, Valérie Pichon et Giacomo Ceccone ainsi que le Dr. Yann Chevolot - qui ont accepté de relire ce manuscrit et de s'investir dans son évaluation. Un remerciement particulier au Pr. Giacomo Ceccone et au Dr. Yann Chevolot pour avoir accepté d'être rapporteurs du texte. Je remercie également le Pr. Jacques Devaux de présider ce jury.

Un remerciement tout particulier au Pr. Christine Dupont qui a fait partie de mon comité d'accompagnement pour ses conseils précieux à la réalisation de mon travail ainsi que pour m'avoir donné accès aux équipements de QCM-D et d'XPS de son laboratoire.

Je souhaiterais également remercier Pascal Mertens et Olivia Lefèvre de la société Coris BioConcept qui nous ont fourni plusieurs produits essentiels à

la réalisation de ce projet ainsi qu'un aide précieuse dans l'établissement de certains protocoles ou lors du projet de mémoire de Catherine.

Je continuerai ces remerciements par exprimer ma gratitude aux organisateurs de l'école doctorale européenne IDS-FunMat sans qui ce projet n'aurait pas pu avoir lieu. Merci d'avoir organisé les "spring schools" d'IDS qui ont été une formidable plateforme d'échange entre tous les doctorants du programme dans différents domaines.

Speaking about IDS, I'll switch to English here to thank all the students from the school. It was great meeting you all and share these moments along the years. I won't risk myself in giving specific names since I'll forget half of you but good luck to you all for the end of your projects (especially the 2010 promotion)! I hope that we will continue to interact in our future positions.

I also have to thank all my colleagues in the SIMS group in Louvain. I think about all the people I shared my office with along the years: Taoufiq, Vanina, Roussin, Catherine... Thanks for keeping a good spirit and for inspiring discussions! But I shouldn't forget the "theoreticians' office": Oscar, Anneesh, Bartek, Henok, and Mohammad. Thank you guys for the great tea breaks and nice discussions!

Merci également à Claude de m'avoir formé à l'utilisation du ToF-SIMS et pour son travail quotidien au sein du groupe nous permettant d'utiliser la machine dans les meilleures conditions. J'aimerais également remercier ici Michel et Pierre, les rois de l'XPS pour leur disponibilité et pour m'avoir aidé dans l'analyse de mes résultats. J'ai également une pensée pour tous les membres du pôle BSMA avec qui j'ai eu le plaisir de travailler pendant ces années.

Acknowledgments

Pour terminer le chapitre louvaniste, je remercie particulièrement Sami et Guilhem qui ont été mes acolytes au quotidien. Merci pour toutes ces discussions, parfois enflammées, souvent autour d'une Duvel mais toujours passionnantes. Bonne chance à vous deux dans vos projets futurs !

Je voudrai également remercier mes collègues parisiens que j'ai côtoyé moins souvent mais qui m'ont toujours bien accueilli et ce depuis mon master (il y a plus de 4 ans...) ! Merci à Jessem qui a toujours été là pour m'accompagner. Merci à mes collègues de bureau au fil des années : Charlotte, Manel, Nesrine, Faiza... et ceux que je n'ai croisés que quelques semaines. Merci à tous les membres du LRS pour ces bons moments lors des pauses café ou des apéros du vendredi : Jessie, Vincent, Anne-Fée, Catarina, Sarah, Dimitri, Christophe (x2)... J'en oublie sûrement !

Finalement, ces remerciements ne seraient pas complets sans un mot pour mes amis et ma famille. Il me serait impossible de citer tout le monde ici mais merci à tous d'être présent au quotidien et de m'avoir apporté un équilibre en dehors du monde parfois très prenant de la recherche. Je remercie en particulier Thomas, il faut qu'on joue plus souvent au billard ! Merci également à ma sœur, Marion, à son mari Thony, ainsi qu'à mon frère Martin qui, je le sais, sont toujours là dans les bons moments mais également dans ceux de doute. Merci à mes neveux Maceo et Ethan pour leur sourire et leur insouciance qui m'apportent chaque fois un grand bonheur. Je terminerai par un grand merci à mes parents qui ont su être là depuis le début de toutes ces années d'études et qui m'ont permis de poursuivre ma voie. Merci à eux de leur soutien quotidien et inconditionnel.

A tous, MERCI !

Content

Acknowledgments	3
Content	7
Abstract.....	11
Résumé	13
List of Abbreviations	15
1 Introduction	17
1.1 Interaction of Proteins with Surfaces	18
1.1.1 Structure of Proteins.....	18
1.1.2 Adsorption of Proteins on Solid Surfaces	22
1.1.3 Characterization of Adsorbed Proteins.....	26
1.1.4 Quantity of Adsorbed Protein on SAMs.....	28
1.1.5 Physical Status of Proteins on Surfaces	32
1.2 Goals and Experimental Strategy.....	36
1.3 Outline	37
2 Methodology for Protein Film Study	39
2.1 ToF-SIMS and PCA.....	40
2.1.1 Theoretical Background	40
2.1.2 Experimental Description	44

2.1.3	Characterization of Protein Films	46
2.1.4	PCA Applied to ToF-SIMS Datasets	49
2.2	XPS	53
2.2.1	Theoretical Background	53
2.2.2	Experimental Description	57
2.2.3	XPS Characterization of Organic Layers	60
2.3	PM-IRRAS	65
2.3.1	Theoretical Background	65
2.3.2	Experimental Description	68
2.3.3	Analysis of PM-IRRAS Spectra	69
2.4	QCM-D	71
2.4.1	Theoretical Background	71
2.4.2	Experimental Description	75
2.4.3	Protein Films Characterization.....	76
3	Chemical Modification of Gold Surfaces Using SAMs.....	77
3.1	Characterization of SAMs with Conventional Methods.....	78
3.1.1	SAMs Formation.....	78
3.1.2	PM-IRRAS	79
3.1.3	XPS	81
3.1.4	Activation of the –COOH-terminated SAMs	88

3.2	SAMs Characterization in ToF-SIMS Using Ar_n^+ Clusters Ions	90
3.2.1	Analysis Parameters.....	90
3.2.2	Low Masses Fragments.....	91
3.2.3	$[M-H]_x Au_{x-1}^-$ Molecular Clusters	95
3.3	Conclusion.....	97
4	Studying the Adsorption of Model Proteins on SAMs	99
4.1	Samples.....	100
4.2	Adsorption of β -Lactoglobulin	102
4.2.1	Results.....	102
4.2.2	Discussion	111
4.3	Adsorption of bovine serum albumin	115
4.3.1	Results.....	115
4.3.2	Discussion	121
4.4	Conclusion.....	130
5	Toward a More Realistic System – Antibody Adsorption and Grafting	133
5.1	Samples.....	134
5.2	Results.....	137
5.2.1	Anti-GDH Adsorption on SAMs	137
5.2.2	Exploring Anti-GDH Adsorption Using ToF-SIMS and PCA..	141
5.2.3	Testing Biorecognition of GDH by Anti-GDH.....	145

5.3	Discussion	146
5.3.1	Orientation of the Antibody.....	146
5.3.2	Influence of Orientation on Biorecognition.....	148
5.4	Conclusion.....	152
6	Conclusion and Perspectives	155
6.1	Principal Results.....	155
6.2	What's Next?.....	157
A	Nanoparticles Functionalization Using Antibodies.....	161
A.1	Samples.....	162
A.2	Dried-Drops Samples Study	167
A.3	Antigen Immobilization on Si for Biorecognition with NPs.....	173
A.3.1	Grafting of GDH on Silicon	173
A.3.2	Biorecognition Tests	178
A.4	Conclusions	179
	Bibliography.....	181
	Dissemination	201

Abstract

In this work we studied protein adsorption on chemically well-controlled surfaces. The focus is put on linking physico-chemical properties of surfaces (hydrophobicity/charge) to the structural properties of the adsorbed proteins. To this end, alkyl thiols differing by their end group were used to build self-assembled monolayers on gold substrates (SAM) that serve as templates for protein adsorption or covalent grafting.

SAM surfaces before and after protein adsorption were characterized with a combination of techniques. *Ex situ* analysis were carried out, in air with polarization-modulated infrared reflection absorption spectroscopy (PM-IRRAS), or in vacuum using X-ray photoelectron spectroscopy (XPS) and time-of-flight secondary ion mass spectrometry (ToF-SIMS). ToF-SIMS results were analyzed statistically in principal component analysis (PCA) to reveal preferential orientations based on amino acids fragments distributions. Protein adsorption was also followed directly *in situ* (*i.e.* in the liquid phase) with quartz crystal microbalance with dissipation monitoring (QCM-D).

Two model proteins – β -Lactoglobulin (β LG) and bovine serum albumin (BSA) – were first studied. They are both model globular proteins with different structural properties (β LG is *hard* while BSA is *soft*). Different orientations were proposed for both proteins on each SAM surface. A more complex case was then studied with the adsorption and grafting of a monoclonal antibody on the SAM. Again differences in orientations were determined and correlated to biorecognition measurements. In conclusion, this thesis establishes a methodology for the direct label free determination of protein orientation on surfaces.

Résumé

Dans ce travail, nous étudions l'adsorption de protéines sur des surfaces chimiquement contrôlées. Le but est d'établir le lien entre les propriétés physico-chimiques de la surface (hydrophobicité /charge) et la structure physique de protéines. Des couches auto-assemblées de thiols ayant des groupements terminaux différents sont formées sur des surfaces d'or (SAM) et servent de support à l'adsorption ou du greffage de protéines.

Les SAM sont caractérisés, avant ou après l'adsorption de protéines, avec une combinaison de techniques. Des analyses *ex situ* sont réalisées, dans l'air, en spectroscopie infrarouge en lumière polarisée (PM-IRRAS) ou, sous ultra-vide, en spectroscopie des photoelectrons X (XPS) et en spectrométrie de masse d'ions secondaires (ToF-SIMS). L'analyse en composante principale (PCA) des résultats ToF-SIMS aide à révéler l'orientation des protéines adsorbées grâce à la répartition des fragments d'acides aminés. En microbalance à quartz avec mesure de la dissipation (QCM-D), l'adsorption des protéines est suivie *in situ* (*i.e.* en phase liquide).

Deux protéines globulaires ayant des propriétés structurales différentes sont d'abord étudiées, la β -Lactoglobuline (β LG) est dite *dure* quand l'albumine de sérum bovin (BSA) est dite *souple*. Des orientations différentes sont proposées après adsorption sur les SAM. Un cas plus complexe est ensuite étudié avec l'adsorption ou le greffage d'un anticorps sur les surfaces. De nouveau, différentes orientations sont proposées et elles sont corrélées à des mesures de bio-reconnaisances. En conclusion, cette thèse établie une méthodologie de détermination directe et sans marquage de l'orientation de protéines adsorbées.

List of Abbreviations

a.a.	Amino acid
Ab	Antibody
AES	Auger electron spectroscopy
AFM	Atomic force microscopy
Ag	Antigen
BSA	Bovine serum albumine
β LG	β -Lactoglobulin
DSC	Dual source column
EDC	1-Ethyl-3-(3-dimethylaminopropyl)carbodiimide
ESCA	Electron spectroscopy for chemical analysis (= XPS)
GCIB	Gas cluster ion beam
(Anti-) GDH	(Anti-) Glutamate dehydrogenase
IgG	Immunoglobulin G
IMFP	Inelastic mean free path
LMIG	Liquid metal ion gun
MVA	Multi-variate analysis
NHS	N-Hydroxysuccinimide
NPs	Nanoparticles
PCA	Principal component analysis
pI	Isoelectric point
PM-IRRAS	Polarization modulated infra-red reflection absorption spectroscopy
QCM-D	Quartz crystal microbalance with dissipation monitoring
SAMs	Self-assembled monolayers
SPR	Surface plasmon resonance
ToF-SIMS	Time-of-flight secondary ion mass spectrometry
UHV	Ultra-high vacuum
UPS	Ultraviolet photoelectron spectroscopy
XPS	X-ray photoelectron spectroscopy

1 Introduction

God made the bulk; surfaces were invented by the devil
Wolfgang Pauli

In this introductory chapter, the concept of protein adsorption will be discussed with a focus on surface characterization. Understanding the interaction of proteins with surfaces of biological interest is important since it will mediate further interactions with the surrounding environment. As a matter of fact, protein adsorption is the first step in numerous biological processes. On one hand, it could be interesting to control initial steps of protein adsorption to avoid the inflammatory response and for a better integration of implanted devices. On the other hand, avoiding this initial adsorption is of crucial importance to avoid biofouling of surfaces in certain environments (at sea or in food production facilities for example).¹

Particularly, protein interactions with metal or reactive surfaces will be fundamental in the biomedical field. One of the main applications is the development of diagnostic platforms often described as biosensors. In 1999, Thévenot *et al.* described a biosensor as “a self-contained integrated device, which is capable of providing [...] analytical information using a

biological recognition element [...] which is retained in direct spatial contact with an electrochemical transduction element.”² The biochemical receptor can vary from enzymes to antibodies, DNA strands or even whole cells.³ In the case of protein based biosensors, the challenge is to retain the biological properties (bioactivity, biorecognition properties) of the immobilized proteins to allow further detection with the biosensor.^{4,5}

The main focus of this thesis is the understanding of protein adsorption on chemically well controlled surfaces. We want to show that the reactivity of solid surfaces in biological environment can be controlled to devise new applications in the field of biosensors. The link between surface properties (charge/hydrophobicity) and adsorption modes of a protein (orientation /conformation/defolding) will be explored to show the influence on their bioactivity. In this chapter, we want first to present the main parameters driving the interaction between proteins and metal surfaces. This will be followed by the definition of the goals of this particular work and by a description of the experimental strategy developed during this work. Finally, the outline of the manuscript will be presented.

1.1 Interaction of Proteins with Surfaces

1.1.1 Structure of Proteins

Proteins are generally described as polymers of amino acids (a.a.). The 20 natural a.a. form the building blocks of the peptidic chain. Amino acids are described by the general formula $H_2N-CHR-COOH$, where R is the lateral chain which is specific of each a.a. (see Figure 1.1 for the detailed structure

of the 20 natural a.a.). The properties of the side groups such as their polar or charged character will determine the final structure of the protein.

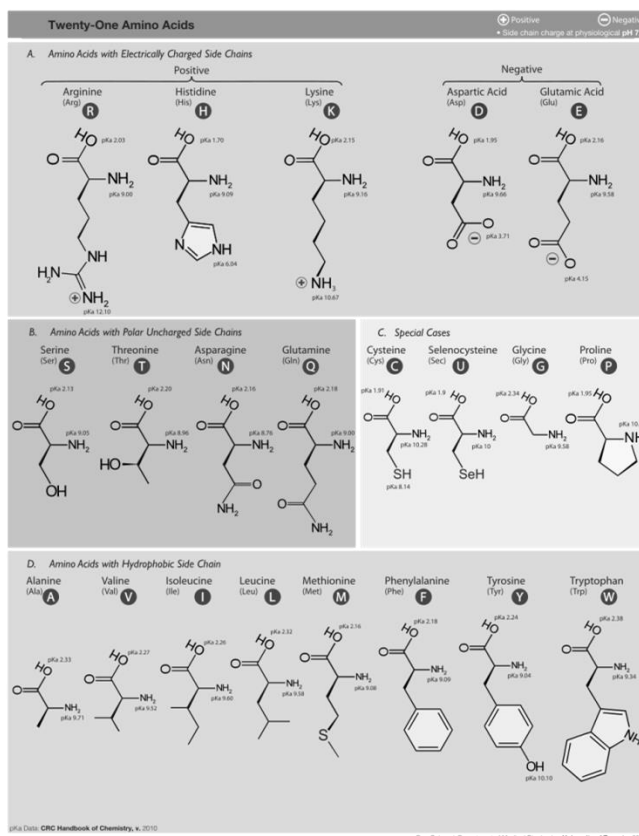


Figure 1.1 Presentation of the 20 natural amino acids (plus the selenocysteine one). Their names are given in the 3 or in the 1 letter code. (This image is provided under the GNU Free Documentation Licence by Dan Cojocari)

The backbone of the protein is described as a repetition of peptide units forming the peptidic chain. The structure of the peptide unite is presented below in Figure 1.2. The number of different chains formed using the 20 a.a. *i.e.* the theoretical number of proteins is infinite. The sequence of a.a. in the polypeptide chain is called the *primary structure* of the protein. This

Chapter 1

sequence will govern the interactions in the protein and with its environment.

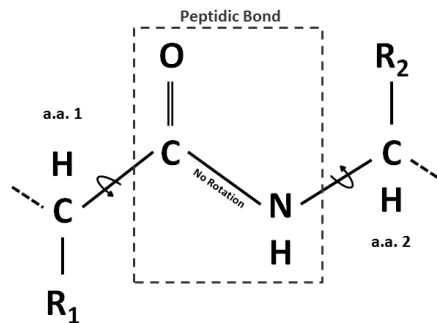


Figure 1.2 Structure of a peptide unit in a polypeptide chain. Two of the three bonds in the peptidic function are allowed to rotate helping in the folding of proteins

The 3D structure of a protein is acquired after its folding. The *secondary structure* is described as the arrangement of the peptidic backbone excluding the a.a. side groups. The most common *secondary structures* are β -sheets or α -helix, they will not be described in details here but they correspond to an ordered organization of the backbone stabilized by hydrogen bonds between NH and C=O groups in the peptidic chain. The *tertiary structure* represents the interaction of side groups in the chain and describes the 3D organization of the protein. These structures are stabilized by hydrophobic interactions between apolar side groups, by hydrogen bonding between polar ones, and by electrostatic interactions between (de)protonated a.a. side chains. Finally, the *quaternary structure* is defined as the non-covalent interaction of several *tertiary structures* in complex proteins. The different levels of a protein structure are described in Figure 1.3.

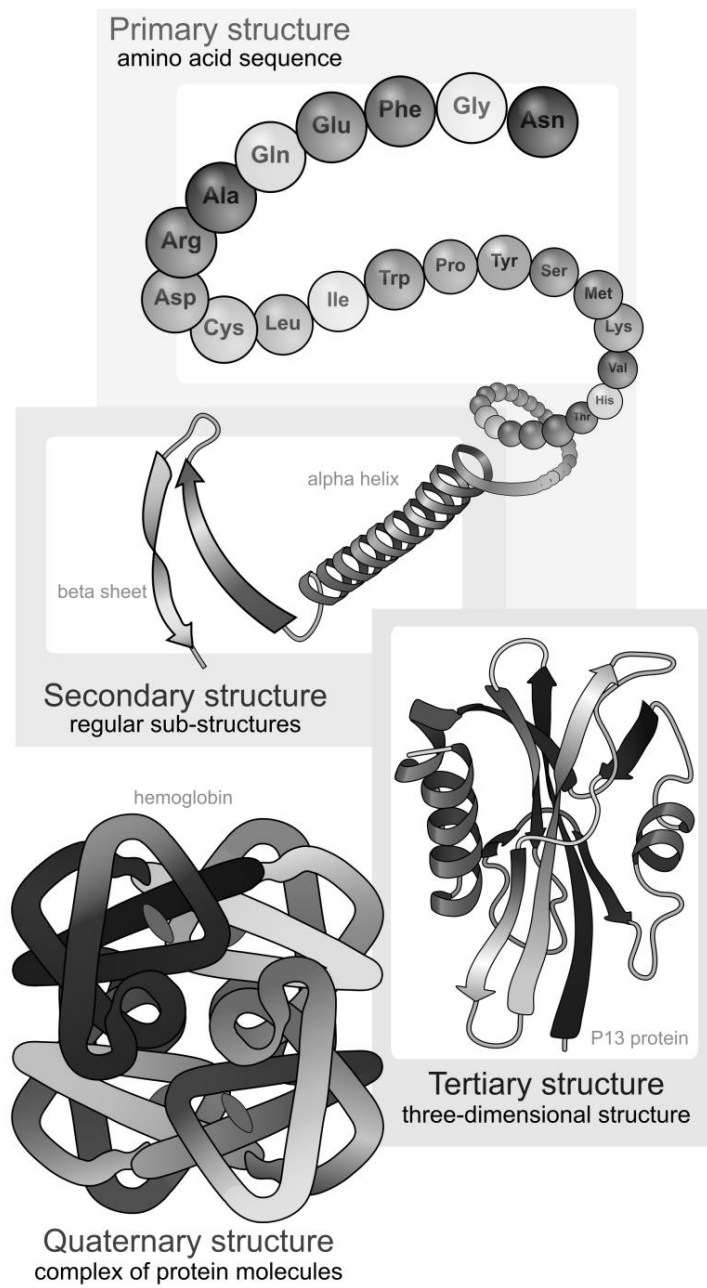


Figure 1.3 Schematic of the main protein structure levels (Public domain illustration)

As stated by Norde et al.,⁶ three main observations can be made after the folding of globular proteins:

They adopt a **spherical or ellipsoidal** form with a dimension of a few to a few tens of nm.

Apolar residues responsible for hydrophobic interactions are buried in the **heart of the protein** where they are shielded from the surrounding water.

Almost all **charged groups are on the outer part of the protein**. If charges are buried in the molecule they will exist as ion pairs.

Proteins are thus polyampholytes molecules bearing numerous charges on their surface in addition with hydrophobic (apolar) patches. We will now explore their interactions with solid surfaces.

1.1.2 Adsorption of Proteins on Solid Surfaces

Both the protein and the surface properties will influence the adsorption process in addition with the experimental conditions. The first parameter to consider is the adsorption pH that will determine the charge of both the surface and the protein. At its isoelectric point (pI), a protein will have a net charge of zero corresponding to a balance between positive and negative charges on its surface. At $pH > pI$, proteins are negatively charged and when $pH < pI$, proteins are positively charged. A better adsorption will generally be observed when the protein and the surface bear opposite charges due to electrostatic interactions. However, it is usually considered that protein

tend to adsorb at a higher packing density at the isoelectric point since less protein-protein repulsion will occur.⁷

Nevertheless, electrostatic repulsions can be overcome by the hydrophobic interactions. When polar surfaces are considered, water is most likely retained between the surface and the protein after adsorption.⁸ On apolar surfaces and/or proteins, dehydration of the contact points will favor the adsorption due to strong hydrophobic interactions.^{6,7,9} Water molecules at the contact point are released in the bulk solution resulting in an increase of the entropy of the system. This entropy increase contributes to a decrease in free energy favoring the adsorption.¹⁰ In adsorption studies, one should also take into account the “Vroman effect”. In the 60’s, Vroman *et al.* demonstrate that upon plasma adsorption, exchanges of protein happen at the surface.¹¹ Small proteins as albumins first adsorb and are progressively replaced with fibrinogens and finally by high molecular weight kinases. This phenomenon is now known as the “Vroman effect” and describes the replacement of low molecular weight proteins by bigger ones during successive adsorption steps.

In addition, a distinction has been defined between the so called *hard* or *soft* globular proteins.⁹ A *hard* protein will generally have little tendency to lose its structure upon interaction with a surface whereas for a *soft* protein, surface-induced structural changes are more severe and can lead to the loss of ordered secondary structures (α -helix or β -sheets). The hydrophobic core of the protein is exposed to the surface by the unfolding, which leads to a larger adsorption in the case of labile proteins. This could also be explained

by the notion of conformational entropy. By losing secondary structures such as α -helix, a *soft* protein will undergo a conformational entropy gain that will favor its adsorption.⁹ As a general rule of thumb, proteins retain more structure on electrostatically neutral hydrophilic surfaces than on hydrophobic or charged surfaces.¹² In Table 1.1, is presented a summary of the best conditions for protein adsorption.

Table 1.1 General prediction of whether ("Yes") or not ("No") a protein tends to adsorb on a surface (reproduced from Norde⁹)

		Surface			
		Hydrophobic (apolar)		Hydrophilic (polar)	
		+	-	+	-
Protein	Hard				
	+	Yes	Yes	No	Yes
	-	Yes	Yes	Yes	No
	Soft				
	+	Yes	Yes	Yes	Yes
	-	Yes	Yes	Yes	Yes

"+" or "-" refer to the electric charge of the protein or the surface

Looking at Table 1.1, one could almost say that "any protein will adsorb to any surface".¹³ But when studying protein/surface interactions, several questions arise:

- (1) How to control the **surface properties** to control protein adsorption?
- (2) What is the **quantity** of proteins adsorbed on the surface?
- (3) What are the **structural properties**, and physical status of the adsorbed proteins?

- (4) What is the biological **function** of the adsorbed proteins? The biological function can refer to enzyme activity, antigen-antibody binding or to adsorbed protein interaction with cell.⁸

Many strategies have been developed to answer the first question. They include both the chemical modifications of surfaces and the topographical ones.^{14,15} Chemical modifications can be performed in order to decrease or increase protein/surface interactions. In addition to polymer grafting¹⁶ or the use of zwitterionic materials,¹⁷ chemical control of metal surfaces has been achieved in the past few decades by developing the self-assembly of organic monolayers (SAMs), especially on gold.^{18–20} Thiolate SAMs on gold have been described as a good template for protein adsorption due to the tunability of alkyl-thiol molecule end-groups ($-\text{COOH}$, $-\text{NH}_2$, $-\text{CH}_3\dots$) and lengths.^{20–22} Figure 1.4 presents the main characteristics of SAMs on gold. Topographical control of the surface is not explored here but it is generally admitted that rough surfaces will expose more sites suitable for interactions and lead to an increase of protein adsorption.¹⁴

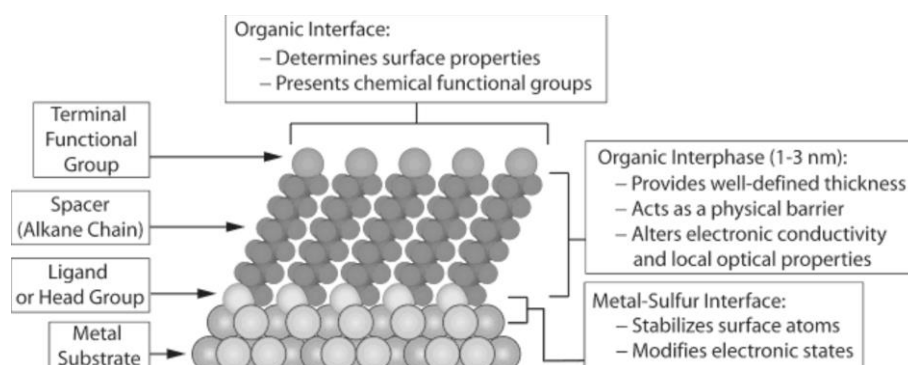


Figure 1.4 Schematic diagram of an ideal, single crystalline SAM of alkanethiolates supported on a gold surface with a (111) texture. The anatomy and characteristics of SAMs are highlighted (reproduced from Love et al.²⁰)

In order to answer the three last questions and characterize the protein adsorption, a large panel of surface characterization techniques has been developed over the years. The next paragraphs will focus on how surface characterization techniques can help in determining the quantity and physical status of adsorbed proteins and on the use of SAMs as a template for protein adsorption.

1.1.3 Characterization of Adsorbed Proteins

In the past decades, numerous studies of protein adsorption can be found in the literature with the introduction of new surface characterization techniques and their combination. We will quickly present here most of these techniques in a few words and show some applications to the characterization of proteins adsorbed on SAMs surfaces in the next paragraph. It is difficult here to be exhaustive but we will try to present the most important techniques currently in use:

Ellipsometry is an optical method that allows the determination of thin film composition, structure or thickness by following changes in the dielectric properties of a light beam reflected on the surface.^{23,24}

Infrared spectroscopies probes the chemical functions present on a surface. This is important in protein characterization since the intensity of protein-related bands (Amide I and II mostly) indicate the adsorbed quantity of proteins. Careful analysis of the amide band can also lead to the detection of secondary structures for the

adsorbed proteins and helps in the determination of its conformation.^{25,26}

The chemical state of atoms in thin films (i.e. their environment) is followed using **X-ray photoelectron spectroscopy (XPS)**. It can also help in the determination of adsorb proteins quantities and of the thickness of the film.^{15,27}

Time-of-flight secondary ion mass spectrometry (ToF-SIMS) probes the surface with energetic primary ions that fragment the top surface layers (over a few nm) and produce secondary ions giving the chemical composition of the extreme surface. It will mainly give information on the amino acids at the extreme surface of a protein adsorbed sample and help in determining the orientation, folding or conformation of adsorbed proteins.^{15,28}

Water **contact angle** measurements give information on the hydrophilic or hydrophobic character of a surface by checking the angle formed by a drop of solvent when deposited on a surface. The evolution of the contact angle before or after adsorption of proteins is a good sign of a successful adsorption.^{29,30}

Atomic force microscopy (AFM) can probe the topography of a surface by scanning a tip over it either in liquid phase or in air. This gives information on the local adsorbed quantities on a surface together with the adsorb state (spreading of the proteins or adhesion properties by force measurements for example).^{31,32}

In the liquid phase, **quartz crystal microbalance with dissipation monitoring** (QCM-D) or **surface plasmon resonance** (SPR) follow the adsorption of biomolecules on surfaces over the time with a great sensitivity (up to the ng.cm^{-2}).^{33,34}

We presented here the most common surface characterization techniques for protein adsorption analysis. A comprehensive review by Yano in 2012 In presents the use of other techniques such as sum-frequency generation or second harmonic generation for characterizing the orientation of proteins or the kinetic of protein unfolding at interfaces.³⁵ In addition to all the techniques presented above, circular dichroism (CD) measurements performed in solution can help in determining a likely conformation of proteins right before the adsorption.³⁶ We will not focus here on the possibilities of this technique but just say that it can quantify the amount of secondary structures (α -helix, β -sheets or random coils) in a protein and show its evolution in different conformations. We will now presents a summary of different studies using the above mentioned techniques for the study of adsorbed proteins on SAM surfaces.

1.1.4 Quantity of Adsorbed Protein on SAMs

In the early 90's, Prime and Whiteside demonstrated the possibility to use SAMs as a model system for studying adsorption of proteins at surfaces.²² Their first studies examined the effects of the length and number of ethylene oxide chains in mixed SAMs to prevent protein adsorption.³⁷ Using ellipsometry and XPS they could demonstrate that terminally attached ethylene oxide oligomers (from 2 to 17 monomers) prevent the adsorption

of four different proteins (Fibrinogen, Pyruvate Kinase, Lysozyme and Ribonuclease A) depending on their chain length. After these initial studies, thiol SAMs with different oligomers modifying the hydrophobicity (ethylene oxide, ethylene glycol, acrylamide, N,N-dimethylacrylamide...) were probed for non-specific protein adsorption resistance.^{38,39} The non-specific adsorption of proteins being avoided, it was proposed to graft specific ligand on the SAMs to promote specific adsorption of proteins.⁴⁰⁻⁴² In 2001, mixed ethylene glycol/biotinylated thiols monolayers were formed to adsorb specifically streptavidin on the surface.⁴³ Since streptavidin has binding sites for biotin on opposite sides of the molecule, it can be used as a linker for other biotinylated molecules (Figure 1.5).¹⁵ These studies are the starting point of using SAMs to build biosensors system.

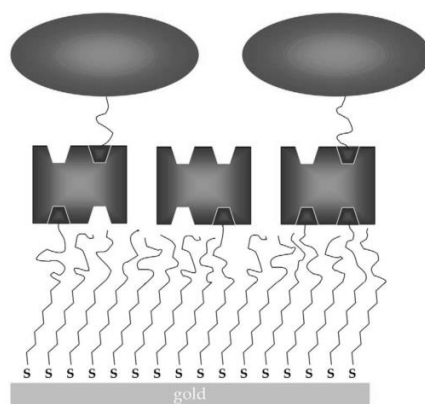


Figure 1.5 Selective immobilization of streptavidin on a mixed ethylene glycol / biotinylated thiols for specific binding of biotinylated biomolecules. From the gold substrate and going up, one first observe the biotinylated SAM layer, then the streptavidin and finally the biotinylated biomolecules (reproduced from Castner *et al.*¹⁵)

In parallel to the protein repulsion or to specific adsorption studies on complex modified SAMs, other groups worked on much simpler systems. They are usually formed of homogeneous SAMs only differing by their end-

group or by mixture of such simple thiols. Already in 1996, Silin *et al.*⁴⁴ were able to study the non-specific adsorption of two different proteins (one human antibody and BSA) on six SAMs with terminal groups as $-\text{CH}_3$, $-\text{PheOH}$, $-\text{COO}^-$, $-\text{NH}_2$, $-\text{OH}$ and ethylene oxide (EO). The protein concentrations measured by SPR, followed the order: $-\text{CH}_3 \approx -\text{PheOH} > -\text{COO}^- > -\text{NH}_2 > -\text{OH} > \text{EO}$.

In a series of paper from the early 2000's, the groups of Barbosa and Ratner studied the influence of hydrophobicity on albumin (HSA) adsorption. To this aim, they used a combination of contact angle, XPS, IRRAS and ellipsometry measurements. They first showed that the amount of adsorbed HSA increased in the following order on SAMs: $-\text{OH} < -\text{COOH} < -\text{CH}_3$ -terminated surfaces.⁴⁵ Then, they studied mixture of $-\text{CH}_3$ - and $-\text{OH}$ -terminated SAMs and showed a decrease in HSA adsorption when increasing the number of $-\text{OH}$ -terminated thiols in the SAMs. Moreover, with 65% of $-\text{OH}$ -thiols (in solution before formation of the SAMs), even if the amount of adsorbed HSA is lower than on pure $-\text{CH}_3$ surfaces, it seems to be stabilized by the presence of $-\text{OH}$ groups and exhibit a resistance to competitive adsorption of fibrinogen.⁴⁶ Finally, another paper showed that the modification of an $-\text{OH}$ -terminated SAM with a C18 alkyl chain compound that gradually increase the thickness and hydrophobicity of the SAM will have a positive influence on HSA adsorption.⁴⁷

Also in an attempt to probe the influence of surface wettability over protein adsorption on SAMs, Sethuraman *et al.* performed a complete AFM study of the interaction of eight different thiols SAMs with different wettabilities

and seven proteins with variable molecular weights. Proteins were first covalently immobilized on a –COOH-terminated SAMs using an activation steps and adhesion forces for each type of SAMs were recorded using gold coated tips functionalized with the eight different thiols. All the proteins showed a similar behavior with an increased adhesion with the increased hydrophobicity of the SAMs. Moreover they studied protein-protein and SAM-SAM interactions and showed that the secondary structures normalized to the molecular weight of proteins can help in predicting protein self-adhesion and their adhesion to the SAM substrate.

In our group, the work of Briand et al.,⁴⁸ is a good example of how –COOH SAMs mixed with other thiols can influence the covalent binding of Protein A on the surface. Protein A immobilization on a surface could be the first step for building a biosensor due to its high affinity for the constant part of antibodies. Again, results were obtained using a combination of polarization modulated IRRAS (PM-IRRAS) and XPS. A similar approach was conducted by Patel *et al.* when they demonstrate a better accessibility of the –COOH groups necessary to bind covalently proteins to the SAMs when mixing them with shorter length thiol molecules upon formation of SAMs.⁴⁹ In this study they also benefits of insight from ToF-SIMS and AFM measurements.

The common idea of all those studies is to probe the adsorbed quantity of proteins regarding the electro-chemical properties of the SAMs (hydrophobicity / polarity / hydrophilicity / charge). Results are in good agreement with the theoretical predictions presented in the previous paragraph (see Table 1.1). We can thus conclude that SAMs can be tuned to

promote specific adsorption of proteins but no, or very few, information was yet deduced about the conformation or orientation of proteins at the interface and on their possible bioactivity. Those parameters will be explored below.

1.1.5 Physical Status of Proteins on Surfaces

In order to develop interesting applications in the field of biosensors or biomaterials, not only the quantity but the orientation or conformation of adsorbed proteins will be of major importance to enhance their bioactivity. In the common case of antibodies, their active sites must be indeed oriented opposite to the surface to ensure a good recognition of antigens.^{50,51} Conclusions about the orientation of a protein on a surface can be drawn by following the antibody/antigen interaction, for example in QCM-D.⁵¹⁻⁵³ This methodology was successfully applied in our group by studying the adsorption and activity of a rabbit IgG antibody on three different immunosensing platforms.⁵⁴ The first one based on biotin/avidin recognition system (NAV biosensor), the second one on the affinity of protein A for the constant part of the IgG (Protein A biosensor), and the third one using an Anti-IgG to catch the rabbit antibody (SAb biosensor). Figure 1.6 presents the different biosensors with their different building blocks. The first step is the functionalization of gold samples with an amine terminated SAMs followed by the immobilization of intermediate proteins before interaction with the antibody that will interact with the antigen. Exact steps are detailed in Figure 1.6, the adsorption of BSA correspond to a saturation step to avoid nonspecific recognition. The protein A platform was proved to be the most efficient in the capture of the antigen revealing

a better orientation or accessibility of the antibody. However, the techniques used for detection did not provide any direct information about the orientation or conformation of the adsorbed proteins.

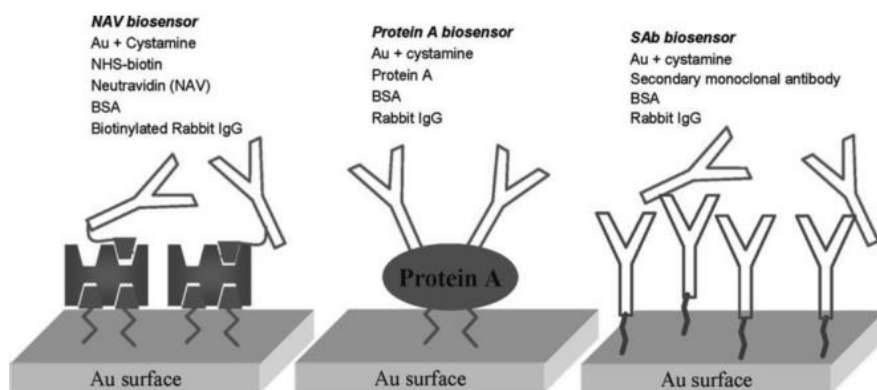


Figure 1.6 Schematic representation of the controlled immobilization of antibodies for biosensing applications (reproduce from Boujday et al.⁵⁴)

ToF-SIMS, in the static regime, was proposed to probe protein conformation and orientation upon adsorption thanks to its very low sampling depth (a few nanometers).⁵⁵ In ToF-SIMS measurements, fragments corresponding to each amino acid (a.a.) are detected. These a.a. fragments have been identified by studying a.a. homopolymers films.^{56,57} The relative intensities of each fragment give information about the outmost a.a. on the surface. Comparing this information to the structure of the protein indicates directly which part of the protein is exposed.⁵⁸⁻⁶¹

Seminal studies of adsorbed proteins in ToF-SIMS were carried out by Lhoest et al., with fibronectin adsorbed on polystyrene, before and after oxygen plasma treatment, and led to the detection of different conformations/orientations by monitoring the evolution of the amino acids

(a.a.) fragment peaks.⁶² Due to the very low sampling depth of ToF-SIMS (a few nm), it is accepted that a.a. fragments come from the outmost part of the adsorbed proteins. By comparing with the structure of the protein one can determine which part is exposed. This principle is detailed in the next chapter. Other studies from Wagner et al. showed the interest of ToF-SIMS combined with XPS and radiolabeling in identifying the structure of binary and ternary adsorbed protein films formed by a mixture of BSA, IgG and fibrinogen.⁶³ In early 2001, Tidwell *et al.* demonstrated that the sensitivity of static ToF-SIMS helped in probing the structure of adsorbed protein films in relation with the protein type, the substrate type and the adsorption conditions.⁶⁴ But rapidly, direct interpretation of adsorbed proteins ToF-SIMS spectra was shown to be a really complicated and tedious work; multivariate analysis (MVA) treatment of data was thus introduced.^{65,66} Principal component analysis (PCA) is the most common technique for statistical treatment of large ToF-SIMS datasets.²⁸ It allows the detection of specific fragmentation patterns in adsorbed protein films and the identification of the amino acid fragments relevant for the separation of several samples to elucidate the orientation/conformation of an adsorbed protein.

Since the early 2000's, PCA has been applied in numerous studies using ToF-SIMS for adsorbed protein characterization. It was first used to characterize adsorption from single protein solutions and detect the different a.a. composition of proteins.⁶⁷⁻⁶⁹ As an example, 13 different proteins could be identified after adsorption on mica, PTFE and silicon wafers.⁶⁶ Mixture of proteins were also analyzed using PCA in the study of

competitive adsorptions of insulin and albumin on various polymers^{70,71} or the differentiation of fibrinogen/collagen mixtures adsorbed on silicon.⁷² However, the main results drawn from MVA on ToF-SIMS datasets concern the study of conformation and of orientation of adsorbed proteins.

Xia et al. studied the protection of antibodies by trehalose (a disaccharide known for its ability to inhibit protein unfolding at high temperature) to reduce the effect of drying before UHV study.⁷³ PCA showed a clear structural difference between protected and un-protected antibodies. The effect of glutaraldehyde in preserving protein structure upon adsorption was also demonstrated in a second study.⁷⁴ In our group, this methodology was successfully applied to detect conformational changes of albumin on polycarbonate membranes.⁷⁵ The orientation of adsorbed proteins was also probed. Some examples are the detection of the orientation of antibodies presenting their antigen binding side or their constant one on different substrates,⁷⁶⁻⁷⁸ and the immobilization of small proteins on surfaces that could influence the orientation through their charge or hydrophobicity.^{58,59} In a recent study, Giambianco *et al.* combined QCM-D measurements with ToF-SIMS and PCA results to demonstrate the influence of the co-adsorption of albumin on the conformation and bioactivity of fibronectin.⁷⁹ Numerous other examples of the use of PCA in ToF-SIMS data treatment could be given, a review on the subject was written by Graham and Castner²⁸ showing the great input of MVA techniques to reveal the information from complex datasets such as ToF-SIMS spectra.

1.2 Goals and Experimental Strategy

In the context of protein adsorption presented previously, the main goal of this project is to devise **chemically well-controlled surfaces** and to monitor the resulting **orientation and bioactivity of immobilized proteins**. In the literature, the interaction of proteins with complex surfaces have been largely studied but rarely fully explained **from the molecular level in UHV to the macroscopic level of bioactivity in the liquid phase**. Here we adopt a novel fundamental approach with the development of the **ToF-SIMS/PCA** combination to study protein **orientation/conformation/defolding** and its correlation to **measurements in different media** (UHV, air and the liquid phase in XPS, PM-IRRAS and QCM-D).

The main focus in this thesis is to make the link between the **molecular structure of the protein** upon adsorption or grafting and the **surface properties**. In this work, intrinsic parameters of the surface are studied together with external ones depending on the protein itself and on its environment. The protein composition is taken into account to explain the orientation. Based on protein models, charged residues or hydrophobic patches will be identified on the outer part of proteins and will help in the determination of most likely orientation in the considered adsorption conditions. External conditions for protein adsorption are for example the **solution** in which adsorption is carried out (concentration, buffer, pH...), the **influence of drying the sample** before analysis in ToF-SIMS, XPS or PM-IRRAS, and moreover, the influence of the **UHV environment** on the results. By adopting a multi-technique approach we can study the influence of such parameters.

Finally, the aim is to probe:

The **structure** of the surface and its **physico-chemical properties**: hydrophobic/hydrophilic, polar/apolar, charge.

How the surface properties influence the **adsorption modes** of proteins, and mainly their **orientation**, upon adsorption.

The influence of these parameters on the **bioactivity** of adsorbed species.

The templates chosen for these studies are homogeneous SAMs of thiolates on gold. All the thiol molecules used have the same chain length (10 carbon atoms) and only differ by their endgroups ($-\text{CH}_3$, $-\text{COOH}$ and $-\text{NH}_2$). This will change the hydrophobicity and charge of the gold substrate. After SAM formation, proteins are simply adsorbed to or covalently grafted on the surface. First, two model globular proteins (β -Lactoglobulin and BSA) were explored before the study of a more realistic and complex system using antibodies. Finally, some preliminary studies have been conducted to transpose the obtained results to adsorption on nanoparticles (NPs).

1.3 Outline

This introductory chapter is directly followed by a detailed description of the techniques in use during this work revealing how they will each contribute in the study of adsorbed protein films or SAMs characterization (Chapter 2). Results obtained during this work are then presented in three different chapters.

Chapter 1

The first one (Chapter 3) will present how SAM were characterized using first conventional techniques such as XPS or PM-IRRAS, and then in ToF-SIMS using the newly introduced Ar cluster source. This chapter aims to demonstrate how gold surfaces were chemically controlled and characterized before protein adsorption. It also shows new methodological developments in organic thin film study using ToF-SIMS.

Chapter 4 presents the results of adsorption of two model proteins on –COOH-, –NH₂- and –CH₃-terminated SAMs. β -Lactoglobulin (β LG) is a *hard* globular protein and bovine serum albumin (BSA) is a *soft* one. We will discuss the influence of protein properties on their adsorption and how it is related to surface properties.

Chapter 5 presents the study of a more realistic case with the exploration of adsorption or grafting of an antibody on SAMs. In addition to the direct determination of protein orientation with ToF-SIMS and PCA, the influence on bioactivity is probed using PM-IRRAS and PCA.

Chapter 6 will conclude this manuscript by drawing a summary of the main results and presenting perspectives for future work.

An annex is added to the present manuscript to show preliminary results on the adsorption of antibodies on nanoparticles. This part will be mainly focused on the challenge of studying such complex systems using surface characterization techniques such as XPS or ToF-SIMS.

2 Methodology for Protein Film Study

Here will be presented the different techniques in use during this project. As exposed in the introduction, a multi-technique approach was chosen in order to get a full picture of the adsorption mechanisms during protein adsorption. It will involve several techniques applied in various media ranging from the ultra-high vacuum (UHV) to the liquid phase. Time of flight secondary ion mass spectrometry (ToF-SIMS) and X-ray photoelectron spectrometry (XPS) are performed in UHV while polarization modulated infra-red reflection absorption spectroscopy (PM-IRRAS) is operated in air and quartz crystal microbalance with dissipation measurements (QCM-D) in the liquid phase. The theoretical background for all these techniques will be provided together with the relevant information obtained for self-assembled monolayers (SAMs) and protein films analysis.

2.1 ToF-SIMS and PCA

2.1.1 Theoretical Background

In secondary ion mass spectrometry (SIMS), ionized atoms or molecules are collected after bombardment of a surface by energetic particles. Primary species can be atomic, molecular or cluster ions (Bi^+ , Bi_n^+ , Cs^+ , O_2^- , C_{60}^+ , Ar_n^+ ...) with an energy of several kV. In a classical model, incident atomic ions will trigger a collision cascade in the material that will lead to the ejection of material from the surface. The main part of the sputtered material (atoms or molecules) is neutral but SIMS only allows the detection of charged species (secondary ions).⁸⁰ The detection of neutral species can be improved by using laser post-ionization methods.⁸¹

Dynamic SIMS (D-SIMS) was the first application of SIMS. In this technique, the studied material is sputtered with high dose of primary ions causing an etching of the specimen. D-SIMS reveals the elemental and isotopic composition of the sample but is only able to follow one (or few) specific mass at a time.⁸² Most of the applications of D-SIMS can be found in the domain of the semiconductors, in metallurgy or in geology. In order to retrieve the molecular information in organic or biological materials it was necessary to introduce new concepts. In the 70's Alfred Benninghoven defined the principles of *static* SIMS.⁸³⁻⁸⁵ He established that, in the case of atomic primary ions, using a very low current for primary ions (low particle flux density at the surface $< 1 \text{ nA.cm}^{-2}$), and analyzing a large surface (about 0.1 cm^2) the surface monolayer lifetime under bombardment becomes higher than the analysis time. Statistically, each analysis point on the

surface will only be impacted one time by primary ions.^{80,86} SIMS, in the static mode, is thus a very “surface sensitive” technique since the spectral information comes from undamaged part of the surface. The static limit is generally set at a maximum primary ion dose of 10^{13} ions.cm⁻² throughout all the analysis time.

Theoretical background behind the SIMS technique is extensively described in the literature,^{87,88} only the basic concepts will be presented here. The main principles of the technique and the relevant parameters are described by the basic equation of SIMS for a specific chemical *m* on the analyzed surface:

$$I_m = I_p y_m \alpha^\pm \theta_m \eta$$

Where:

I_m is the secondary ion current for species *m*

I_p is the primary ion current (or primary particle flux)

y_m is the sputter yield of *m*

α^\pm is the ionization probability of *m* in positive or negative ions

θ_m is the fractional concentration of *m* in the surface layer

η includes the transmission factor by the analyzer and the detection by the detector

Most relevant physical parameters in this equation are y_m and α^\pm . The sputter yield will represent the way the species *m* will be ejected from the surface after primary ion impact. It depends on the type of analyzed materials (inorganic/organic) and on the projectile. In the past decade, large cluster ions were introduced as projectile (Ar_n^+ with $n > 1000$ for

example) with two main advantages: a lower damage to the chemical structure of the surface (1) and an increase in the sputtering yield for organic species (2). The first effect is due to the repartition of the total energy of the cluster to all of its atoms upon breaking when impacting the surface. The penetration depth being dependent on the impact energy, ion cluster provoke less damage to the subsurface. However, the second effect is observed because more atoms bombard the surface after breaking of the cluster and each one can interact to form secondary species.⁸⁹

The ionization process leading to detection of the secondary ions is less understood and can occur during the collision cascade or after sputtering by interaction between ejected particles (neutrals, electrons, protons...). Nevertheless, several solutions are explored to increase it. Examples are post-ionization of ejected particles using lasers⁹⁰ and electrons,⁹¹ or the injection of water vapor to enhance charge transfers to the sputtered material.⁹² Looking at the basic SIMS equation, one can easily see that SIMS is not a quantitative technique since the ionization probability is difficult to calculate. However, qualitative and semi-quantitative information can still be extracted from SIMS spectra by comparing several characteristic peaks or different spectra.

After sputtering, secondary ions must be sorted according to their mass. Only time-of-flight (ToF) analyzers are described here but other detection systems such as magnetic sectors or quadrupole analyzers exist.⁸⁷ In a ToF analyzer, secondary ions are first accelerated with a strong electric field. Ions acquire a kinetic energy E_k proportional to the applied difference of

potential: $E_k = \frac{1}{2}mv^2 = zV$ where m is the mass of the considered ion and v its velocity, z the charge of the particle and V the applied voltage of the electric field. Negative and positive ions are detected separately by switching between negative and positive electric field for the extraction. In the ToF drift tube, the velocity is described as $v = \frac{d}{t}$ (with d the path distance in the analyzer and t the time-of-flight) we thus obtain:

$$t = \frac{d}{\sqrt{2V}} \sqrt{\frac{m}{z}}$$

$\frac{d}{\sqrt{2V}}$ being a constant for the analyzer, the time-of-flight is directly linked to the mass over charge ratio of the ion m/z . In this kind of analyzer, ions cannot be detected continuously; the primary ions are then grouped in pulse of 10 ns that are bunched down to about 1 ns when impacting the surface. Secondary ions from the same z are all accelerated at the same energy before entering the ToF analyzer allowing their separation. The energy and angular dispersion of secondary ions after sputtering and acceleration is compensated by an ion mirror (a reflectron) in the analyzer to increase the mass resolution. The reflectron is formed of successive electrodes creating a retarding field for the ions. Ions with a mass m at a higher energy will penetrate deeper in the reflector and travel a longer distance. Conversely, ions with the same mass m but with a slightly lower energy travel a shorter distance. The detector is placed in a way that reflected ions with different energy but the same mass hit it at the same time. The reflectron thus allow improving the mass resolution and reducing the length of the analyzer needed for ions separation (see Figure 2.1).^{93,94}

After reflection on the reflectron and just before hitting the detector, secondary ions can be post-accelerated with an energy of a few kV allowing the enhancement of the detection of high masses ion that would arrive on the detector with a very low energy. The post-acceleration takes place right before the detector to have the smallest influence possible on the time-of-flight. A technical description of our ToF-SIMS equipment together with the different surface analysis modes and parameters used for this work are presented below.

2.1.2 Experimental Description

The general principle of the equipment is presented in Figure 2.1. The spectrometer used for this work is a TOF.SIMS 5 (ION-TOF GmbH, Münster, Germany) equipped with three different primary ion columns (4 sources). The first one is a Bi liquid metal ion gun (LMIG); generated primary ions are: Bi^+ , Bi_3^+ or $^{++}$, and Bi_5^+ with an energy of 30 kV. The LMIG is used as an analysis gun in the static mode. The second one is a dual source column (DSC) producing O^- and Cs^+ primary ions. It is used mostly to sputter inorganic materials. Finally, a gas cluster ion beam (GCIB) is available to produce large clusters Ar_n^+ as primary ions ($n = 500$ to 10000) with an energy ranging from 2.5 to 20 kV. This gun is used either in analysis or in sputter mode for organic materials.

After sputtering, secondary ions are accelerated at 2 kV by the extractor before entering the analyzer. They travel in the ToF analyzer and are reflected on the detector to produce a mass spectrum. In our setup, the post-acceleration is set at 10 kV but it can be pushed up to 20kV. For non-

conductive samples, a low energy electron gun compensates the charges created at the surface when bombarding the sample and during the sputtering process.

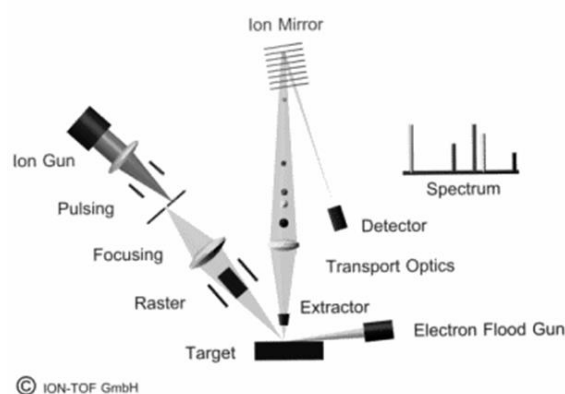


Figure 2.1 Schematic description of the ToF-SIMS equipment (reproduced from www.ion-tof.com)

In ToF-SIMS, four analysis modes are available:

Surface spectroscopy probes the chemical composition of the extreme surface (a few nm) of a sample using very low primary ion dose (static conditions) over a limited region of the sample.

Surface imaging is equivalent to spectroscopy but the beam is scanned over an area from μm^2 to cm^2 (if tiling several images) to provide a chemical map of the surface. Each pixel of the resulting image is a mass spectrum.

Depth profiling gives information on the chemical composition of a sample in the z direction. The analysis is performed in the dual beam mode by alternatively sputtering to create a crater and analyzing the bottom of the crater.

3D analysis is the combination of imaging and depth profiling to reconstruct a chemical map of the analyzed volume in a sample.

In this work, only the surface spectroscopy mode is used with Bi^+ (and Ar_n^+ occasionally) as primary ions. Bi^+ primary ions were chosen over the Bi_n^+ since no differences can be observed between both sources over SAMs analysis as shown in the literature.⁹⁵ In the case of protein film study, most of our work is based on the analysis of low mass peaks corresponding to a.a. fragments in the protein. The formation of such fragments is favored when using atomic primary ions sources. Moreover, our PCA calculations showed no differences in sample separations when using Bi^+ or Bi_3^+ ions. The analyzed area for each spectrum is a square of $500 \times 500 \mu\text{m}^2$ and the acquisition time is fixed at 60 s to ensure a primary ion dose lower than $2 \cdot 10^{11} \text{ ions.cm}^{-2}$ well below the static limit. The mass resolution $m/\Delta m$ in these conditions is of about 8000 at m/z 70 for each sample. Spectra are calibrated using CH_3^+ , C_2H_3^+ , C_3H_5^+ , and C_7H_7^+ ($m/z = 15, 27, 41$ and 91) in the positive mode and CH^- , C_2H^- , C_3H^- and C_4H^- ($m/z = 13, 25, 37$ and 49) in the negative mode. Charge compensation was not necessary in our studies since SAMs and proteins were adsorbed on a conductive gold layer over silicon wafers allowing the evacuation of the charge brought by primary ions bombardment on the surface.

2.1.3 Characterization of Protein Films

ToF-SIMS presents several advantages for the study of organic films, most important ones being its high mass resolution (up to $m/\Delta m = 10000$) and its very low sampling depth (a few nm).⁵⁵ ToF-SIMS will probe only the one or

two first layers of the surface while XPS retrieve information from the top ten layers or so.⁹⁶ Moreover, ToF-SIMS is more sensitive with detection limits in the order of 10 to 100 ppm (depending on the sample and especially the ionization probability) compare to 1000 ppm for XPS. Sputtering proteins with an energetic primary ion (Bi^+ at 30 kV) leads to their fragmentation. In previous studies,^{57,66,75} characteristic protein fragments peaks have been identified in the negative or in the positive ion mode. In the negative mode, only the CN^- ($m/z = 26$) and the CNO^- ($m/z = 42$) peaks corresponds to protein fragments. These peaks are not specific of one amino acid and are thus not used to identify specific proteins. In the positive mode, 44 peaks have been identified that correspond to specific amino acids fragments in proteins; they are displayed in Table 2.1. Looking at the relative intensities of these peaks give information on the adsorbed proteins orientation or conformation.¹⁵

Table 2.1 Characteristic positive amino acids fragments detected for protein analysis in ToF-SIMS with the corresponding a.a. in the one letter code

Mass	Fragment	a.a.	Mass	Fragment	a.a.	Mass	Fragment	a.a.
28.02	CH_2N^+	G	68.05	$\text{C}_4\text{H}_6\text{N}^+$	P	87.06	$\text{C}_3\text{H}_7\text{N}_2\text{O}^+$	N
30.04	CH_4N^+	DERMS HYFKLG	69.04	$\text{C}_4\text{H}_5\text{O}^+$	T	88.04	$\text{C}_3\text{H}_6\text{NO}_2^+$	D
42.03	$\text{C}_2\text{H}_4\text{N}^+$	AF	70.03	$\text{C}_3\text{H}_4\text{NO}^+$	N	98.02	$\text{C}_4\text{H}_4\text{NO}_2^+$	N
43.03	CH_3N_2^+	R	70.07	$\text{C}_4\text{H}_8\text{N}^+$	P	100.09	$\text{C}_4\text{H}_{10}\text{N}_3^+$	R
44.01	CH_2NO^+	N	71.01	$\text{C}_3\text{H}_3\text{O}_2^+$	S	102.06	$\text{C}_4\text{H}_8\text{NO}_2^+$	E
44.03	CH_4N_2^+	R	72.08	$\text{C}_4\text{H}_{10}\text{N}^+$	V	107.05	$\text{C}_7\text{H}_7\text{O}^+$	Y
44.05	$\text{C}_2\text{H}_6\text{N}^+$	ALFYHS MKDE	73.07	$\text{C}_2\text{H}_7\text{N}_3^+$	R	110.07	$\text{C}_5\text{H}_8\text{N}_3^+$	RH
44.98	CHS^+	C	74.06	$\text{C}_3\text{H}_8\text{NO}^+$	T	115.05	$\text{C}_4\text{H}_7\text{N}_2\text{O}_2^+$	G
47.00	CH_3S^+	C	80.05	$\text{C}_5\text{H}_6\text{N}^+$	P	120.08	$\text{C}_8\text{H}_{10}\text{N}^+$	F
56.05	$\text{C}_3\text{H}_6\text{N}^+$	FKM	81.04	$\text{C}_4\text{H}_5\text{N}_2^+$	H	127.10	$\text{C}_5\text{H}_{11}\text{N}_4^+$	R
58.07	$\text{C}_3\text{H}_8\text{N}^+$	E	82.05	$\text{C}_4\text{H}_6\text{N}_2^+$	H	130.07	$\text{C}_9\text{H}_8\text{N}^+$	W
59.00	$\text{C}_2\text{H}_3\text{S}^+$	C	83.05	$\text{C}_5\text{H}_7\text{O}^+$	V	131.05	$\text{C}_9\text{H}_7\text{O}^+$	F
60.05	$\text{C}_2\text{H}_6\text{NO}^+$	S	84.05	$\text{C}_4\text{H}_6\text{NO}^+$	EQ	136.08	$\text{C}_8\text{H}_{10}\text{NO}^+$	Y
60.06	CH_6N_3^+	R	84.09	$\text{C}_5\text{H}_{10}\text{N}^+$	K	170.06	$\text{C}_{11}\text{H}_8\text{NO}^+$	W
61.01	$\text{C}_2\text{H}_5\text{S}^+$	M	86.10	$\text{C}_5\text{H}_{12}\text{N}^+$	IL			

Chapter 2

Figure 2.2 illustrates how a.a. fragment peaks study can lead to detect different conformation/orientation of adsorbed proteins on a surface. The a.a. sequence is characteristic for each protein and will determine its structure. In the case of two separated conformations/orientations of the adsorbed protein, the a.a. fragments distribution in the mass spectrum will thus be different. By comparing these distributions to the structure of the studied protein one can infer the different orientations/conformations. However, this work can sometime be complicated because really small differences are at stake. Principal component analysis was introduced to compare mass spectrum of adsorbed proteins and try to determine which a.a. are the most presents on the outmost layer. It will help getting a better understanding of how proteins are adsorbed on a surface without checking individually all the intensities of a.a. fragments peaks. This multivariate analysis technique is presented in the next paragraph.

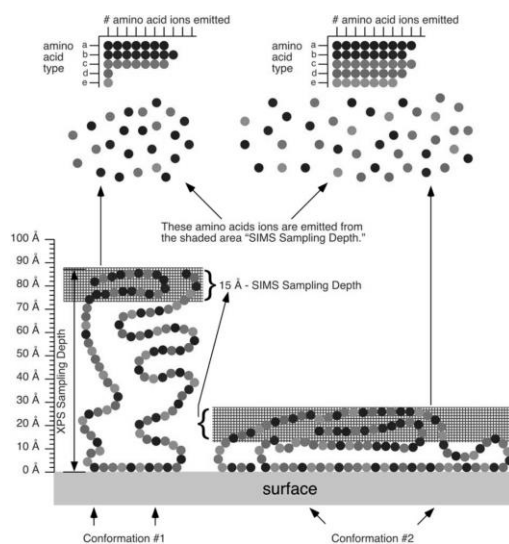


Figure 2.2 Schematic representation of how a protein adsorbed in two different conformations on a surface can give two different a.a. fragments repartition in ToF-SIMS due to the low sampling depth of the technique (reproduced from ¹⁵)

2.1.4 PCA Applied to ToF-SIMS Datasets

Since numerous peaks (more than 40) are involved in the identification of proteins in ToF-SIMS, comparison of individual peaks can lead to a tedious work. SIMS data are a multi-variate system; the relative intensities of several peaks in one spectrum are related due to the fact that ions come from the same surface species.⁹⁷ In order to simplify the analysis of large groups of SIMS data, statistical multi-variate analysis (MVA) methods were introduced. The applications of MVA for ToF-SIMS data treatment has been recently reviewed by Graham and Castner. They show the growing importance of MVA in the analysis of organic materials such as proteins, lipids, polymers or cells.²⁸

A lot of different MVA methods exist but the most common is principal component analysis (PCA). Figure 2.3, gives a graphical representation of PCA. The main idea is to lower the complexity of ToF-SIMS data by representing them in a new space. In this graphical example, each spectrum is characterized by 3 peaks (m_1 , m_2 , m_3) and is plotted as one point in the space where each mass correspond to one axis. The principal components (PCs) are new orthogonal axes summarizing the information contained in the original dataset. In this case, PC1 represents the maximum of variance between samples when PC2 represents the statistical differences between each spectrum of the same sample.

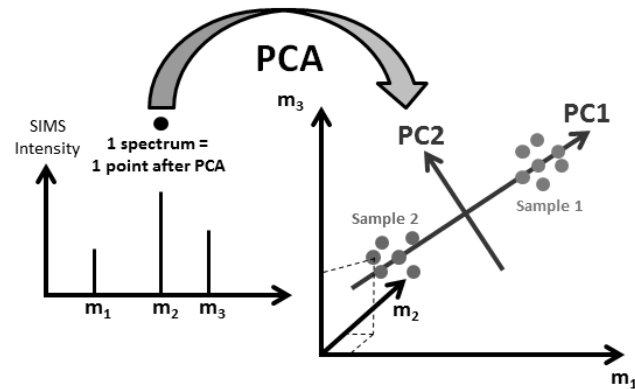


Figure 2.3 Graphical representation of PCA applied to SIMS spectrum [adapted from ⁹⁸]

Considering now the more realistic case of n spectra with k peaks, they can be represented in a hyperspace of k -dimensions (the k -space). Practically, data are ordered in a matrix X with n rows and k columns. Each $x_{i,j}$ cell in the data matrix is filled with the corresponding peak area for the specific spectrum.⁹⁹ The PCA algorithm finds a new space with m -dimensions ($m < k$) describing the maximum of variance within the dataset. Axes in this new space are the different orthogonal PCs. The output of PCA calculations is a linear combination of the initial values which is stored in three different matrices described as the scores, the loadings, and the residual.

Scores are the projection of each sample (spectra) on the PC axes in the new m -space, they give the relationships between samples and how they can be separated.

Loadings are the cosines of the angle between the new axis (PC1, 2, 3...) and the original ones in the k -space ($m_1, 2, 3...$). They describe how much a variable contributes to the new axes, *i.e.* PCs.

The **residual** matrix contains only the noise not described in any PCs.

The actual PCA calculations will not be elaborated here but precise descriptions can be found in the literature.^{100,101} During this work, the NESAC/BIO MVA Toolbox (<http://mvsa.nb.uw.edu>, developed by Dr. Dan Graham in University of Washington) for MATLAB (The MathWorks, Inc., Natick, MA) was used to perform PCA calculations. After uploading the data matrix in the toolbox, it calculates the scores and loading matrices. Scores are then plotted with the 95% confidence limit; the methodology of the script was described by Wagner et al. in 2001.⁶⁶

Before performing PCA, one should carefully select the peaks to analyze (variables). In the case of protein films analysis, only the 44 peaks corresponding to a.a. fragments are analyzed. PCA is indeed used to detect the relationship between these peaks and their relative importance in the separation of different samples. Moreover, to detect only the variation due to chemical differences between samples in PCA, several pre-treatments can be performed on the data. They are summarized in three categories:

Normalization refers to the division of the intensity of each peak by a scalar. It is performed to take into account the fluctuations in secondary ion yields between different spectra. These can emerge from variations in the experiment itself like a fluctuation of the primary ions beam current, the roughness of the sample or possible charging effect on the surface. Many ways are possible to normalize data the most common ones being the normalization on the total

counts of each spectrum, the normalization on the sum of the selected peaks for PCA analysis or on one specific peak. The detailed influence of normalization on the data is discussed in the literature.¹⁰² In the case of protein film analysis, it was chosen to normalize the data over the sum of all selected peaks for PCA to take into account variations between samples and detect relative differences in fragment distributions.

Mean centering of the data is done to make them fluctuate around a common zero. It is then considered that most of the chemical information is represented by the variation of the data around the mean.

Scaling is done to account for differences in the scales between variables. Several methods are described such as auto-scaling (where each variable of a mean centered data set is divided by its standard deviation), square root scaling, or Poisson scaling...¹⁰² Scaling of SIMS data is still an open debate.²⁸ The intensity of ToF-SIMS peaks decreasing with increasing mass, some would argue that scaling should be done to restore the weight of high mass peaks in the data sets separation; other would argue that these differences are not relevant since all secondary ions are coming from the same machine and no scaling should be performed. In addition, scaling could lead to an artificial increase of the weight of the noise in high masses measurements. In this work, no scaling has

been performed on data in order to keep most of the original information contained in SIMS spectra.

Once PCA calculations are finished, one should carefully analyze scores and loadings keeping in mind the assumption made when pre-processing the data. As it is underlined by Graham and Castner,²⁸ one should always ask the three following questions: (1) Are the results logical? (2) Do the results agree with the other data collected on the samples? (3) Are the results reflected in the original data? In general, samples with high scores on one side of a given PC axis will have higher intensities for the peaks showing large loadings on the same side of this given PC axis. All the information is already contained in the original data but PCA helps unraveling the differences. In the case of adsorbed proteins, PCA will reveal the set of a.a. most likely to be exposed on the surface. By comparison with models of the studied proteins, their orientation or conformation can thus be deduced.

2.2 XPS

2.2.1 Theoretical Background

In the 50's, Siegbahn *et al.* introduced the Electron Spectroscopy for Chemical Analysis (ESCA) also known as X-ray photoelectron spectroscopy (XPS).¹⁰³ Photoelectron spectroscopy exploits the photoelectric effect evidenced in 1887 by Hertz¹⁰⁴ and theoretically formalized in 1905 by Einstein.¹⁰⁵ In photoelectron spectroscopy, a photon excites an atom and leads to the ejection of an electron with a certain kinetic energy (E_k). For the photoelectron, E_k is related to the binding energy (E_b) of the electron in

the considered element and to the photon energy ($h\nu$) of the photon. The general photoemission equation can be written as $E_K = h\nu - E_B$. However, one must also take into account the work function needed to extract the produced photoelectrons. In Figure 2.4 the energy levels implicated for the extraction of the photoelectron from the sample and its transmission to the spectrometer has been represented. Since both the sample and the spectrometer are grounded, their Fermi levels are aligned. The binding energy is defined in reference to the Fermi level. The work function (Φ) of the spectrometer or of the sample will be equal to the difference between the Fermi level and the vacuum level for the considered system.

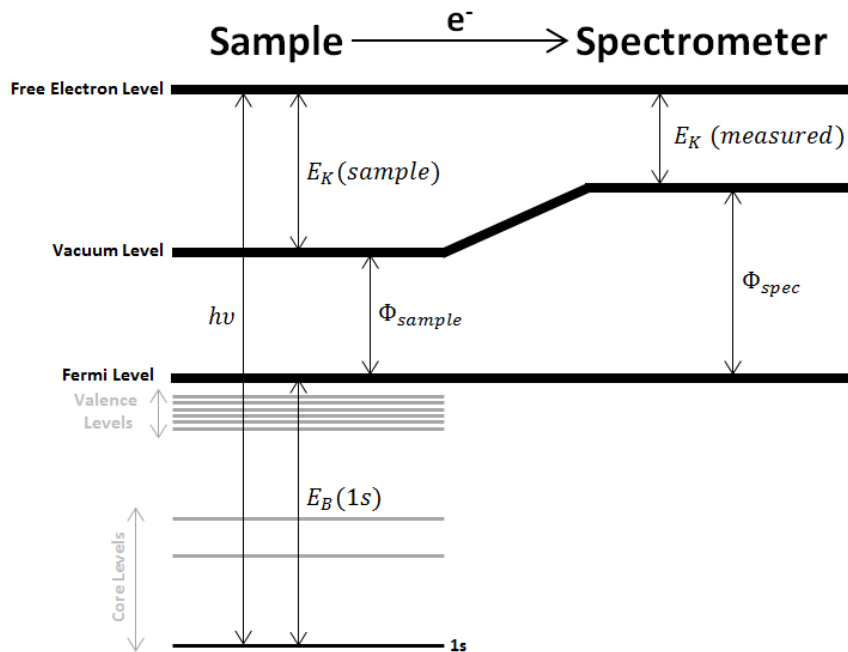


Figure 2.4 Schematic representation of the different energy levels during the photoelectron emission and its transmission to the spectrometer. E_K is the kinetic energy, E_B is the binding energy, $h\nu$ is the photon energy and Φ_n is the work function of the sample or of the spectrometer.

When escaping the sample, the photoelectron has a kinetic energy described as:

$$E_{K(sample)} = h\nu - E_B - \Phi_{sample}$$

After transmission to the spectrometer, the difference in work functions between the sample and the spectrometer must be taken into account:

$$E_K = E_{K(sample)} - (\Phi_{spec} - \Phi_{sample})$$

So finally, the kinetic energy of the photoelectron in the spectrometer is:

$$E_K = h\nu - E_B - \Phi_{spec}$$

By measuring the kinetic energy of photoelectrons one can easily retrieve their original binding energy that depends only on their origin in the sample (elements, core level, valence level...), the photon energy and the work function being fixed parameters in the experiment.

Photoelectron spectroscopies probe differences in binding energies of electrons from photo-ionized elements. The photon energy used for the analysis will define the kind of electrons probed. X-ray excitation in XPS allows probing the electrons from the core levels when UV excitation (UPS) gives access to valence electrons. Alongside with photoelectrons, the Auger electrons can also be emitted (see Figure 2.5). Auger electron spectroscopy (AES) will generally use an electron gun as the excitation source but Auger electrons are also produced during XPS measurements. The different processes are summed-up in Figure 2.5.

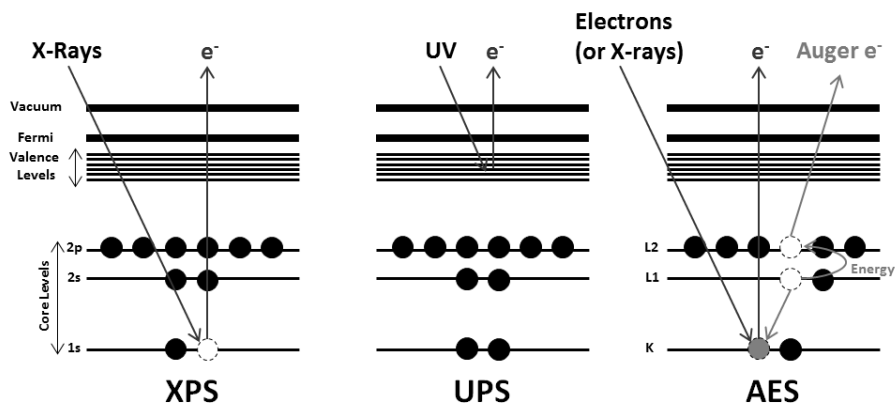


Figure 2.5 Schematic representation of the excitation in different photoelectron spectroscopies. e^- = electrons [adapted from ¹⁰⁶]

The photoelectron binding energy (E_B) depends on the element the electron originates from and on its chemical environment. Each element will then have several peaks corresponding to its core levels (1s, 2s, 2p...) based on its electronic structure. Peak intensities will describe the quantity of each element in the sample taking into account acquisition parameters. Each peak can be decomposed in several components corresponding to the different chemical functions in which the atom can be in the sample. For levels superior to 2s, spin-orbit coupling appears and give rise to doublets of peaks. These doublets have specific area ratios based on the quantum numbers of the analyzed elements. Details can be found in reference but won't be developed here.¹⁰⁶ As an example, on the 2p level, the two peaks of the doublet are labeled $2p_{1/2}$ and $2p_{3/2}$ and have an area ratio of 1:2. More details on spectral decomposition will be given below after a short experimental description.

2.2.2 Experimental Description

The XPS spectrometer used for this work is a Kratos Axis Ultra (Kratos Analytical, Manchester UK). Practically, samples are fixed on a stainless steel multispecimen holder using insulating tape and introduced in a UHV chamber maintained at 10^{-6} Pa. Then the analyzed sample is irradiated with an X-ray beam. In the laboratory this source is an X-ray tube with a fixed energy but synchrotron radiation can be useful for higher brightness and to tune the photon energy ($h\nu$). In Figure 2.6 is depicted a schematic XPS spectrometer, details of our experimental setup are given below.

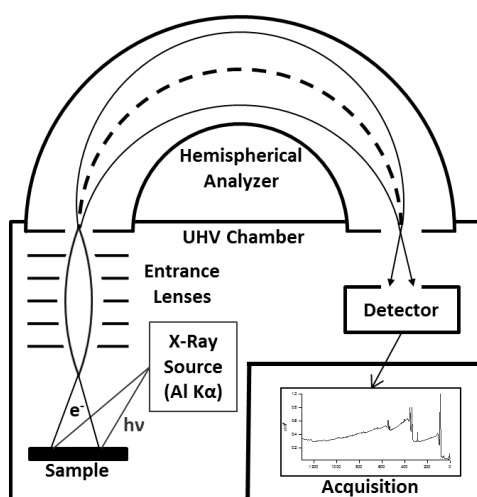


Figure 2.6 Schematic description of an XPS analyzer

X-rays are produced in a monochromatized aluminum X-ray source. It is operated at 10 mA and 15 kV and has a fixed photon energy of $h\nu = 1486.6$ eV corresponding to the Al $K\alpha$ ray. Photoelectrons are generally collected at an angle of 0° from the normal to the sample but this angle is variable. The analyzed area is $700 \times 300 \mu\text{m}^2$. The analysis depth is about 10 nm and

depends on the inelastic mean free path (IMFP) of electrons in the analyzed material. The IMFP correspond to the average distance an electron can travel in the material without collisions. It varies principally in function of the electron energy and of the nature of the material the electron travel through. It is generally considered that the analysis depth is of about three times the IMFP.

The analysis is performed in the hybrid lens mode, with a combination of magnetic and electrostatic lenses collecting photoelectrons. The electrostatic lenses labeled entrance lenses on Figure 2.6 are set to accept electron escaping the surface with a low solid angle (usually around 20°). In the hybrid lens mode a magnetic lens is placed under the sample and redirect electrons escaping the sample with a large angle toward the stack of electrostatic lenses. This mode improves the sensibility of the instrument by increasing the number of photoelectrons collected.

After collection, photoelectrons enter the hemispherical analyzer. A difference of potential is applied between the inner and the outer shell of the analyzer. Electron having a kinetic energy corresponding to the median potential will have a curved path to the exit slit and will be detected. The energy resolution (ΔE) of the analyzer depends on its radius (R_0), on the width of the exit slit (W) and on the pass energy (E_p) as follows:²⁷

$$\Delta E = \frac{E_p W}{2R_0}$$

Increasing the pass energy decreases the energy resolution. For survey scan pass energy of 160 eV was used when it was set at 40 eV for narrow scans.

In the latter, a full width at half maximum (FWHM) of 0.9 eV is obtained for Ag 3d_{5/2} peak of a standard silver sample. Practically, it is difficult to scan the whole range of kinetic energies by changing the difference of potential in the analyzer. Photoelectrons are then retarded or accelerated in the entrance lenses to reach the fixed pass energy. The whole energy range below the Al K α line is scanned by applying different retarding or accelerating field in the electrostatic lenses.

The detection is finally made by an eight channeltrons detector. Charge stabilization is achieved by using an electron source (semicircular filament) mounted coaxially to the electrostatic lens column and a charge balance plate used to reflect electrons back toward the sample. The magnetic field of the immersion lens placed below the sample acts as a guide path for the low-energy electrons returning to the sample. The electron source is operated at 1.8 A filament current and a bias of -1.1 eV. The charge balance plate is set at -2.8 V.

For each experiment, a specific sequence of spectra is recorded. First a survey spectrum is recorded to identify each element present on the surface of the sample and narrow scans are recorded for one core-level of each specific element (C 1s, O 1s, N 1s, S 2p, Si 2s...). The sequence is generally started and ended by the C 1s measurement to check for the absence of degradation and charge stability over time. Finally, the C-(C,H) component of the C 1s peak is fixed at 284.8 eV to set the binding energy scale.

2.2.3 XPS Characterization of Organic Layers

The data treatment is performed with the CasaXPS software (Casa Software Ltd., UK). The peaks are decomposed using a linear baseline, and a component shape is defined by the product of a Gauss and Lorentz function, in the 70:30 ratio, respectively. Atomic % for the sample are calculated using peak areas normalized on the basis of acquisition parameters after a linear background subtraction, experimental sensitivity factors based on those of Wagner¹⁰⁷ and transmission factors provided by the manufacturer. Elemental atomic percentages, excluding hydrogen which is not detected in XPS, are calculated to determine the surface composition.

In our studies, XPS is used to characterize organic layers formed either of SAMs or of adsorbed proteins. A first indication of the adsorption of an adlayer on a surface can be found by looking at the attenuation of the signal coming from the substrate. In our case we follow the atomic percentage of gold (Au 4f peak) before and after SAMs formation or protein adsorption. The thickness of the adlayer can be estimated using the Beer-Lambert law. The gold signal will be attenuated as follows:

$$I_{Ad}^{Au} = I_0^{Au} e^{-\frac{d}{\lambda_{Ad}^{Au} \cos \theta}}$$

In this equation I_x^{Au} represents the intensity of the gold signal before or after formation of the adlayer ($x = 0$ or Ad), d is the thickness of the film, λ_{Ad}^{Au} is the IMFP of gold photoelectrons traveling through the adlayer and θ is the take-off angle of photoelectrons (i.e. the angle formed between the

detector and the normal to the surface). Figure 2.7 sums up the situation. The intensities are measured during the XPS analysis while the IMFP can be calculated, one can thus easily retrieve the thickness of the film by studying the attenuation of the substrate signal. However, such calculations must be interpreted carefully since photoelectrons reach the analyzer with a distribution of angles (especially in the hybrid lens mode).

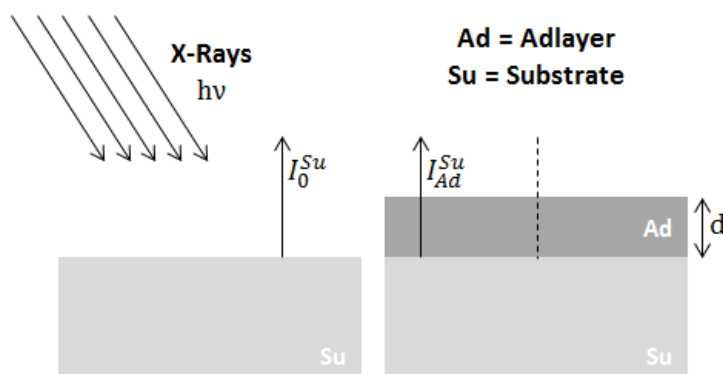


Figure 2.7 Schematic representation of an overlayer on a substrate

Since the IMFP is fixed for a certain material, by changing θ one can enhance the signal coming only from the surface. For large θ angles, photoelectrons collected by the analyzer come mostly from the adlayer and not from the substrate since they have a longer path to travel to escape from the sample and will most likely be involved in collisions (see the $\cos \theta$ in the attenuation equation). To determine the surface composition of a film it could be interesting to record different XPS spectra at different θ and see if a component is more localized at the surface or buried in the interface. This has been applied for example in SAM characterization⁴³ or in determination of their contamination.¹⁰⁸ In our case, such measurements

were not performed since we used the hybrid mode that increases greatly the angle of acceptance of the analyzer cancelling partially the change in θ .

Further analysis is required to identify the different chemical functions at the surface. The positions of XPS lines for each component in biochemical compounds have been tabulated.²⁷ They are presented in Table 2.2 for C 1s, O 1s and N 1s peaks. We will present here in detail how XPS spectra were decomposed for this work. Decompositions have been performed using the CasaXPS software. Before decomposition, all spectra are recalibrated by fixing the C 1s component corresponding to carbon only bound to carbon or hydrogen $\underline{\text{C}}\text{-(C,H)}$ at 284.8 eV as the energy reference. Decomposition was carried out by fixing the lowest number of constraint. Nevertheless, within one element, all components are fixed to have the same full width at half maximum (FWHM). For S 2p peaks, 3/2 and 5/2 doublets are given an area ratio of 2:1 and an energy separation of 1.18 eV.¹⁰⁹ We will now detail the decomposition applied for C 1s, O 1s, N 1s and S 2p peaks found during this work.

The C 1s peak was decomposed in four components: with the lower binding energy one (fixed at 284.8 eV) attributed to carbon only bound to carbon or hydrogen $\underline{\text{C}}\text{-(C,H)}$; the second one (fixed at 286.3 eV) to carbon singly bonded to oxygen or nitrogen $\underline{\text{C}}\text{-(O,N)}$; the two high binding energy ones are attributed to carbon doubly bonded to oxygen in amides or in carboxylates ($\underline{\text{C}}\text{=O}$ amide, $\underline{\text{C}}\text{OO}^-$ at about 288 eV), and to carbon in carboxyl groups ($\underline{\text{C}}\text{(=O)-OH}$ (at about 289 eV)).²⁷ The O 1s peak was decomposed in two components. The first one at lower binding energy was attributed to

oxygen doubly bonded to carbon, $C=O$, in amides or carboxyls, and to oxygen in carboxylates,²⁷ while the second component, at higher binding energy, is likely due to oxygen singly bonded with carbon ($C-OH$).²⁷ The N 1s peak also shows usually two components, one at lower energy attributed to amide or amine NH/NH_2 and another at higher energy, indicating the presence of protonated amines NH_3^+ . In the case of SAM characterization, the S 2p peak was decomposed in two doublets, respectively attributed to sulfur in $S-Au$ bonds, at low binding energy (S 2p_{3/2} at about 161.9 eV), thus confirming the chemisorption of thiols to gold, and unbound sulfur groups (labeled S_{free} with S 2p_{3/2} at 163.3 eV).

Table 2.2 Binding energy of elements in chemical functions of biochemical compounds, [Reproduced from Genet *et al.*²⁷]

Element and function	Position (eV)	Compound of reference
CARBON		
$C-(C,H)$	284.8	Hydrocarbon, adventitious contamination
$C-N, (C=O)-N-C$	286.1	Amine; amide, peptidic link
$C-O$	286.3	Alcohol
$(C=O)-O-C$	286.8	Ester*
$C=O, O-C-O$	287.8	Aldehyde, (hemi)acetal
$(C=O)-N-C, O=C-O^-$	288.0	Amide, peptidic link; carboxylate
$(C=O)-O-C$	289.0	Ester*
$(C=O)-OH$	289.0	Carboxylic acid
OXYGEN		
$O=C-O^-$	531.1	Carboxylate
$(C=O)-N$	531.3	Amide, peptidic link
$(C=O)-OH$	531.8	Carboxylic acid
$(C=O)-O-C$	531.9	Ester*
$C-OH, C-O-C-O-C$	532.6	Alcohol, (hemi)acetal
$(C=O)-O-C$	533.4	Ester*
$(C=O)-OH$	533.4	Carboxylic acid
NITROGEN		
$C-NH_2$	399.3	Amine
$(C=O)-NH$	399.8	Amide, peptidic link
$C-NH_3^+$	401.3	Protonated amine

* determined on glycerol tristearate (unpublished)

Chapter 2

Using these values, one can identify which moieties are represented at the surface. After decomposition, the atomic % of each component is calculated. Protein layers are characterized by the components corresponding to the peptidic link. The peptidic link can be described as (C=O)-N-C (see Figure 1.2). On the C 1s peak it will give two contributions at 288.0 and 286.3 eV (see Table 2.2). The first one, at higher energy, corresponds to carbon atoms doubly bonded to oxygen ones, this function is also observed on the O 1s peak with a component at low energy. The second one is characteristic of the CN moiety in the peptidic function and is observable on the N 1s peak with a component at low energy. Atomic %, derived from the areas of these components give direct information on the adsorbed protein quantity on the surface.

In the case of SAM characterization, the evolution of the components corresponding to thiol endgroups is followed compared to a blank gold sample. In the case of a -COOH-terminated SAMs, two components on the carbon peak can be observed. The first one at about 288 eV corresponds to a carbon atom linked to two oxygen atoms in a carboxylate (COO⁻). The second one at about 289 eV is associated to the carbon atom in a protonated carboxylic acid (COOH). Their relative intensities give information on the protonation state of the terminating layer. On a -NH₂-terminated SAM a similar effect is observed with two components in the N 1s peak corresponding to NH₂ and NH₃⁺ (399.3 eV and 401.3 eV respectively). To characterize the formation of the SAM, the S 2p peaks are also analyzed. They help in the determination of the quality of the thiol layer. The S_{Free} component represents sulfur atoms that are not bound to

the gold surface and is found at an higher energy (163.3 eV) than when sulfur atoms are covalently bound to Au (161.9 eV). The S_{Free} component is observed when free thiol molecules interact with the SAM without interacting with the Au surface.

2.3 PM-IRRAS

2.3.1 Theoretical Background

In infra-red spectroscopy, the characteristic vibrations between atoms in molecules are detected. Due to infra-red selection rules, only vibrations with a dipole moment change are active. In the late 50's, Francis and Ellison¹¹⁰ reported the first theoretical and experimental work studying monolayers on metal mirrors with infra-red. This work was pursued by Greenler¹¹¹⁻¹¹³ who formalized the optimum conditions for infra-red reflection absorption spectroscopy (IRRAS) experiments in the 60's.

Figure 2.8 describes the reflection of an IR beam on a metal surface. It is represented by an electromagnetic wave \vec{E} that is separated in the E_p and the E_s components. They are respectively parallel and perpendicular to the plane of incidence.

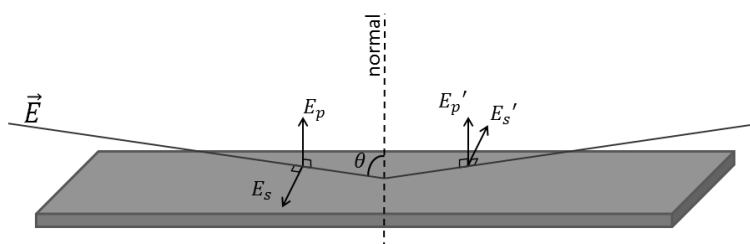


Figure 2.8 Geometry of the reflection of an IR beam on a metal surface at grazing incidence for the p- and s-component in the electric field

Chapter 2

Figure 2.9 represents the phase shift for each component. For the s-light, one can observe a nearly 180° phase shift for all angles of incidence that will create destructive interferences leading to a vanishing of this component at the surface. On the other hand, the p-light shows much lower phase shift for a large panel of incidence angles. A 90° phase shift of the electric field is observed at grazing incidence ($\Phi = 80 - 88^\circ$) resulting in an enhancement of the p-polarized component but only in a direction normal to the surface.¹¹⁴

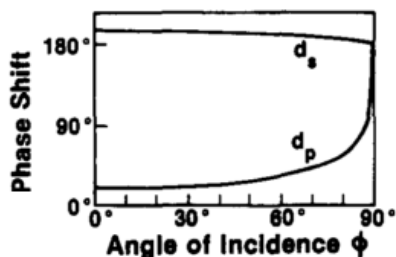


Figure 2.9 Reflection of IR light at a clean metal surface: Phase shifts d_s and d_p versus angle of incidence Φ . Figure reproduced from Hoffman¹¹⁴

Finally, the two **surface selection rules** of IRRAS measurements are stated as follows:

For metal surfaces, only the component of the electromagnetic vector normal to the surface is effective in exciting dipole-active vibrations.¹¹²

The experiment is only effective for high angles of incidence from the normal to the surface ($\Phi=80-88^\circ$) and for a given polarization of the light.^{111,113}

After adsorption of molecules on metal surfaces, the IR light will interact with dipoles from the adsorbates and from the environment. The s-component of the reflectivity spectrum (R_s) will contain information on the absorption from the gaseous environment. The p-component of the reflectivity spectrum (R_p) records the absorption from both the volume and the surface. In regular IRRAS experiments, a reference spectrum without the adsorbate is first recorded. A second spectrum after adsorption is then acquired and normalized with the reference one. The main drawback in this technique is the mandatory recording of a reference spectrum to get rid of the working environment.

In PM-IRRAS we combine the IR reflectivity measurements with a rapid modulation of the polarization of the incident beam. In order to achieve this modulation between p (parallel to the plane of incidence) and s (normal to the plane) polarizations a photo-elastic modulator (PEM) is used. Both signals (R_p-R_s) and (R_p+R_s) are detected simultaneously and give a direct access to the normalized reflectivity signal:

$$\frac{\Delta R}{R} = \frac{(R_p - R_s)}{(R_p + R_s)}$$

Recording both signals in parallel allows the direct separation of polarized absorptions from the surface and from the environment. The acquisition of a separated reference spectrum is no longer necessary.

PM-IRRAS thus combines three different techniques:

IRRAS measurements characterized by the “surface selection rules”.

Rapid **modulation in polarization** of the incident electric field between p- or s-light.

Synchronic detection of signals avoiding to record reference spectrum.

2.3.2 Experimental Description

Figure 2.10 presents an experimental scheme showing the path of the IR beam during the experiment. Samples are placed in the external beam of the FT-IR instrument (Nicolet Nexus 5700 FT-IR spectrometer) and the reflected light is focused on a nitrogen cooled Mercury-Cadmium-Telluride (MCT) wide band detector. Infrared spectra are recorded at 8 cm^{-1} resolution, with co-addition of 128 scans. A ZnSe grid polarizer and a ZnSe photo-elastic modulator are placed prior to the sample to modulate the incident beam between p and s polarizations (HINDS Instruments, PEM90, modulation frequency = 36 kHz). The MCT detector and the PEM are coupled to a lock-in amplifier allowing the synchronic detection of both channels. The detector output is sent to a two-channel electronic device that generates the sum and difference interferograms. Those are processed and undergo Fourier transformation to produce the PM-IRRAS signal ($\Delta R/R$).

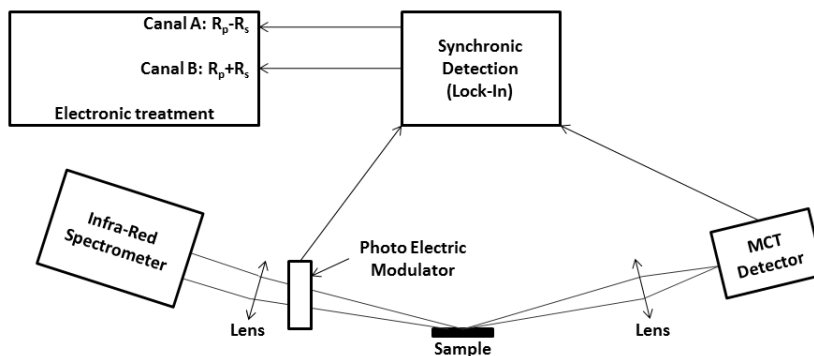


Figure 2.10 Schematic representation of the PM-IRRAS experiments

2.3.3 Analysis of PM-IRRAS Spectra

The PM-IRRAS signal is thus given by the differential reflectivity $\Delta R/R$. A typical absorption spectra obtained with this technique is presented on Figure 2.11. For chemical moieties with vibrational modes inducing a dipole moment change fulfilling the requirements described by the surface selection rules, absorption bands will be observed. These bands are attributed to different chemical functions using reference tables.¹¹⁵ Different regions of the electromagnetic spectra will be interesting for us. We will focus on the one around 2900 cm^{-1} that gives information on alkyl bonds and especially on the CH_2 or CH_3 asymmetric or symmetric stretchings. The second region of interest will be localized between 1900 and 1100 cm^{-1} and is characteristic of organic moieties. Such features as carboxylic acids or amine can be identified with information about their protonation state.

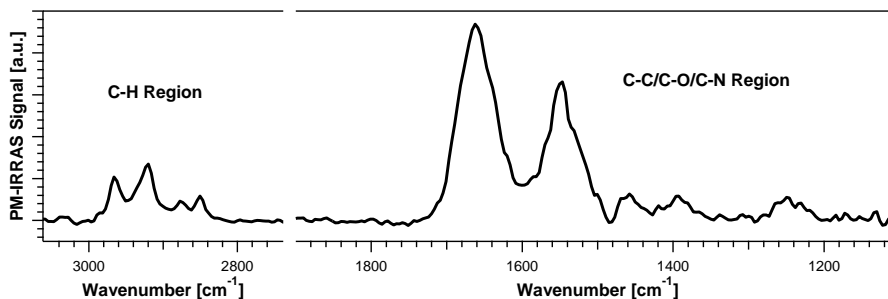


Figure 2.11 Typical PM-IRRAS spectra of a protein film on SAMs after correction of the baseline

In this study, PM-IRRAS is used first to characterize the integrity of thiol-SAMs on gold surfaces (see Chapter 3). To characterize protein adsorption the amide I and II bands are followed. The amide I band around 1660 cm^{-1} corresponds to the stretching of the C=O group in the amide bond. The amide II band at about 1550 cm^{-1} corresponds to the combination of the stretching of CN and the deformation of the NH moiety. The intensity of these bands will be proportional to the quantity of adsorbed proteins on the surface. Figure 2.12 below illustrate this principle. Practically, the area of amide I and II bands will be calculated and compared to estimate the quantity of proteins adsorbed in different cases. Such applications of protein studies have been reviewed by Tengvall *et al.* in the late 90's.²⁶ They presented different results from single protein adsorption or from complex solution such as plasma or serum. Moreover, decomposition of the Amide I band can lead to the identification of secondary structures in the adsorb proteins.^{115,116}

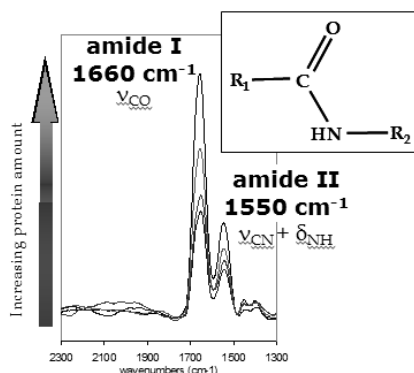


Figure 2.12 Protein films characterization in PM-IRRAS

2.4 QCM-D

2.4.1 Theoretical Background

Quartz crystal microbalance (QCM) is based on the piezoelectric properties of quartz crystals discovered in 1880 by the Curie brothers.¹¹⁷ When excited by a proper voltage, a quartz crystal starts to oscillate at its resonance frequency. As represented on Figure 2.13, AT-Cut of quartz crystal will resonate laterally in the thickness shear mode (TSM) when a voltage is applied. When an overlayer is deposited on the crystal, the resonance frequency will decrease: this change in frequency (Δf) is monitored in QCM. In 1959, Sauerbrey demonstrated the linear relation between the Δf and the change in adsorbed mass.¹¹⁸ By linking the calculated mass to the density of the deposited material, it is then possible to calculate the deposited film thickness in air or in vacuum.¹¹⁹ Another possible application is gas detection by coating the crystal with a specific sorbent. The Δf will in this case be related to the detection of certain gas in the environment (gas sensors).^{120,121}

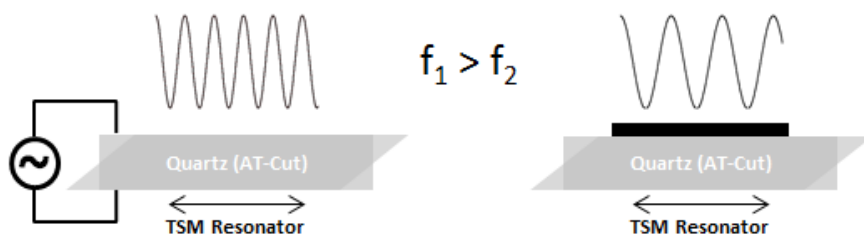


Figure 2.13 Modification of the resonance frequency in presence of an adlayer for a quartz crystal AT-cut acting as a thickness-shear-mode (TSM) resonator

Since first QCM measurements were performed in air or in vacuum, it was not possible to follow biomolecule adsorption. In the 80's, the first circuits capable of QCM measurements in liquid were introduced.¹²² This opened the way for bioanalytical applications. Moreover, QCM-D was introduced in the 90's by Kasemo *et al.*^{123,124} In this case the "D" stands for dissipation monitoring. By regularly switching off the excitation of the quartz, the exponential decay of the oscillation is recorded. The dissipation parameter D is defined as $D = 1/\pi f \tau$ where f is the resonance frequency and τ the decay time. D will give information about the density and viscoelasticity of the ad-layer since it can also be defined as a loss of energy in the system. Figure 2.14 illustrates those principles. When a soft ad-layer is added to a surface, two phenomena will occur:

A decrease of the resonance frequency ($\Delta f < 0$) of the quartz due to the added mass on the quartz.

An increase of the dissipation parameter ($\Delta D > 0$) due to a stronger attenuation of the oscillation of the quartz since more energy is dissipated in a softer adlayer.

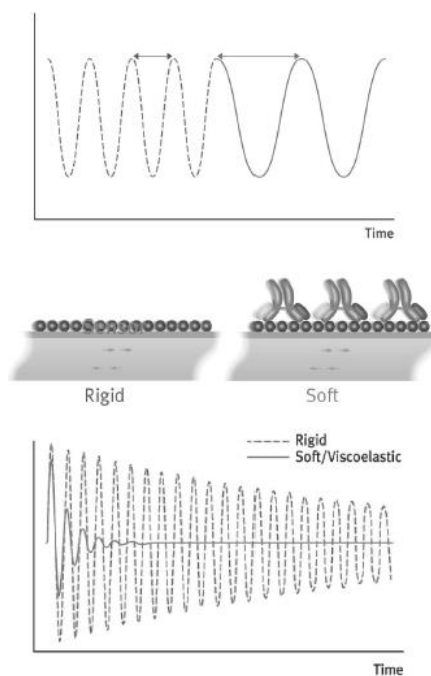


Figure 2.14 Illustration of parameters measured in QCM-D. Adsorption of soft over a rigid film will lead to a decrease of the resonance frequency (increase of the mass, top) and of the decay time (increase of the dissipation, bottom) [from www.qsense.com]

QCM-D allows sensing the mass uptake on a surface with a sensitivity of about 1 ng.cm^{-2} . In the Sauerbrey model,¹¹⁸ the adsorbed mass (Δm) is in linear relationship with the frequency shift (Δf):

$$\Delta m = -C_f \frac{\Delta f}{n}$$

Where n is the considered overtone and C_f is the mass sensitivity factor. In modern systems, the Δf is directly expressed in regard of the considered overtone. Differences in frequency will be then noted $\Delta f_n = \frac{\Delta f}{n}$ with $n = 1, 3, 5, \dots$ the overtone. The C_f factor depends only of the fundamental

frequency and of material properties of quartz. It is equal to $17.7 \text{ ng.cm}^{-2}.\text{Hz}^{-1}$ for $f = 5 \text{ MHz}$.

In the case of adsorption in the liquid phase, one should be careful in applying the Sauerbrey model. The linear relationship of the mass and the frequency shift is indeed dependent on the viscoelastic properties of the adlayer. In 2011, Reviakine et al.¹²⁵ explored the limit of several model for QCM-D data interpretation to determine in which cases they can be applied. Two main approaches are described with on one side the application of the Sauerbrey model and on the other side models taking into account the viscoelastic properties of the adlayer. It appears that either in the case of laterally homogeneous film or for monolayers of discrete particles, if the dissipation parameter is small ($\Delta D / \Delta f_n \ll 4 \cdot 10^{-7}$) and if there is a low dispersion in the Δf_n measurements for different overtone, one can reasonably apply the Sauerbrey model. Otherwise, more complicated models including the dissipation must be used for data interpretation.¹²⁶

In any case, one should remember that the absolute mass calculated from QCM-D measurements takes into account molecules deposited on the surface but also the water (or solvent) trapped into the layer.^{127,128} It has been reported in the literature depending of the nature of adsorbed molecules, the mass uptake calculated from QCM-D can be over-estimated by a factor of 1.5 to 4. One should be particularly careful in comparing the values derived from QCM-D measurements with the adsorbed molar mass

derived with other techniques. However, QCM-D can still provide relative information about adsorption on different surfaces.

2.4.2 Experimental Description

The QCM-D systems in use in this thesis were developed by Q-Sense (Gothenburg, Sweden). Two separate apparatus are used: the E1 (in UPMC) or E4 system (in UCL) with respectively one or four cells in parallel. The advantage of the E4 system is to measure simultaneously 4 samples. Measurements are performed under a controlled temperature of 20.0 ± 0.1 °C. The crystals used are thin AT-cut gold-coated quartz with a nominal resonance frequency f of 5 MHz (Lot-Oriel, France). Functionalized gold crystals are placed in a flow cell allowing the measurement of the frequency and dissipation shifts when flowing a biomolecule solution (Figure 2.15).



Figure 2.15 Flow cell from the Q-Sense system presented with an AT-Cut quartz crystal coated with gold

Solutions are injected into the measurement cells using a peristaltic pump (Ismatec IPC-N4) at a flow rate of $50 \mu\text{L}\cdot\text{min}^{-1}$. Oscillations of the crystal at the resonance frequency (5 MHz) or at one of its overtones (15, 25, 35, 45, 55, and 65 MHz) are obtained when applying AC voltage. The variation in resonance frequency (Δf) or in dissipation (ΔD) are monitored throughout the all experiment for all overtones.

2.4.3 Protein Films Characterization

As described earlier, QCM-D allows retrieving information about adlayers in the liquid phase. During this work, it was mainly used to characterize protein adsorption on several SAMs. In a second part, QCM-D was used as a tool to probe the biorecognition efficiency of antibodies adsorb on different surfaces. For all experiments, low dissipation measurements ($< 3 \cdot 10^{-6}$) and a ratio $\Delta D/\Delta f < 4 \cdot 10^{-7}$ are observed. As mentioned earlier, in these conditions the Sauerbrey model can reasonably be applied and the adsorbed layer is considered as rigid.^{51,125} Frequency shifts in QCM-D measurements are then directly interpreted as protein mass uptakes upon adsorption on the different system considered. Moreover we will be interested in comparing the QCM-D results with those obtained in XPS or PM-IRRAS. This will help in understanding the influence of the liquid phase on adsorption measurements. The applications of QCM-D as a tool for characterizing protein or biomolecules adsorption are reviewed in the following references.^{34,129}

3 Chemical Modification of Gold Surfaces Using SAMs

The first step of the chemical control of the gold surfaces is the formation of self-assembled monolayers (SAMs). SAMs of thiolates on gold have been well studied in the past few decades^{18,19,130} and they constitute adequate substrates for controlled protein adsorption due to the tunability of their chemical properties.^{20–22,39,131} During this work, three different alkyl thiols, differing by their end-group ($-\text{COOH}$, $-\text{CH}_3$ and $-\text{NH}_2$), were used to build up self-assembled monolayers (SAMs) on gold substrates and subsequently adsorb proteins. Moreover, the $-\text{COOH}$ -terminated SAMs could be activated using N-Hydroxysuccinimide (NHS) and 1-Ethyl-3-(3-dimethylaminopropyl)carbodiimide (EDC) to enable a covalent grafting of proteins. The first part of this chapter is dedicated to the study of thiolate SAMs on gold using conventional techniques such as XPS or PM-IRRAS while the second part is focused on the advantages of using new large Ar_n^+ clusters as primary ions in ToF-SIMS to study such systems.

3.1 Characterization of SAMs with Conventional Methods

3.1.1 SAMs Formation

Gold surfaces are obtained by metallization of 3 inches silicon wafers with a 5 nm chromium or titanium layer (to enhance gold adhesion on the wafer) and 100 nm of gold on top. Before functionalization, wafers are cut in 1 cm² samples, cleaned using UV/O₃ treatment for 15 min, and thorough absolute ethanol rinsing before drying with N₂.

Chemical control of the gold surfaces was obtained by forming self-assembled monolayers (SAMs) of the following alkyl thiols, HS-(CH₂)₁₀-R with R = COOH (11-Mercaptoundecanoic Acid, 95 %, 450561, Sigma-Aldrich), CH₂-NH₂ (11-Amino-1-undecanethiol hydrochloride, 99 %, 674397, Sigma-Aldrich) or CH₃ (1-Undecanethiol, 98 %, 510467, Sigma-Aldrich). Thiols were chosen with a length of eleven carbons to favor interactions between alkyl chains ensuring a better organization of the SAM.^{18,19} Moreover, 11-carbon thiols molecule are available with several endgroups (-CH₃, -NH₂, -COOH, -OH...) that ensure different chemical properties of the SAM surfaces. As previously described in the literature,^{20,130} gold samples were immersed in 10 mL of 1 mM thiol solutions in absolute ethanol for 24 h under gentle agitation on an agitation table at room temperature. The thiol solution is then replaced with 10 mL of ethanol for 10 min two times in a row and dried under N₂ to form the SAMs. Samples were then characterized using PM-IRRAS and XPS. These conditions were kept identical during all the work in the two different labs.

To perform a chemical attachment (grafting) of proteins, the –COOH layer was activated with a mixture of NHS (130672, Sigma-Aldrich) and EDC (E6383, Sigma-Aldrich) in 10 mL of MilliQ water at respectively 60 and 30 mM for 90 min at room temperature under gentle agitation on an agitation table.¹³² Samples were then rinsed two times for 10 min in 10 mL of MilliQ water and dried under N₂. The activation will be followed in ToF-SIMS and PM-IRRAS.

3.1.2 PM-IRRAS

Due to the principle of PM-IRRAS, detailed in the previous chapter, this technique is particularly suitable for SAMs characterization. In this infra-red setup, no signal from trapped water or from the environment is recorded allowing the characterization of chemical functions at the solid-air interface. Results obtained for each type of SAMs in use during this work are presented in Figure 3.1. The two regions of interest around 2900 cm⁻¹ and 1500 cm⁻¹ are studied.

Bands at 2925 and 2850 cm⁻¹ are attributed to the asymmetric and symmetric stretches of CH₂ in the alkyl chain ($\nu_{CH_2}^{as}$ and $\nu_{CH_2}^s$) respectively. The small band at 1455 cm⁻¹ can be attributed to the scissoring mode of CH₂ in the alkyl chains. These bands are observed for all types of SAMs and their positions suggest the formation of SAMs. Moreover, it is indicated in the literature that the band around 2925 and 2850 cm⁻¹ will slightly change in position regarding the crystallinity of the SAM structure.^{133,134} Their positions are shown to shift from 2924 to 2918 cm⁻¹ (and 2855 to 2851 cm⁻¹ respectively) when going from a “liquid-like” structure of the alkyl chains in

the SAM to a crystalline one. Looking carefully at Figure 3.1, one can see bands are in a slightly lower position for the $-\text{CH}_3$ surface indicating a better organization of this SAM.

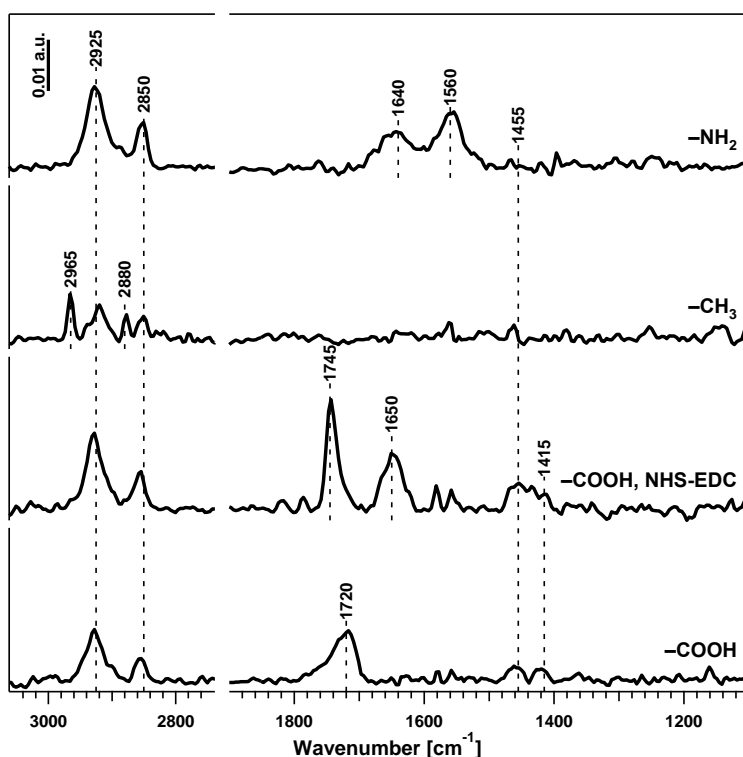


Figure 3.1 PM-IRRAS characterization of SAMs terminated with different groups: $-\text{COOH}$, activated $-\text{COOH}$, $-\text{CH}_3$ or $-\text{NH}_2$

We now want to characterize the chemical state of the terminal end-group. The $-\text{COOH}$ -terminated SAM is characterized by bands at 1720 and 1415 cm^{-1} , attributed to the stretching vibration of $\text{C}=\text{O}$ in COOH and to the symmetric stretching of COO^- ($\nu_{\text{COOH}}^{\text{C}=\text{O}}$ or $\nu_{\text{COO}^-}^{\text{S}}$) respectively. The strong band at 1720 cm^{-1} and weaker one at 1415 cm^{-1} are strong indications that most acidic groups are in the protonated form, coexisting with carboxylates

in lower quantity. As for the $-\text{CH}_3$ terminated surface, bands are observed at 2965 and 2880 cm^{-1} . They correspond to the asymmetric and symmetric stretches in CH_3 ($\nu_{\text{CH}_3}^{\text{as}}$ and $\nu_{\text{CH}_3}^{\text{s}}$) respectively. Finally, $-\text{NH}_2$ -terminated surfaces show principally two large bands at 1640 and 1560 cm^{-1} . The first one at about 1640 cm^{-1} includes stretching vibration of NH in an unprotonated amine (NH_2) in addition to the asymmetric deformation vibration in a protonated one (NH_3^+). The band at 1560 cm^{-1} corresponds to the symmetric deformation vibration of NH in NH_3^+ .¹³² The comparatively stronger band at 1560 cm^{-1} and the contribution of the NH_3^+ moiety in the one at 1640 cm^{-1} indicate that the amines are predominantly protonated after formation of the SAMs.

3.1.3 XPS

On the XPS survey spectra (not shown), peaks corresponding to C, O, N, S and Au are observed. The atomic % derived from the C 1s, O 1s, N 1s, S 2p and Au 4f peak areas are presented in Table 3.1. Table 3.2 shows the SAM composition excluding the gold signal together with the theoretical value calculated for each thiol molecule. Presented values correspond to three measurements on three separate samples prepared at three different occasions for each SAM. In Figure 3.2, one example of high resolution XPS spectra in the C 1s, O 1s, N 1s and S 2p regions is presented before or after formation of each thiol SAM.

First, the attenuation of the gold signal was followed to ensure the formation of the SAMs. In Table 3.1, the percentages of gold in the different SAMs are: 47.7% for the $-\text{COOH}$ SAMs, 57.9% for the $-\text{CH}_3$ and 35.8% for

the $-\text{NH}_2$ ones. Those values are in reasonable agreement with what was found in the literature. For thiols with the same chain lengths as the ones used in the present study, Apte *et al.*¹³⁵ report values of 51.5% of gold for the $-\text{CH}_3$ - and 44.4% for the $-\text{COOH}$ -terminated SAMs. In another paper, Baio *et al.*⁶⁰ report values of 36.9% of gold for the $-\text{NH}_2$ SAMs and 43.7% for the $-\text{COOH}$ ones. It is also observed that all layers include a fraction of thiols not bound to gold (S_{Free} component on S 2p peaks), with the higher amount of “weakly” bound thiols observed on the $-\text{NH}_2$ -terminated SAM. This feature will be further discussed after characterization of the endgroups on each surface. To assess the protonation states and the good formation of the SAMs, detailed regions of the C 1s, O 1s, N 1s and S 2p peaks were then studied.

On the $-\text{COOH}$ terminated surface, $\underline{\text{C}}\text{OO}^-$ of carboxylates (at 287.7 eV) and $(\underline{\text{C}}=\text{O})\text{-OH}$ components (at 289.1 eV) appear in the C 1s spectrum, with a large excess of the latter (3.2% vs 0.8%), indicating that carboxylic acid functions are predominantly in the protonated form (see Table 3.1). Moreover, on the O 1s peaks (see Figure 3.2 and Table 3.1), two components are observed corresponding to oxygen simply or doubly bond to carbon (at higher or lower binding energies respectively). This also indicates that carboxylic acids are found in both protonated or deprotonated forms. Table 3.2 indicates that the atomic percentages for the organic part are in good agreement with the theoretical composition of the $-\text{COOH}$ thiol molecule. Nevertheless, the carbon percentage is higher than expected due to adventitious carbon contamination often observed in XPS.

Table 3.1 Atomic % of C 1s, O 1s, N 1s, S 2p and Au 4f peaks as assigned on a blank gold sample or on the different thiol SAMs

	(eV)	C 1s				O 1s				N 1s			S 2p			Au 4f
		C-(C,H)	C-(O,N)	$\begin{matrix} \text{C} \\ \text{COO}^- \\ \text{C=O} \end{matrix}$	C(O)-OH	C _{tot}	C=O	C-OH	O _{tot}	$\begin{matrix} \text{NH} \\ \text{NH}_2 \end{matrix}$	NH_3^+	N _{tot}	S-Au	S _{free}	S _{tot}	
Blank		284.8	286.3	287.7	289.1		532.2	533.3								
	+/-	20.5	2.9	1.3	0.9	25.7	2.3	0.7	3.0	-	-	1.0	-	-	1.3	69.0
-COOH	(eV)	284.8	286.3	287.7	289.1		532.2	533.5					162.3	163.8		
	+/-	37.3	3.1	0.8	3.2	44.5	3.2	2.3	5.5	-	-	0.4	1.2	0.5	1.8	47.7
-CH ₃	(eV)	284.8	286.3										162.6	163.8		
	+/-	38.8	1.0	-	-	39.8	-	-	0.1	-	-	0.1	1.7	0.5	2.2	57.9
-NH ₂	(eV)	284.8	286.3	288.1			531.2	532.8		399.3	401.3		162.0	163.7		
	+/-	45.7	5.3	1.6	-	52.5	5.2	1.3	6.5	1.3	1.8	3.2	1.2	0.9	2.0	35.8
						1.9	1.9	0.3	1.6	0.6	0.8	0.2	0.1	0.2	0.2	1.3

Table 3.2 XPS determined composition of all three SAMs. Results are presented excluding the gold with C, O, N and S signals renormalized to 100 at%.

Theoretical values are presented in italic font for all thiols.

	C 1s	O 1s	N 1s	S 2p
-COOH	85.1 ± 1.1	10.6 ± 1.8	0.8 ± 0.7	3.5 ± 0.1
	<i>78.6</i>	<i>14.3</i>	-	<i>7.1</i>
-CH ₃	94.3 ± 0.6	0.3 ± 0.5	0.1 ± 0.2	5.2 ± 0.1
	<i>91.7</i>	-	-	<i>8.3</i>
-NH ₂	81.9 ± 1.9	10.1 ± 2.4	4.9 ± 0.4	3.9 ± 0.2
	<i>84.6</i>	-	<i>7.7</i>	<i>7.7</i>

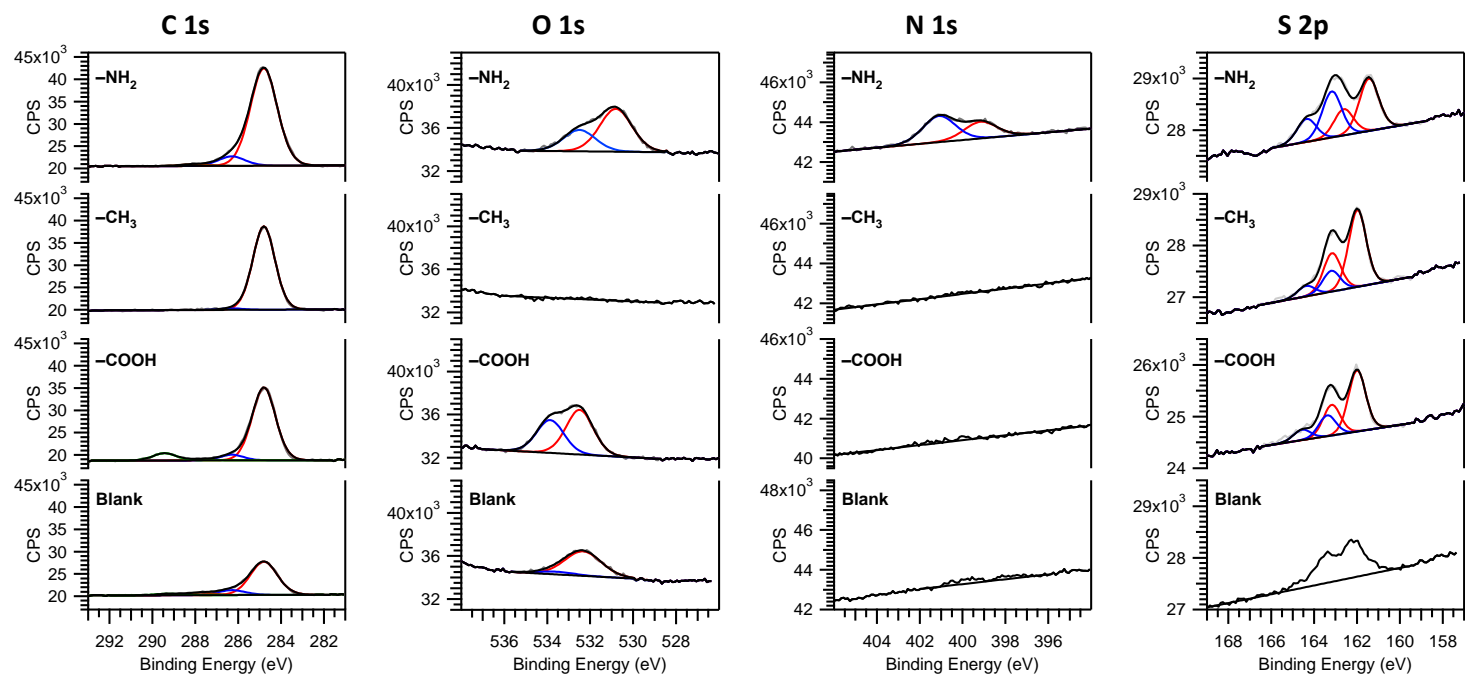


Figure 3.2 XPS Spectrum for the C 1s, O 1s, N 1s and S 2p peaks before or after the formation of each different thiol SAMs

On the $-\text{CH}_3$ terminated surface, the $\underline{\text{C}}$ -(C,H) component is, as expected, predominant, corresponding to the CH_2 function in the alkyl chain and the $-\text{CH}_3$ termination of the thiol. In this case, the observed and theoretical compositions of the organic part are really close (Table 3.2) which is again an indication of the high degree of organization of the $-\text{CH}_3$ SAM. This SAM is most likely less contaminated than the others with a good crystallinity of the alkyl chains (see PM-IRRAS results).

For the $-\text{NH}_2$ -terminated surface the N 1s peak displays a small component at low energy, 399.3 eV ($\underline{\text{N}}/\underline{\text{NH}_2}$), and a dominating one at higher binding energy, 401.3 eV, showing the coexistence of neutral and protonated amines, as already observed on the PM-IRRAS spectrum where the protonated form was also predominant. In Table 3.2, the oxygen contamination observed for this SAM influence the results. Nitrogen and sulfur percentage are however in the same range and in a good ratio compare to carbon and to the theoretical composition of the thiol.

On the $-\text{NH}_2$ terminated SAMs, an unexpected amount of 6.5 atomic % of oxygen is detected. This was already observed in previous studies reporting values between 5 and 8 atomic % of oxygen for such SAMs.^{76,136,137} Two main hypothesis have been proposed: either the SAM is covered with other oxygen containing species or the layer is oxidizing over time. In a study by Baio et al.,¹⁰⁸ it was demonstrated that the first hypothesis is the most probable of both. The study pointed out to a reasonably ordered surface with low indications of oxidation. Using a combination of XPS, ToF-SIMS,

NEXAFS and SFG, they propose that oxygen is coming from water molecule tightly bound to the amine groups.

In our case, we want to establish a correlation between carbon and oxygen amounts in our decomposition to determine the most likely contamination. Carbon simply bonded to oxygen or nitrogen ($\underline{\text{C}}\text{-(N,O)}$ at 286.3 eV) represents 5.3 at%. We have to remove the contribution from nitrogen (3.2 at%); that gives 2.1 at% of carbon simply bond to 1 atom of oxygen. We must now add the component at 288.1 eV (1.6 at%) that is either coming from a carbon bonded to 1 (double bond) or 2 (carboxylates) oxygen atoms and will thus count as 1.6 or 3.2 at% for the oxygen signal. Based on carbon decomposition, oxygen should then represent between 3.7 and 5.3 at% (2.1 + 1.6 or 3.2 at%) in the total composition. The total oxygen amount is measured at 6.5 at%. It is slightly higher than what is calculated but still indicates a most likely contamination with oxidized organic compounds. The remaining 1.2 at% could be explained by the presence of sulfates on the layer. In the case of SO_4 molecules on the surface, we would have 1 sulfur atom for 4 oxygen ones resulting in a sulfur component 4 times lower (about 0.3 at%). Looking carefully at Figure 3.2, one can observe a small component around 168 eV that could correspond to these sulfates. The large variation of the oxygen component at lower energy (5.2 ± 1.9 at%) could come from a variable amount of sulfates in the different samples.

We will now discuss the amount of unbound thiols on all surfaces. In the case of $-\text{COOH}$ and $-\text{CH}_3$ surfaces, the amounts are relatively low and are mainly explained by, respectively: hydrogen bonding of free thiols with

bounded ones or by hydrophobic interactions. In the case of the $-\text{NH}_2$ surfaces, in addition to hydrogen bonding of free thiols, the relatively larger amount of free sulfur atoms detected could also be explained by the direct interaction of amine moieties with the gold surfaces (thiols bounded upside down) resulting in thiols moieties exposed on the surface. As shown earlier, the presence of oxidized contaminant in this layer could also disturb the SAM structure and retain more free thiols at the surface.

Despite the rinsing procedure, all surfaces still present unbound thiols after formation of the SAMs. However, in our conditions, the surfaces showed mostly the presence of protonated amine groups for the $-\text{NH}_2$ -terminated SAM and of a mixture of unprotonated and protonated carboxylic acid groups for the $-\text{COOH}$ -terminated surface. In order to check the hydrophilic properties of the SAM, contact angle measurements were performed. The contact angle is the angle formed by the liquid/vapor interphase when a liquid is in contact with a solid. In our setup we used the static sessile drop method to measure the contact angle. Since we wanted to probe hydrophobicity/hydrophilicity of the SAM, measurements were performed using water droplets on the functionalized surfaces. A low contact angle will characterize a hydrophilic surface while a high value is characteristic of a hydrophobic one. Measurements were performed with 0.3 μL water drops 5 s after deposition. A total of eight points is measured for each surface: four drops on two separated samples prepared in the same conditions.

Contact angle measurements are presented in Table 3.3, they showed that a likely hydrophobic surface is obtained using the $-\text{CH}_3$ -terminated thiols

(angle $> 90^\circ$) and two hydrophilic surfaces are obtained with one being negatively charged ($-\text{COOH}$ SAMs) and one positively charged ($-\text{NH}_2$ SAMs). For the $-\text{NH}_2$ surface the contact angle of 61.1° indicates the formation of an hydrophilic layer but the angle is still higher than on the $-\text{COOH}$ surface. This is in good agreement with the observation of a higher S_{Free} component in XPS measurements. A larger amount of unbound thiol molecules interact with the surface in that case resulting in an increase of the contact angle due to free alkyl chains on the surface together with the previously evidenced organic contamination. All three surfaces were used as a platform for protein adsorption without further modifications or after activation of the carboxylic acid SAMs to promote covalent grafting of proteins.

Table 3.3 Contact angle measurements using water droplets after formation of the three different SAMs

SAM	Contact Angles
$-\text{COOH}$	$24.4 \pm 1.2^\circ$
$-\text{NH}_2$	$61.1 \pm 0.8^\circ$
$-\text{CH}_3$	$100.7 \pm 1.3^\circ$

3.1.4 Activation of the $-\text{COOH}$ -terminated SAMs

The process of activation and covalent linking of proteins is described in Figure 3.3. The EDC molecule will first interact with the carboxylic acids at the surface of the SAM to form a non-stable o-acylisourea active ester. In a first reaction path, this product couples the NHS molecule to the carboxyl forming a more stable activated group that can react with primary amines in proteins. In a second reaction path, the remaining grafted EDC molecules that did not react with NHS can directly form an amide bond with primary amine.¹³⁸ Activation of the $-\text{COOH}$ SAMs is monitored first by PM-IRRAS

(see Figure 3.1). The main band characteristic of the activation is the one at 1745 cm^{-1} corresponding to the vibration of the C=O moiety in the ester function formed by the grafting of NHS. This band is characteristic of the covalent grafting of NHS. Another characteristic feature comes from the vibration of the two C=O groups in the succinimide moiety of NHS at 1650 cm^{-1} .

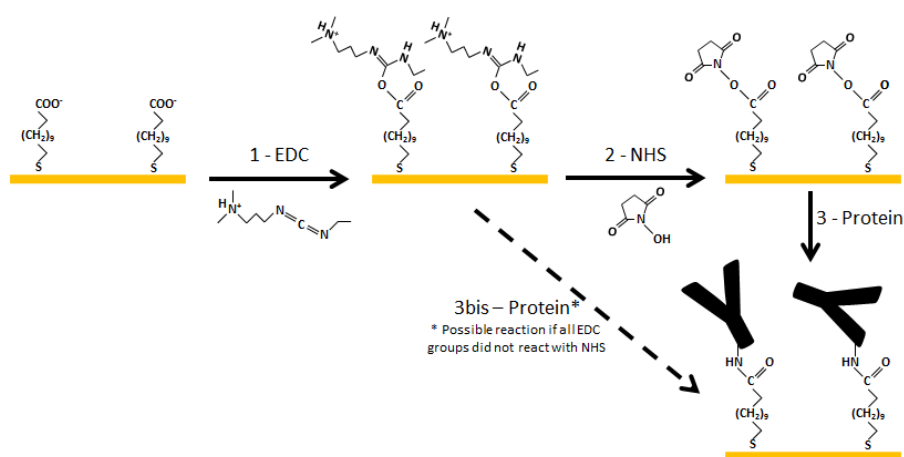


Figure 3.3 Grafting of the Antibody on the –COOH-terminated SAMs using the NHS-EDC activation

In ToF-SIMS, the main characteristics of the grafting of NHS on the –COOH-terminated SAMs are evidenced in the negative mode. It was shown in the literature¹³⁹ that the activation could be followed by the CN^- , the $\text{C}_4\text{H}_4\text{NO}_2^-$ and the $\text{C}_4\text{H}_4\text{NO}_3^-$ peaks. On Figure 3.4, these three peaks are evidenced after the activation (green curves) of the bare –COOH SAMs (red curves) showing the successful grafting of NHS. The two last peaks correspond to a fragmentation of the ester moiety (between carboxylic acids and the NHS molecules) before or after the oxygen atom bounded to nitrogen in the succinimide function (see Figure 3.3).

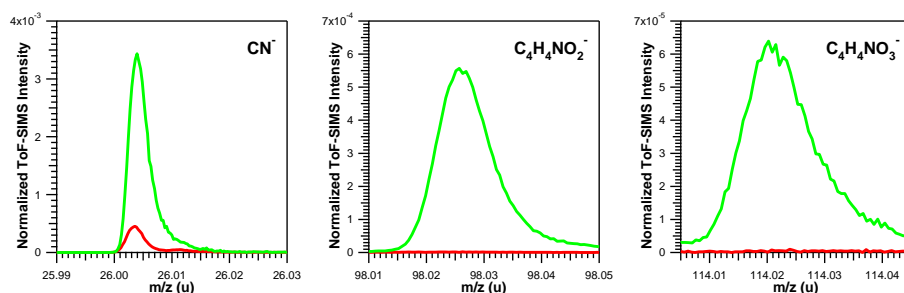


Figure 3.4 Peaks of the covalent binding of NHS group to the $-\text{COOH}$ SAMs followed before (red) or after activation (green)

3.2 SAMs Characterization in ToF-SIMS Using Ar_n^+ Clusters Ions

As shown before, SAMs are model organic thin films that can be easily obtained and used as substrate for bio-molecules adsorption. Seminal studies in our group were performed by Arezki *et al.*^{140–143} either theoretically with molecular dynamic simulations or experimentally with ToF-SIMS measurements of alkanethiol SAMs using conventional Ga^+ source. The aim of this study was to find ways to improve the detection of SAMs in ToF-SIMS. By using the newly introduced Ar_n^+ clusters source with a tunable cluster size and energy, the effect on fragmentation and of the energy per atom in clusters is studied. This paragraph focuses on results obtained for $-\text{CH}_3$ -terminated SAMs.

3.2.1 Analysis Parameters

Both ion polarities were measured but only negative spectra are presented. As it was shown in the literature most of the molecular information corresponding to SAMs formation is described in this mode when

adsorption is performed on gold.^{140,141} As mentioned earlier, the IonToF gas cluster ion beam (GCIB) allows tuning the energy of the clusters from 2.5 to 20 keV and the size of the clusters from about 500 to 10000 atoms. Modifying one or both of these parameters will influence the energy per atom in the cluster. Parameters used in this study are summed-up in Table 3.4. Due to the design and principles of the GCIB (Wien magnetic filter and 90° deflection unit for mass selection and pulsing of the beam), current of the beam in the analysis mode was very low (about 0.05 pA). It was then difficult to calculate the yield for specific ions in the mass spectra; results were thus normalized on the total counts for each spectrum. Results presented here correspond to the mean of 12 spectra (2 series x 3 samples x 2 spectra per sample).

Table 3.4 Analysis parameters used for Ar_n⁺ clusters

Cluster Energy		10 keV			
Cluster Size (n)	700	1500	3000	5000	
E per Atom (eV)	14.3	6.7	3.3	2	
Cluster Energy		20 keV			
Cluster Size (n)	700	1500	3000	5000	
E per Atom (eV)	28.6	13.3	6.7	4	

3.2.2 Low Masses Fragments

In Figure 3.5 are presented the characteristic mass spectra obtained with different primary ion sources between m/z 0 and 300 for the -CH₃-terminated SAMs. If Bi⁺ or Bi₃⁺ are used as primary ions source, no differences are observed in mass spectrum. This is in good agreement with studies by Tuccito *et al.* in 2008 that demonstrate no interest in the use of polyatomic beams in SAM study.⁹⁵ In both cases, low mass fragment peaks are dominant. They correspond to CH⁻, C₂H⁻ and SH⁻ at m/z = 13, 25 and 33.

Chapter 3

These peaks have been evidenced in previous studies^{140,141} and they correspond to the fragmentation of thiols molecules under keV bombardment. The mechanism behind the ejection of such fragments is not fully understood but it is proposed that they results from momentum transfer during the collision cascade. In addition the peak corresponding to the substrate (Au^- at $m/z = 197$) is clearly observed when using Bi_n^+ sources. Finally, the molecular thiols peaks ($[\text{M}-3\text{H}]^-$, $[\text{M}-\text{H}] + \text{S}^-$ and $[\text{M}-\text{H}] + \text{CH}_4\text{S}^-$, with M the complete thiol molecule, and at m/z 185, 219 and 235) are observed but remains low compared to fragment ones.

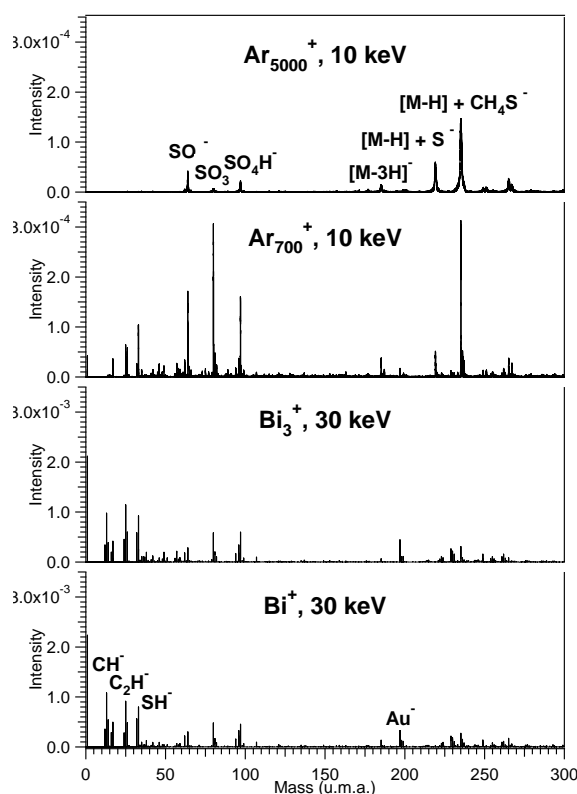


Figure 3.5 Effect of primary ion Argon clusters on fragmentation at low masses compare to Bi^+ or Bi_3^+ for the study of $-\text{CH}_3$ -terminated thiol SAM

When using Ar_n^+ clusters as primary source, ions characteristics of the unfragmented thiol molecules are dominant on the mass spectra over the fragment ones especially in the case of very low energy per atom; Ar_{5000}^+ at 10 keV represents 2 eV per atom in the cluster. At masses $m/z = 64, 80$ and 97 the sulfate ions ($SO_x(H)^-$) are largely represented on Ar_n^+ spectrum. This corresponds to an enhancement of the yield for these ions even if the quantity on the surface is very low as observed in XPS measurements (oxygen amount lower than 0.5% on the $-CH_3$ surfaces, see Table 3.1). This is explained by a good ionization probability of these species in the negative mode. Moreover, sulfates are a contamination that is not covalently bonded to the surface; they will thus be easily sputtered when the argon clusters interact with the surface.

In Figure 3.6, the evolution of the normalized intensity of CH^- , C_2H^- , SH^- and Au^- peaks have been represented in function of the energy per atom. This shows that fragmentation of thiols molecules upon emission under Ar_n^+ bombardment is mainly governed by the energy per atom in the clusters. The general trend is that molecules remain intact during emission (less CH^- , C_2H^- and SH^- fragments) and that the substrate is less perturbed (less Au^- fragments) with low energy per atom clusters. In addition, $[M-3H]^-$, $[M-H]^- + S^-$ and $[M-H]^- + CH_4S^-$ thiols molecular clusters are dominant on the spectrum. Molecular dynamics theoretical studies by Rzeznik *et al.*¹⁴⁴ showed similar processes under large and low energy Argon clusters sputtering of polystyrene molecules adsorbed on metal surfaces. On Figure 3.6, curve corresponding to different size and energies of the primary clusters (see Table 3.4) are overlapping. It is shown here that the influence

Chapter 3

of the cluster size and of the total energy in the cluster on the sputtering process is low. The main parameter in the sputtering process is thus the energy per atom in the primary clusters.

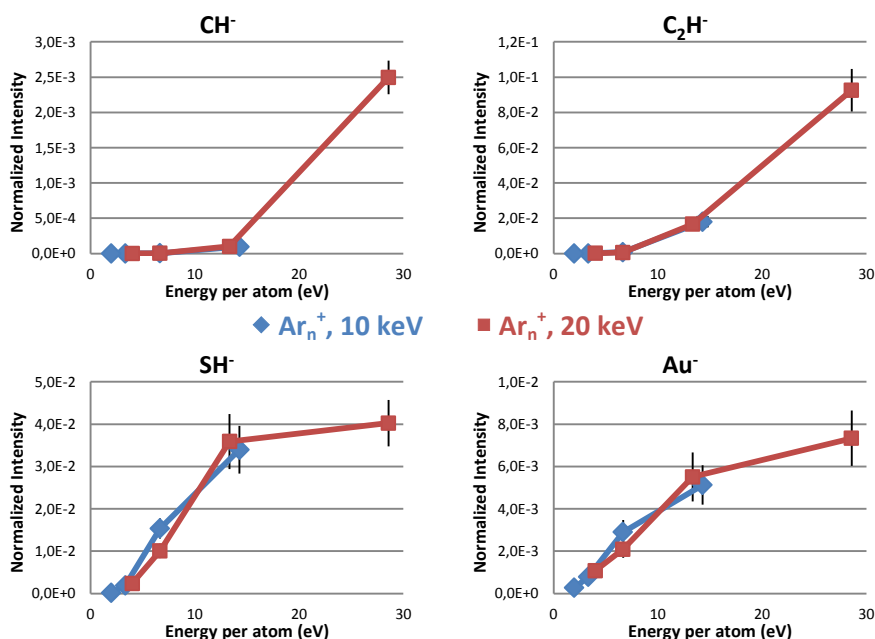


Figure 3.6 Intensity of characteristic fragmentation peaks normalized over the Total Counts and function of the energy per atom in Ar_n^+ clusters. Results are presented for a $-CH_3$ -terminated SAM surface.

On Figure 3.6, two different trends are observed for fragments intensities. The first trend, observed for CH^- and C_2H^- peaks, is characterized by a very low emission under 15 eV of energy per atom and a higher yield when the energy is over this threshold. The second trend is observed for SH^- and Au^- peaks and corresponds to a more linear increase of the emission with increasing energy per atom in the clusters. This could be explained by the fact that a certain amount of energy is needed to break the alkyl chain and form CH^- and C_2H^- fragments during the collision cascade. In the case of SH^- ,

the similar behavior as for the substrate peak Au⁻ indicate that the covalent link between thiols and the substrate influence the sputtering of sulfur. Since sulfur atoms are buried in the SAM, they behave as the substrate itself while the alkyl chain acts as an overlayer. The sputtering of substrate species is difficult to explain and we would gain more understanding by performing molecular dynamic simulations. Unfortunately, such simulations are very time consuming and we could not hold them in the timeframe of this project.

3.2.3 [M-H]_xAu_{x-1}⁻ Molecular Clusters

In studies by Arezki *et al.*,¹⁴¹ gold-thiolate clusters described as [M-H]_xAu_{x-1}⁻ (with M the complete thiol molecule) were identified as characteristic of SAM formation on gold surfaces. In Figure 3.7, the intensity of these gold-thiolate clusters for x = 2, 3 and 4 in function of their mass and of the energy per atom in the analysis argon cluster beam is represented. The energy per atom is, again, the relevant parameter in comparison with the size or the energy of the analysis cluster (same relative intensities measured at 10 or 20 keV). Conversely to peaks corresponding to fragmentation or to the substrate, a large increase of the gold-thiolate clusters intensity is observed with low energy per atom argon clusters. In addition, one can see that the probability of emission decreases with the gold-thiolate cluster size (when x increase) in agreement with the SIMS emission process.

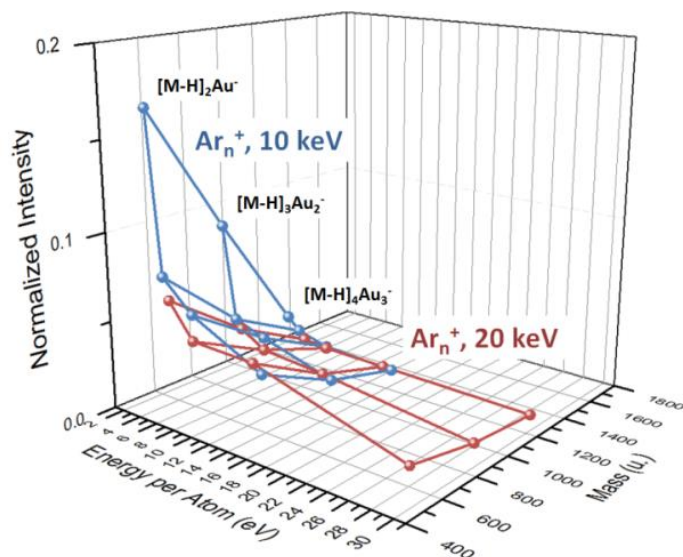


Figure 3.7 Intensity of the $[M-H]_xAu_{x-1}^-$ thiol clusters for a $-CH_3$ -terminated SAM in function of their mass and of the energy per atom in the Ar_n^+ analyzing cluster beam

Results presented above correspond to the study of the $-CH_3$ -terminated SAM, but the same studies with Ar_n^+ clusters have been conducted on both $-COOH$ - and $-NH_2$ -terminated surfaces. On Figure 3.8 the intensities of the $[M-H]_xAu_{x-1}^-$ gold-thiolate clusters are presented in the case of the $-COOH$ and $-NH_2$ SAMs. For the acid-terminated layer, the gold-thiolate clusters intensities regarding the energy per atom in the primary Ar_n^+ clusters follow the same trend as for the $-CH_3$ -terminated SAM. However, the normalized intensities are lower in this case indicating a probably lower ionization probability of the gold-thiolate structures with the thiols bearing $-COOH$ endgroups in the negative polarity.

In the case of the amine-terminated layer, one can observe that no clear trends in the intensities of the gold-thiolate clusters can be determined. Two explanations are proposed:

As already observed by XPS studies, the -NH_2 SAM tend to have a less organized structure with contamination. This could disturb the formation of the gold-thiolate clusters upon sputtering and therefore influence the detection of such clusters.

In addition, the -NH_2 thiol could be less favorable for the ionization of the gold-thiolate clusters in the negative polarity. That would lead to poor detection using the Ar_n^+ clusters. Unfortunately, based on previous studies¹⁴¹ and time constraint, the positive polarity was not measured during this study.

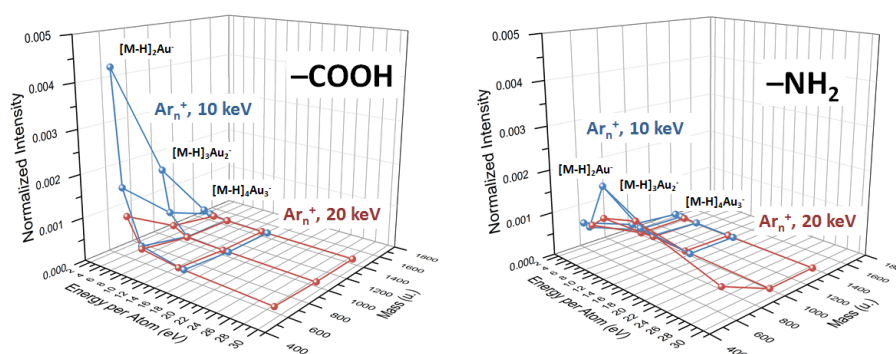


Figure 3.8 Intensity of the $[\text{M-H}]_x\text{Au}_{x-1}$ thiol clusters for the -COOH- and -NH_2 -terminated SAM in function of their mass and of the energy per atom in the Ar_n^+ analyzing cluster beam

3.3 Conclusion

It was shown in this chapter that chemical control of gold surfaces has been achieved using SAMs. After characterization using PM-IRRAS, XPS andToF-SIMS it was shown that four different type of surface are obtained:

One **hydrophobic** surface terminated by -CH_3 moieties.

Two **hydrophilic** surfaces **positively** ($-\text{NH}_2$) or **negatively** ($-\text{COOH}$) charged.

One **activated** surface with NHS-EDC expected to allow the **covalent grafting** of proteins.

These surfaces will be used as templates for protein adsorption in the rest of this work. The orientation and/or conformation of the adsorbed biomolecules will be probed to test the influence of the physico-chemical properties of the surface.

The second part of this chapter demonstrated that the use of Ar_n^+ clusters as primary source in ToF-SIMS improve greatly the study of SAMs compare to the use of conventional Bi_n^+ sources. The fragmentation at low masses becomes very low when using the clusters and molecular signals coming from the SAMs are dominant. It was also shown that the detection of gold-thiolates clusters was greatly improved using the primary ion argon cluster source. Moreover, it was shown that the relevant parameter when using argon clusters for organic thin film characterization is the energy per atom and not the energy or the size of the full argon cluster. Further analysis of this system by comparing with results obtained from molecular dynamics calculations are planned but those study are very time consuming and could not be held before writing this manuscript. Theoretical calculations could give more insights about the physical process behind sputtering under Ar_n^+ clusters bombardment.

4 Studying the Adsorption of Model Proteins on SAMs

Results about β -Lactoglobulin (β LG) have been published in 2013 under the title “Probing the Orientation of β -Lactoglobulin on Gold Surfaces Modified by Alkyl Thiol Self-Assembled Monolayers” (J. Phys. Chem. C, **2013**, *117* (22), 11569-11577).

In this chapter, the correlation between the chemical properties of the surface (e.g. hydrophobicity and surface charge) and the adsorption of model proteins, β -Lactoglobulin (β LG) and bovine serum albumin (BSA), is explored. Using ToF-SIMS and PCA, our main goal is to determine the orientation of the proteins on these different surfaces. In the case of β LG, conformational changes in the adsorbed protein will not be investigated nor characterized in this work since it can reasonably be considered as a *hard protein*,⁹ owing to the stability of its tertiary structure. For BSA, the situation could be more complicated to interpret since it is considered as a *soft protein*.⁶ The model substrates chosen for this study were

polycrystalline gold surfaces, conditioned with alkanethiol solutions to form SAMs. Using $-\text{COOH}$, $-\text{CH}_3$ or $-\text{NH}_2$ thiol endgroups, molecular layers with different surface chemistries could be prepared (see previous chapter). Adsorption was carefully characterized using complementary techniques, in the liquid phase (QCM-D), in air (PM-IRRAS) and in vacuum (XPS and ToF-SIMS), in order to obtain a full picture of protein adsorption on the three different SAMs.

4.1 Samples

The formation and characterization of $-\text{COOH}$ -, $-\text{NH}_2$ -, or $-\text{CH}_3$ -terminated SAMs have been described in the previous chapter. In this study we observed the adsorption of two different proteins. βLG , one of the major whey proteins,¹⁴⁵ is an acidic protein ($\text{pI} = 5.1$) bearing a high number of acid functions on its surface as shown on its 3D structure.^{146,147} It is found in a dimer form in physiological conditions¹⁴⁶ with two monomers of 162 amino acids (a.a.). The total mass of the dimer is about 36 kDa. βLG was purchased from Sigma-Aldrich (L3908) and has a purity higher than 90%. BSA is coming from plasma in cows and is also acidic ($\text{pI} = 4.9$). It is formed by a single polypeptidic chain of 583 a.a. and has a molecular weight of about 66.4 kDa. BSA was purchased from Sigma-Aldrich (A8806), its purity is higher than 96%. Proteins were dissolved with no further purification in a phosphate buffer ($\text{pH} 7.1$) at a concentration of 0.1 mg.mL^{-1} .

Thiol functionalized samples were handled 6 by 6 in 24-well plates (6x4 wells). First, 1 mL of the protein solution in phosphate buffer at $\text{pH} 7.1$ was added onto the samples for 2 h incubation at room temperature in the first

line of the plate. The wells in the second line were filled with 2 mL of buffer, while the third and fourth lines of wells were filled with 2 mL of MilliQ water. After adsorption, samples were successively dipped in a buffer well for 2 min, then 2 min in MilliQ water to remove the excess of salt coming from the buffer, and finally in another well of MilliQ water for 10 minutes before drying with N₂ and analyzing in PM-IRRAS, XPS or ToF-SIMS.

PM-IRRAS measurements were carried out on two separate series of three samples prepared in two different occasions. XPS measurements were performed on three separate samples prepared on three separate occasions. For PCA calculations, 20 spectra were selected for each type of protein adsorbed surface. They were issued from about 8 different samples (2 to 3 spectrum per sample) prepared in three separate occasions. The exact number of samples varies for all type of surfaces due to the extreme sensitivity of the ToF-SIMS technique; contamination (even in really small quantity) can influence greatly PCA results as well as variation in the acquisition conditions (mostly the primary beam current). QCM-D monitoring of adsorption were performed after mounting SAM functionalized quartz in the flow cell. The temperature is maintained at 20°C during the all experiment while successive solutions of buffer or of 0.1 mg.mL⁻¹ protein solutions were flowed with a rate of 50 μL.min⁻¹.

4.2 Adsorption of β -Lactoglobulin

4.2.1 Results

4.2.1.1 *Ex Situ* Characterization (PM-IRRAS and XPS)

β LG adsorptions was first investigated on $-\text{COOH}$, $-\text{CH}_3$ and $-\text{NH}_2$ surfaces (after drying of the sample) in air with PM-IRRAS and in UHV with XPS. The evolution of the infrared amide I and II bands at 1660 and 1550 cm^{-1} gives information about the relative amounts of adsorbed proteins on the surfaces. Figure 4.1 shows a series of representative spectra and sums up the results obtained with the evolution of the amide I + II band area. On the $-\text{COOH}$ -terminated SAMs, no clear amide bands are detected after β LG adsorption. On both other surfaces ($-\text{CH}_3$ - and $-\text{NH}_2$ -terminated SAM), intense amide bands are evidenced after β LG adsorption. A stronger intensity of these bands is observed on the $-\text{CH}_3$ SAM compare to the $-\text{NH}_2$ one.

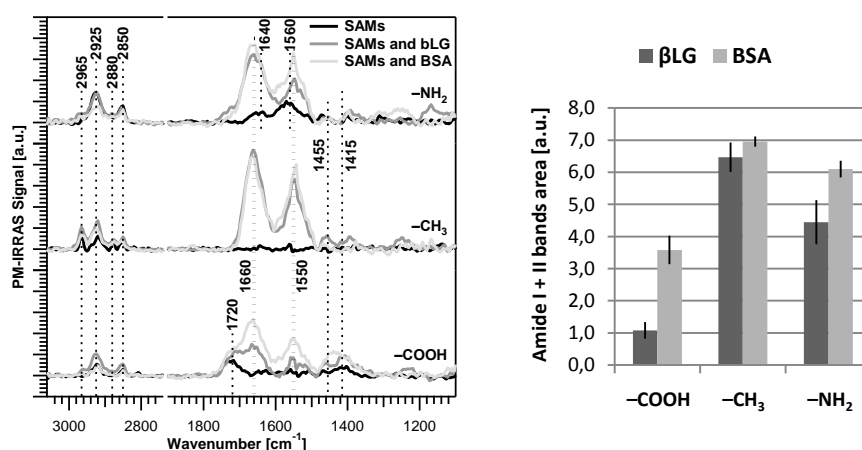


Figure 4.1 PM-IRRAS measurements before and after β LG or BSA adsorption on SAMs (left) together with the evolution of amide I + II bands area (right). Results are presented for $-\text{COOH}$ -, $-\text{CH}_3$ - and $-\text{NH}_2$ -terminated SAMs separately.

In XPS, fingerprints of protein adsorption are found mostly on the C 1s and N 1s peaks. Characteristic spectrum from C 1s and N 1s peaks are presented before or after adsorption of both β LG and BSA in Figure 4.2 together with atomic percent for C 1s, O 1s, N 1s, S 2p and Au 4f in Table 4.1. On the C 1s peak, the two contributions at 286.3 and 288 eV, and corresponding to carbon in $\underline{\text{C}}\text{-(O,N)}$ and $\underline{\text{C}}\text{=O}$, will be characteristic of the amide bonds in proteins. On the N 1s, the amide bonds give a contribution at low energy (about 400 eV) and some a.a. will give a signature due to protonated amine at higher energy (about 402 eV). The overall N 1s raw area follows the amount of adsorbed proteins and is presented in Figure 4.3 for both proteins on the three SAMs.

XPS measurements confirm that β LG adsorbs mainly on the $-\text{CH}_3$ and $-\text{NH}_2$ samples. After adsorption of the protein on the $-\text{COOH}$ surface the very small increase of the N 1s signal (Figure 4.3) together with the slight evolution of the amide components on C 1s and the low attenuation of the gold signal (Table 4.1) indicates, as in PM-IRRAS, a very low amount of adsorbed protein on this surface. Looking now at the evolution of the N 1s signal raw area on Figure 4.3, we can observe a relatively larger increase of the N 1s signal after adsorption on the $-\text{CH}_3$ surface compare to the $-\text{NH}_2$. This observation is in good agreement with the results obtained in PM-IRRAS. The properties of proteins and surfaces (structure, charge, chemistry...) will be taken into account for discussing the amount of adsorbed proteins in a next paragraph; but first, these results will be compared to the one obtained in the liquid phase using QCM-D.

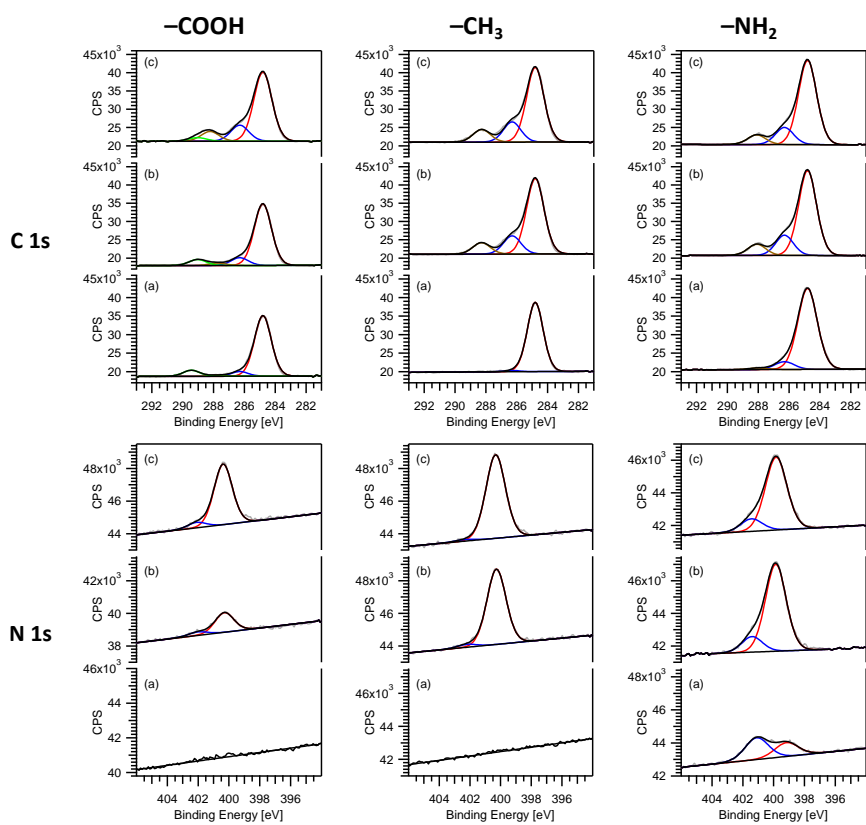


Figure 4.2 XPS Spectrum for the C 1s and N 1s detailed regions on -COOH-, -CH₃- and -NH₂-terminated SAMs before (a) and after βLG (b) or BSA (c) adsorption.

Studying the Adsorption of Model Proteins on SAMs

 Table 4.1 Atomic % of C 1s, O 1s, N 1s, S 2p and Au 4f XPS peaks as assigned on bare thiols SAMs and after β LG or BSA adsorption

		C 1s				O 1s			N 1s			S 2p			Au 4f		
		C-(C,H)	C-(O,N)	$\begin{matrix} \text{COO}^- \\ \text{C=O} \\ \text{Amide} \end{matrix}$	(C=O)-OH	C _{tot}	C=O	C-OH	O _{tot}	$\begin{matrix} \text{NH} \\ \text{NH}_2 \end{matrix}$	NH ₃ ⁺	N _{tot}	S-Au	S _{free}	S _{tot}		
-COOH	(eV)	284.8	286.3	287.7	289.1				532.2	533.5				162.3	163.8		
	SAM	37.3	3.1	0.8	3.2	44.5			3.2	2.3	5.5			1.2	0.5	1.8	47.7
	+/-	1.3	0.4	0.2	0.5	1.3			0.4	0.4	0.8			0.1	0.1	0.1	0.8
	(eV)	284.8	286.3	287.8	289.0				532.0	533.5				162.4	163.9		
	β LG	38.8	5.1	1.6	3.5	48.9			4.3	2.1	6.4			1.2	0.5	1.7	40.9
	+/-	0.3	0.3	0.1	0.4	0.3			0.3	0.4	0.7			0.1	0.1	0.1	0.1
-CH ₃	(eV)	284.8	286.3	288.3	289.2				531.9	533.4				162.5	164.0		
	BSA	35.4	8.2	5.1	1.9	50.5			6.1	1.9	8.0			1.1	0.5	1.5	35.1
	+/-	1.3	0.3	0.1	0.0	1.6			0.1	0.2	0.1			0.1	0.1	0.1	2.0
	(eV)	284.8	286.3											162.6	163.8		
	SAM	38.8	1.0	-	-	39.8					0.1			1.7	0.5	2.2	57.9
	+/-	2.8	0.2			2.6					0.2			0.1	0.1	0.1	2.5
-NH ₂	(eV)	284.8	286.3	288.3					531.8	533.2				162.4	163.9		
	β LG	38.4	9.5	6.0	-	54.0			5.3	1.2	6.6			1.0	0.4	1.4	32.7
	+/-	0.5	0.2	0.1		0.3			0.2	0.3	0.2			0.1	0.1	0.1	0.2
	(eV)	284.8	286.3	288.3					531.8	533.3				162.5	164.0		
	BSA	38.1	10.2	6.4	-	54.7			5.7	1.1	6.8			1.0	0.4	1.4	30.9
	+/-	0.0	0.1	0.0		0.0			0.1	0.1	0.0			0.1	0.0	0.1	0.1
-NH ₂	(eV)	284.8	286.3	288.1					531.2	532.8				162.0	163.7		
	SAM	45.7	5.3	1.6	-	52.5			5.2	1.3	6.5			1.2	0.9	2.0	35.8
	+/-	2.7	0.5	1.1		1.9			1.9	0.3	1.6			0.1	0.2	0.2	1.3
	(eV)	284.8	286.3	288.1					531.3	532.9				162.0	163.8		
	β LG	40.2	9.3	5.2	-	54.7			8.4	1.3	11.2			0.9	0.6	1.5	26.4
	+/-	3.2	0.8	0.6		4.1			0.2	0.1	1.8			0.1	0.2	0.2	3.6
-NH ₂	(eV)	284.8	286.3	288.1					531.3	532.8				162.1	163.8		
	BSA	43.7	9.1	5.0	-	57.7			6.9	1.2	8.1			0.8	0.9	1.8	25.8
	+/-	1.6	0.1	0.2		1.9			0.0	0.2	0.2			0.1	0.1	0.1	1.8

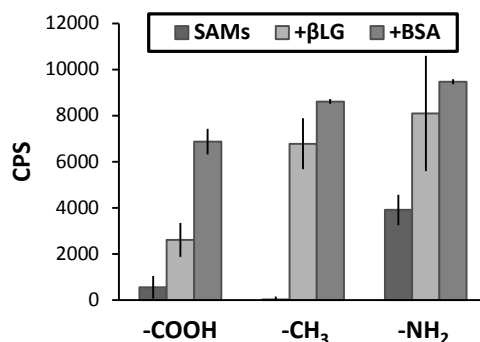


Figure 4.3 Raw Area of N 1s XPS peaks before or after adsorption of βLG and BSA on bare -COOH-, -CH₃- or -NH₂-terminated SAMs

4.2.1.2 *In Situ* Monitoring of Adsorption (QCM-D)

QCM-D results recorded upon the adsorption of βLG are presented in Figure 4.4. On each thiol surface, a rapid adsorption of the protein after stabilization is observed with no noticeable variation in the dissipation measurements, suggesting that protein adsorption leads to the formation of a rigid-like structure layer. On the -COOH terminated surface, the adsorbed protein layer is not stable upon rinsing in a phosphate buffer solution (see Figure 4.4), as shown by the increase in frequency shift indicating the removal of the proteins. Even for longer rinsing times (not shown here), the measured frequency didn't stabilize indicating a progressive desorption of the proteins. This can be correlated to the PM-IRRAS and XPS results indicating that, after rinsing, βLG adsorbed poorly on the -COOH surfaces. For the -NH₂-terminated SAMs, the frequency shift was constant after 20 min of rinsing, indicating no further desorption, while no effect of rinsing was noticeable on the -CH₃ SAMs.

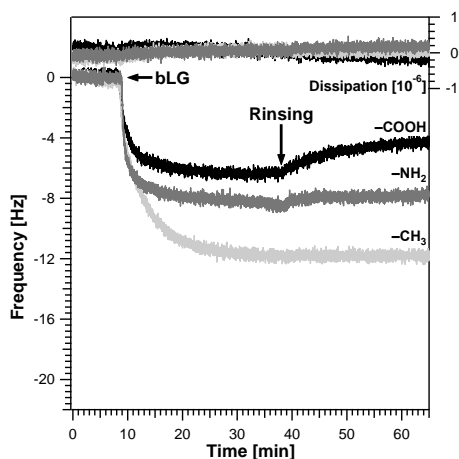


Figure 4.4 Frequency and dissipation shifts obtained in QCM-D for the adsorption of β LG on $-\text{COOH}$ -, $-\text{CH}_3$ - and $-\text{NH}_2$ -terminated SAMs

QCM-D data may provide a rough evaluation of the amount of adsorbed proteins. Low dissipation in QCM-D measurements ($< 1.10^{-6}$) indicates the formation of a “rigid” β LG layer on the surface. The mass of adsorbed protein may be estimated using the Sauerbrey equation:

$$\Delta m = -C_f \frac{\Delta f}{n}$$

Where Δm represents the mass uptake (usually in $\text{ng}\cdot\text{cm}^{-2}$), n is the overtone considered and $C_f = 17.7 \text{ ng}\cdot\text{cm}^{-2}\cdot\text{Hz}^{-1}$ is the mass sensitivity factor (See Chapter 2). Based on QCM-D measurements the amount of β LG adsorbed on $-\text{CH}_3$ and $-\text{NH}_2$ surfaces was calculated as 220 and 140 $\text{ng}\cdot\text{cm}^{-2}$ respectively. The orientation of β LG upon adsorption on the three different SAMs will now be explored using ToF-SIMS coupled with PCA calculations.

4.2.1.3 Exploring the Orientation (ToF-SIMS and PCA)

In order to obtain additional information regarding the orientation of the protein after adsorption, indirect techniques such as bio-recognition measurements or fluorescent tagging can be used. The goal here was to demonstrate that a direct approach can be applied to retrieve such information using ToF-SIMS measurements as described in Chapter 1 and 2. In principle, ToF-SIMS allows us to retrieve chemical information corresponding to the first nanometers of the protein layer and, therefore, to determine which part of the protein is exposed. To achieve that goal, ToF-SIMS measurements were treated by applying PCA to the secondary ion peaks corresponding to amino acid fragments. Prior to PCA calculations, SIMS intensities were normalized to the sum of selected peaks and mean centered. The CH_4N^+ and $\text{C}_2\text{H}_6\text{N}^+$ peaks were removed from the peaklist presented in Chapter 2 because they are characteristic of several a.a. and could not be used to discriminate specific fractions of the proteins.

On an attempt to determine the possibilities of the Ar_n^+ clusters for protein characterization preliminary studies have been performed. They showed that no molecular information was detected. Several questions are raised: is there enough energy in the clusters to sputter an entire protein? What is the ionization probability? Can we detect full protein in our ToF equipment? The two first questions are still an open debate but for the last one we can say that we are limited in the observed mass range by the time for secondary ions to travel in the detector. Mass spectra ranging from 0 to 15 000 m/z were recorded and no big fragments were observed for protein. It does not mean that no information can be found using large argon clusters

for protein analysis but it is another project. In this study, we are interested in the fragmentation pattern in the few first nanometers of adsorbed proteins to detect their orientation. The LMIG source was then used to sputter surfaces with Bi^+ primary ions.

The previous paragraphs showed that βLG is adsorbed on the $-\text{CH}_3$ - and $-\text{NH}_2$ -terminated SAMs in larger quantities than on the $-\text{COOH}$ -terminated surfaces. Multivariate analysis was first performed using samples from the three thiol surfaces but the mass spectra from the $-\text{COOH}$ surfaces after βLG adsorption were not clearly separated from the others on the score plot (see Figure 4.5). Indeed, they presented a large dispersion in principal component scores plot, probably because of the low amount of adsorbed proteins. Thus, PCA calculations were run again but including only spectrum from adsorption of βLG on the $-\text{CH}_3$ and $-\text{NH}_2$ SAMs.

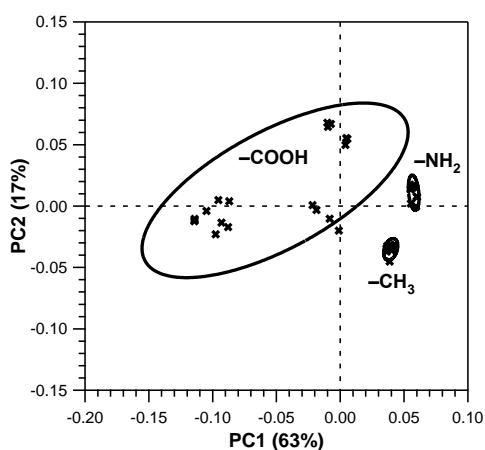


Figure 4.5 Scores plot for PCA calculations performed on ToF-SIMS spectrum after adsorption of βLG on $-\text{COOH}$ -, $-\text{CH}_3$ - and $-\text{NH}_2$ -terminated SAMs

PCA results on $-\text{CH}_3$ - and $-\text{NH}_2$ -terminated surfaces are presented in Figure 4.6. Samples corresponding to these two surfaces are clearly separated on the PC1 axis, which takes into account 86% of the information contained in the original peak series. Surfaces terminated by $-\text{CH}_3$ display negative PC1 scores and $-\text{NH}_2$, positive ones. The PC1 loadings are presented in Figure 4.6 b). Large positive or negative loadings point out the amino acid fragments which allow the separation between samples. Fragment ions corresponding to lysine, methionine, proline and cysteine give the largest positive loadings, while arginine, asparagine, glycine or glutamic acids give the largest negative ones.

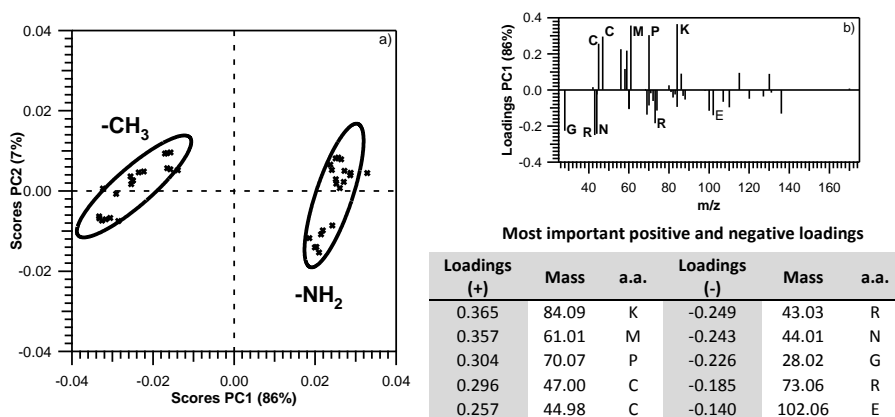


Figure 4.6 PCA calculation results for ToF-SIMS measurements corresponding to $-\text{CH}_3$ - and $-\text{NH}_2$ -terminated SAMS after adsorption of β LG. a) scores for PC1 and PC2, b) loadings for PC1 with most important values in the table

By checking the intensities of the different fragments on both type of surface we can make the link between scores and loadings and determine which amino acids are dominating on ToF-SIMS spectra of one or the other surface. Figure 4.7 presents the average intensity of the considered amino acid fragments after normalization to the sum of all of them, for the $-\text{CH}_3$ -

and $-\text{NH}_2$ -terminated samples. For peaks presenting large positive loadings in PC1 (Figure 4.6), the mean intensity is higher on the $-\text{NH}_2$ -terminated samples. On the contrary, peaks with negative loading have a higher intensity for the $-\text{CH}_3$ -terminated surfaces. Thus, along PC1, negative scores correspond to negative loadings (arginine, asparagine, glycine or glutamic acid), and positive scores to positive loadings (lysine, methionine, proline or cysteine). To determine the most likely orientation of the βLG on each surface, the 3D structure of the protein as well as its adsorption data on each type of surface will be considered.

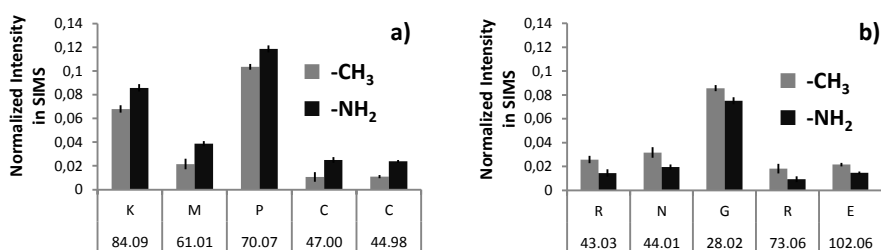


Figure 4.7 Mean peak intensities for most important positive (a) and negative (b) loadings values on PC1 after βLG adsorption on both $-\text{CH}_3$ and $-\text{NH}_2$ SAMs ToF-SIMS measurements

4.2.2 Discussion

4.2.2.1 Amount of Adsorbed βLG

Values of 220 and 140 $\text{ng}\cdot\text{cm}^{-2}$ were obtained when βLG is adsorbed on $-\text{CH}_3$ and $-\text{NH}_2$ SAMs, respectively. Considering the area of a dimeric βLG ¹⁴⁷ as equal to 16 nm^2 in an upright orientation, and 32 nm^2 in a flat lying one, the mass per unit area could thus be calculated for a “theoretical” monolayer coverage, i.e. 380 $\text{ng}\cdot\text{cm}^{-2}$ in an upright orientation and 190 $\text{ng}\cdot\text{cm}^{-2}$ in a flat lying one. From QCM-D, performed in the liquid phase, the calculated mass uptake includes adsorbed proteins and water molecules

that bind or hydrodynamically couple to the macromolecules, it is thus overestimated in comparison with other techniques.^{127,128,148} Moreover, the calculated values for monolayer coverage are an extreme case where all the adsorbed proteins would have the same orientation. Since the calculated mass uptakes from QCM-D are overestimated, dimeric β LG likely form less than one monolayer on both surfaces.

The amount of adsorbed proteins is also probed using XPS; in a qualitative approach the level of nitrogen measured on all samples gives an indication of the protein amount (see Figure 4.3). In addition, the Au 4f atomic percentage decreases from 57.9% to 32.7% for the $-\text{CH}_3$ surfaces and from 35.8% to 26.4% for the $-\text{NH}_2$ ones (Table 4.1). Ratios between the values of each series are equal to 0.56 and 0.74 respectively. This indicates a stronger attenuation of the signal in the case of the $-\text{CH}_3$ SAMs showing that protein adsorption is enhanced on this surface. This is in good agreement with the QCM-D and PM-IRRAS measurements.

Regarding $-\text{COOH}$ SAMs, it must be kept in mind that upon adsorption of β LG, the pH was maintained by a buffer at 7.1. QCM data suggest weak interactions between the $-\text{COOH}$ -terminated surface and the protein. This may be attributed to the repulsive interaction between the negatively charged surfaces (COOH/COO^-) and the globally negatively charged proteins (isoelectric point = 5.1). Hydrophobic interactions can be neglected since the surface is hydrophilic as the outer part of the protein. On the $-\text{NH}_2$ -terminated SAMs, the surface is globally positively charged, thus interacting

favorably with the negatively charged proteins, leading to a significant amount of β LG on the surface.

4.2.2.2 Orientation

Adsorption of β LG was evidenced on both $-\text{NH}_2$ and $-\text{CH}_3$ surfaces. On the $-\text{NH}_2$ -terminated SAM, the terminal amine groups were shown to be predominantly protonated (PM-IRRAS and XPS); moreover, from ToF-SIMS and PCA results, lysine corresponds to the main positive loadings, giving positive scores on $-\text{NH}_2$ -terminated surfaces. Thus, in Figure 4.8 a) which shows β LG in the dimer form (based on the protein data bank - PDB structure 1BEB), with the lysine residues highlighted in gold color, the orientation of the protein is chosen with the lysine residues on top. In contrast, glutamic acid and asparagine have very negative loadings in the PC1. The two red arrows indicate a region rich in these negatively charged or polar a.a. (NH_2 -Glu-Asn-Gly-Glu-COOH from residue 62 to 65) in both chains of the dimer. They are logically in the vicinity of the charged surface. Carboxylic acids, terminating glutamic acid residues, have a pKa of 4.3. Asparagin is a polar a.a. but its carboxamide group cannot be ionized. Considering the adsorption pH (7.1), glutamic acid residues should be mainly negatively charged during the process. It is thus proposed that β LG interacts through electrostatic interactions between the Glu-Asn-Gly-Glu sequence and the $-\text{NH}_3^+$ end-groups on the surface. This is consistent with the expected repulsion between the surface and the lysine-rich regions in β LG.

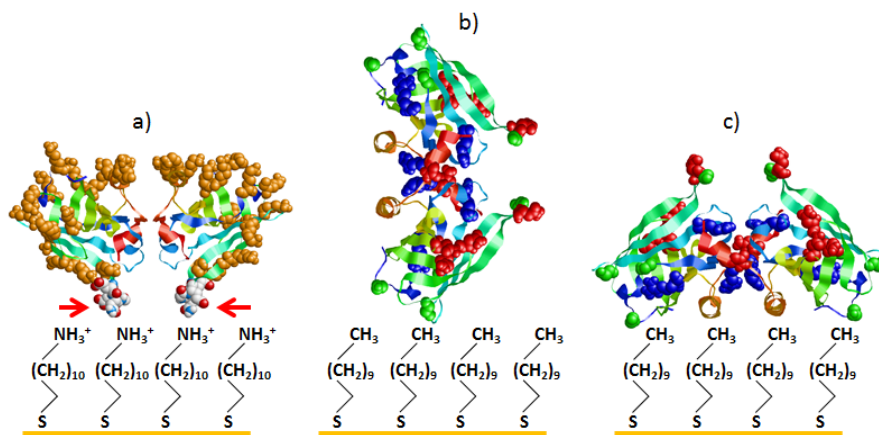


Figure 4.8 Proposed orientation of β LG on $-\text{NH}_2$ (a) and $-\text{CH}_3$ (b & c) terminated SAMs. On a) Lys residues are highlighted in gold color and red arrows indicates a Glu-Asn-Gly-Glu sequence; On b) & c) Arg residues in the protein are in blue, Asp ones in red and Gly ones in green

Unlike the $-\text{NH}_2$ surface, the $-\text{CH}_3$ surface is purely hydrophobic. In that case, the adsorption mechanism of β LG may involve a monomer-dimer exchange. Wahlgren and Elofsson have reported a mechanism based on the adsorption of dimers, favored by lateral interactions with adsorbed monomers.¹⁴⁹ Here two different possible orientations of the protein in the dimer form are proposed based on the PCA results. In Figure 4.8 b), the β LG dimer is presented in upright position, exposing a.a. which were relevant for the separation of the $-\text{CH}_3$ and $-\text{NH}_2$ surfaces in ToF-SIMS measurements (arginine, asparagine and glycine in blue, red and green respectively). This position could be favored by protein-protein interactions with a stabilization of the dimeric form. In Figure 4.8 c) the flat lying orientation, in the opposite way as on $-\text{NH}_2$ surfaces, is proposed. As previously shown in ToF-SIMS measurements, arginine, asparagine and glycine are also well exposed at the protein surface in this orientation.

4.3 Adsorption of bovine serum albumin

4.3.1 Results

4.3.1.1 *Ex Situ* Characterization (PM-IRRAS and XPS)

In PM-IRRAS measurements after BSA adsorption (see Figure 4.1), amide bands are observed for all three surfaces. As in the β LG case, stronger intensities are evidenced for the $-\text{CH}_3$ and $-\text{NH}_2$ surfaces compare to the $-\text{COOH}$ -terminated one. Moreover, the higher intensity of these bands on the $-\text{CH}_3$ surfaces indicates a greater quantity of proteins adsorbed on the $-\text{CH}_3$ than on the $-\text{NH}_2$ functionalized samples. In XPS (see Figure 4.2, Figure 4.3 and Table 4.1), the adsorption is higher on $-\text{CH}_3$ and $-\text{NH}_2$ surfaces and more favorable on the $-\text{COOH}$ surfaces than in the case of β LG. The adsorption of proteins on the $-\text{COOH}$ surfaces will be discussed in more details later taking into account the chemistry, the charges or the structural properties of BSA and of the surface. As observed previously in PM-IRRAS, the N 1s increase is higher on the $-\text{CH}_3$ - than on the $-\text{NH}_2$ -terminated SAMs. This indicates that methyl groups tend to favor the adsorption of proteins as already demonstrated by PM-IRRAS. These observations will now be correlated with QCM-D monitoring of the adsorption in the liquid phase.

4.3.1.2 *In Situ* Monitoring of Adsorption (QCM-D)

In the case of BSA, the protein is adsorbed on all three surfaces (see Figure 4.9). However, two different kinetics of adsorption are observed. In the case of the $-\text{CH}_3$ and $-\text{NH}_2$ surfaces, the adsorption occurs rapidly once the protein is flowed in the QCM-D cell as it was observed for β LG. On the $-\text{COOH}$

COOH surface, the adsorption kinetic is slower. This could be an indication that the protein must change its conformation (secondary structure) or its folding (tertiary structure) in order to adsorb on this surface. This point will be further discussed below but one should keep in mind that electrostatic conditions are (as for β LG) unfavorable for adsorption on this surface (both the surface and the protein are negatively charged).

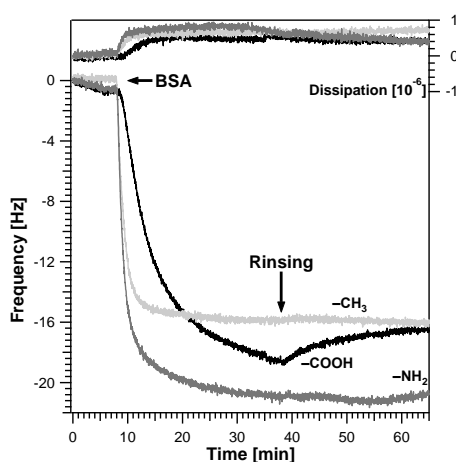


Figure 4.9 Frequency and dissipation shifts obtained in QCM-D for the adsorption of BSA on $-\text{COOH}$ -, $-\text{CH}_3$ - and $-\text{NH}_2$ -terminated SAMs

As a second observation, dissipation is more important than in the case of β LG. This indicates the formation of a less rigid layer compatible with the *soft* character of BSA. The adsorbed protein layer is most likely to be more hydrated due to perturbation of the secondary structure or to an unfolding of the protein upon adsorption. However, dissipation measurements are lower than $1 \cdot 10^{-6}$ which is in agreement with the Sauerbrey conditions giving a frequency shift proportional to the adsorbed mass.

Overall, the adsorbed amount of proteins is higher for BSA than for β LG on all three surfaces (larger frequency shifts). In the case of the $-\text{COOH}$ SAMs, the adsorption of the protein is, again, less stable upon rinsing but more proteins are retained to the surface compare to β LG. On both other surfaces, adsorbed proteins are stable upon rinsing. Compare to what is observed in PM-IRRAS or XPS, the apparent amount seems higher on the $-\text{NH}_2$ surface than on the $-\text{CH}_3$ one. Using the Sauerbrey relation, the adsorbed mass is estimated at about 290, 280 and 370 $\text{ng}\cdot\text{cm}^{-2}$ for $-\text{COOH}$, $-\text{CH}_3$ and $-\text{NH}_2$ surfaces respectively. The amount of adsorbed proteins detected by each technique will be discussed later taking into account the drying step and the fact that QCM-D measurements are taken directly in the liquid phase. We will now explore the orientation of BSA on all surfaces using the already described combination of ToF-SIMS and PCA.

4.3.1.3 Exploring the Orientation (ToF-SIMS and PCA)

In the case of BSA, results in XPS, PM-IRRAS or QCM-D showed that the protein is adsorbed on all three SAMs surfaces. With PCA calculations applied to a.a. fragments peaks in ToF-SIMS, adsorbed proteins on the $-\text{COOH}$, $-\text{CH}_3$ and $-\text{NH}_2$ surfaces were separated, scores and loadings are presented in Figure 4.10. PC1, that sums up 70% of the information contained in the original spectrum, separates BSA adsorbed on $-\text{COOH}$ surfaces (positive PC1 scores) from the two other surfaces. For both $-\text{CH}_3$ and $-\text{NH}_2$ surfaces PCA calculations give negative PC1 scores. They are separated on PC2 (25% of the total variance) with positive scores for $-\text{CH}_3$ surfaces and negative ones for $-\text{NH}_2$ SAMs. Figure 4.10 b) presents the PC1 loadings versus the PC2 ones. Each a.a. fragment peak is represented by a

dot which coordinates correspond to its PC1 and PC2 loadings. As previously shown, the correspondence between scores and loadings is established by looking at the original peak intensities for each fragment with strong loadings in PC1 or PC2. The intensity of peaks responsible for PC1 or PC2 separation of each surface is represented in Figure 4.11.

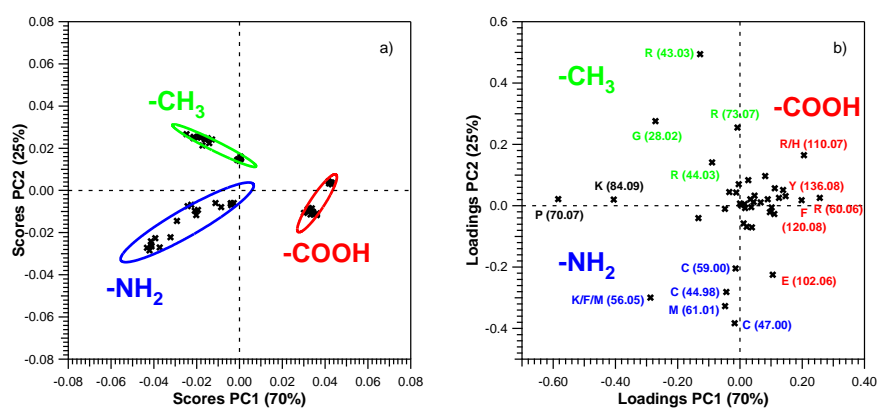


Figure 4.10 Results of PCA calculations performed on ToF-SIMS measurements after BSA adsorption on -COOH-, -CH₃- and -NH₂-terminated SAMS. The a) panel presents the scores for PC1 and PC2, while the b) one represents the loadings for PC1 versus PC2 (most important peaks for separation are labeled with the corresponding a.a. in the one letter code and mass)

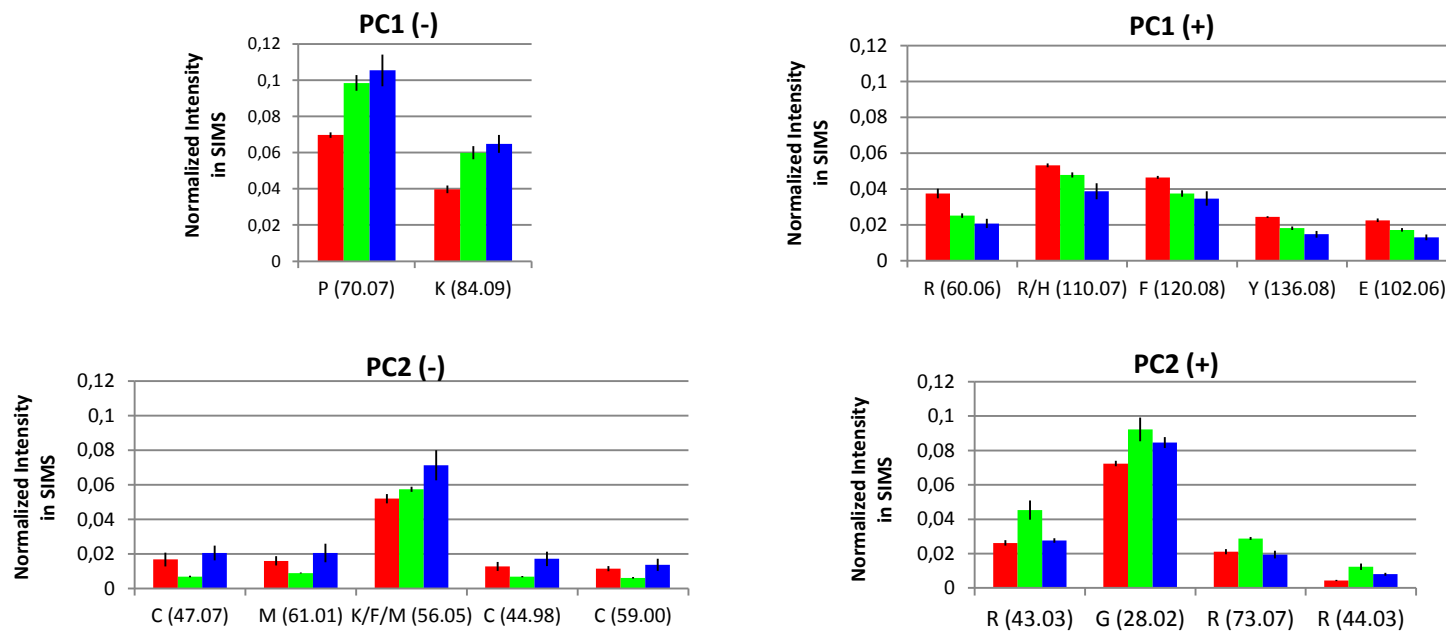


Figure 4.11 Mean peak intensities for most important positive (+) or negative (-) PC1 and PC2 loadings (Red = -COOH, Green = -CH₃ and Blue = -NH₂). Fragments are labeled in the one-letter a.a. code as follows: P = Pro, K = Lys, R = Arg, H = His, F = Phe, Y = Tyr, E = Glu, C = Cys, M = Met.

On Figure 4.10 b), peaks with large PC1 positive loadings have been highlighted in red. They correspond to fragments coming from arginine, histidine, phenylalanine, tyrosine, or glutamic acid and are showing a larger intensity for BSA adsorbed on the –COOH-terminated surface (Figure 4.11). Two peaks corresponding to proline and lysine have large PC1 negative loadings, their mean intensity for all samples are stronger for both the –CH₃ and –NH₂ surfaces in correlation with the score plot indicating the separation of these surfaces on negative PC1 scores. When studying PC2 loadings, one can see that positive loadings correspond to stronger intensities on the –CH₃ surfaces and are correlated to fragments mostly coming from arginine. Arginine was also evidenced in the case of the –COOH surfaces, at m/z 60.06 and 110.07, the fragment CH₆N₃⁺ and C₅H₈N₃⁺ which are attributed to arginine in proteins could interfere with the C₃H₈O⁺ and C₇H₁₀O⁺ fragments most likely originated from the –COOH SAMs itself. Therefore, arginine will be considered as characteristic of the BSA adsorbed on –CH₃ surfaces. Finally, PC2 negative loadings evidence fragments coming essentially from cysteine and methionine and are attributed to the separation of BSA adsorbed on –NH₂ surfaces. For sake of clarity, a.a. evidenced after adsorption of BSA on all three surfaces are summarized in Table 4.2.

Table 4.2 Amino Acids evidenced by PCA after adsorption of BSA on the three different thiol SAMs

–COOH	–CH ₃	–NH ₂
His		Pro
Phe		Lys
Tyr	Arg	Cys
Glu	Gly	Met

4.3.2 Discussion

BSA is one of the most studied proteins in the past decades. It is the most abundant protein in serum and is responsible for numerous physiological reactions (conservation of the blood pH, transport of molecules - such as a.a., drugs, fatty acids... - to organs).¹⁵⁰ As stated in the Chapter 1, the *soft* character of BSA will allow its adsorption on most surfaces and in most adsorption conditions. BSA was then used as a blocking agent for the development of biosensors.^{54,151} However, studies have shown that BSA tends to adsorb in higher quantities on hydrophobic surfaces than on hydrophilic ones.^{44,152} BSA coverage was also studied in function of the adsorption pH and of its concentration in solution.¹⁵³ A maximum coverage was obtained for all considered pH but it was necessary to increase the concentration for pH far from the iso-electric point. In our group, the influence of residual charges at the surface and the influence of the rigidity of a -COOH-terminated SAM surfaces on BSA adsorption were recently shown.¹⁵⁴

Recent studies focused on the influence of the underlying surface on the conformation of adsorbed BSA. It was shown that BSA adsorb on both hydrophilic and hydrophobic SAM with a greater loss of ordered secondary structures in the first case but a larger spreading in the second (unfolding).¹⁵² The influence of conformational changes on BSA ligand ability was also demonstrated.¹⁵⁵ In addition, very recent work shows that doping BSA molecules with small metal-bearing molecules can help in preventing the loss of secondary structures.¹⁵⁶ The fundamental understanding of the unfolding or loss of conformation can be gained by

simulating numerically the adsorption of BSA using molecular dynamics.¹⁵⁷ The adsorption was studied for two initial protein orientations toward a hydrophobic graphite surface. In each case the calculations showed that the protein spreads and unfold on the surface.

As it was stated recently by Vogler in a Leading Opinion Paper,²⁹ the lack of consensus in the protein adsorption literature is striking. BSA being one of the most studied proteins, it is really difficult to extract general conclusions. However, we will try now, in the light of what was found in the literature and with our own results, to determine the influence of the three studied surfaces on BSA adsorption.

4.3.2.1 Amount of Adsorbed BSA

The shape of the BSA protein is more complex to describe than the β LG one; its native structure (N-Form) is shown as a heart-shaped molecule, approximated by an equilateral triangle with sides of 8 nm and a thickness of 3 nm. This native structure can evolve in the F-form (standing for fast migration form) which is a prolate spheroid (a cigar form) with dimensions of 4 by 12.9 nm²; and in a fully extended form (E-Form) as an oblate spheroid (a sphere flattened at its poles) with dimensions 2.1 by 25 nm².^{158,159} The different forms are represented in Figure 4.12. It is complicated to estimate the mass for a one monolayer coverage of BSA due to the different possible shapes and orientations. However, in the intermediate case of the F-Form, a closed pack flat lying monolayer of BSA would lead to an adsorbed mass of about 200 ng.cm⁻² when an upright one would give about 700 ng.cm⁻². In the case of the native form (heart shape),

a flat lying monolayer gives about 250 ng.cm^{-2} and an upright orientation 450 ng.cm^{-2} . Estimated adsorbed mass are 290 , 280 and 370 ng.cm^{-2} for $-\text{COOH}$, $-\text{CH}_3$ and $-\text{NH}_2$ surfaces respectively. Since QCM-D measurements take into account the water contained in the protein films we will consider that less than a monolayer is formed on all surfaces as in the case of βLG .

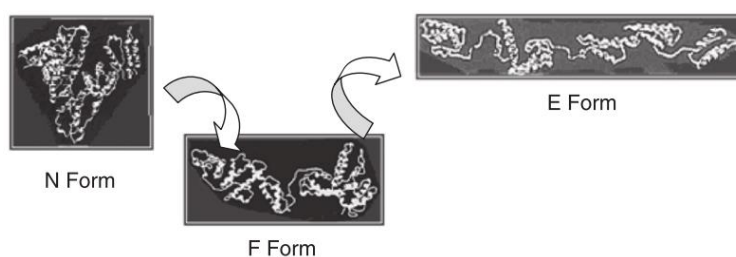


Figure 4.12 Schematic of the different possible folding of the BSA protein in solution (Reproduced from Jachimska *et al.*¹⁵⁸)

In Table 4.1 presenting XPS results, we will now comment on the gold attenuation after BSA adsorption. Before protein adsorption, gold atomic % are calculated as 47.7, 57.9, and 35.8% for $-\text{COOH}$ -, $-\text{CH}_3$ -, and $-\text{NH}_2$ -terminated SAM. After BSA adsorption values are respectively 35.1, 30.9, and 25.8%. Values after are divided by the one before adsorption; calculated ratios are 0.74 for $-\text{COOH}$, 0.53 for $-\text{CH}_3$, and 0.72 for $-\text{NH}_2$ SAM. This indicates a greater quantity of BSA adsorb on the $-\text{CH}_3$ surface (more attenuation of the gold signal) compare to both other surfaces that present similar amounts of adsorbed proteins. PM-IRRAS results (see Figure 4.1) indicate similar results even if the measured amide band signal seems higher for the $-\text{NH}_2$ surface compare to the $-\text{COOH}$ one, signal on the $-\text{CH}_3$ surface is still the strongest. On the $-\text{CH}_3$ surface, BSA most likely interact through hydrophobic interactions. Due to the *soft* character of the protein, the interaction with the SAM influences its folding or conformation. As

explained in Chapter 1, the resulting gain in conformational entropy in the protein favors greatly the adsorption of BSA on this hydrophobic surface.^{8,9}

Nevertheless, QCM-D gave the following order for the adsorbed amount of BSA on thiols SAMs: $-\text{NH}_2 > -\text{COOH} > -\text{CH}_3$. This shows the strong impact of hydration in QCM-D measurements compared to PM-IRRAS or XPS ones performed after drying or in UHV conditions. Water trapped in the protein layer is also measured in QCM-D. The relatively lower adsorption on $-\text{CH}_3$ surfaces observed in QCM-D could indicate that water is expelled from the interface between the surface and the protein. The $-\text{CH}_3$ -terminated SAM is hydrophobic, BSA will most likely interact through hydrophobic interactions with this surface. Less water between the surface and the protein would stimulate the interaction due to a gain in entropy in the bulk solution reducing the free energy necessary for adsorption.^{6,10} The “real” adsorbed amount could then be higher on this surface as it was observed in XPS and PM-IRRAS and underestimated in QCM-D due to a lower amount of water as on the other surfaces. On the contrary, for adsorption on the $-\text{COOH}$ or the $-\text{NH}_2$ SAMs, water is retained between the surface and adsorbed proteins, stimulating adsorption by hydrogen bonding and increasing the calculated mass of adsorbed proteins in QCM-D measurements.⁶ Moreover, most of the external a.a. on the BSA protein are polar residue that can favor such interactions.¹⁵⁰ Structural properties of BSA will be further discussed after studying its adsorption on surfaces using ToF-SIMS en PCA results.

It is worth mentioning here that on the $-\text{COOH}$ surface, electrostatic conditions are unfavorable to the adsorption of BSA. The protein is indeed,

like β LG, an acidic protein that is negatively charged at the adsorption pH of 7.1.¹⁵⁰ As stated earlier, carboxylic acids moiety on the SAM surface are partially unprotonated (mixture of COOH and COO⁻) leading to a globally negatively charged surface. Restructuration of the *soft* BSA protein allows overcoming the repulsion between BSA and the surface as it was explained in the first chapter of the present manuscript. However, BSA adsorption on this –COOH surface is less stable than on the –NH₂ or –CH₃ one where it is favored respectively by electrostatic or hydrophobic interactions. This is confirmed by protein desorption upon rinsing in QCM-D and the lower amount evidenced in PM-IRRAS and XPS. In addition, the slower adsorption kinetic in QCM-D measurements for this surface could show that the protein should change its folding state or conformation in order to adsorb on the –COOH surface. The structural properties of adsorbed BSA (orientation / defolding / conformation) on the three surfaces will now be discussed in greater details using ToF-SIMS/PCA results and physico-chemical considerations.

4.3.2.2 Structural properties upon adsorption

In the case of BSA, it is more complex to detect an orientation solely based on ToF-SIMS and PCA results. As reported in the literature,¹⁵⁹ at pH 7.1 in solution, BSA adopt a defolded state in between the N- and the F-Form which is a prolate ellipsoid with dimensions 4 x 14 nm². It is not evidenced that this structure is strictly retained upon adsorption. However, no 3D model of the F-Form is available, only the native structure is found on PDB (structure 4F5S, see left panel of Figure 4.13). The N-Form has a heart-shape and is formed of three different domains (I, II and III). Transition

between the different structures of the protein is characterized by a loss in the α -helix percentage (N = 55% > F = 45% > E = 35%)¹⁵⁹ causing the spreading of the protein and its opening at the “tip” of the heart in the domain-II.¹⁵⁸

Change in α -helix, β -sheets or random coil composition in proteins can be followed with the shape of the amide I band in IR spectroscopies.^{115,116} β -sheets structures are characterized with a component around 1675-1665 cm^{-1} , random chains with one at 1670-1660 cm^{-1} , and α -helix around 1655-1645 cm^{-1} . In our case, the amount of adsorbed proteins is low (less than a monolayer) and it was then not possible to decompose the amide I signal in PM-IRRAS measurements (see Figure 4.1). The relative composition in protein secondary structures could not be determined exactly. This would have helped in showing which BSA form is predominant upon adsorption on the different surfaces. However, PCA calculations gave us necessary information on the most likely a.a. composition at the surface to determine possible unfoldings and orientations of BSA in each case.

In order to determine an orientation/defolding of BSA on each surface, important a.a., evidenced with PCA calculations, have been highlighted in the BSA structure. On the right panel of Figure 4.13, BSA is shown with Pro in blue and Lys in red. These two a.a. had strong negative PC1 loadings and allowed the separation of the $-\text{CH}_3$ and $-\text{NH}_2$ surfaces versus the $-\text{COOH}$ one. The sum of Pro and Lys residues in the BSA sequence represent 15% of the total of the a.a. (Uniprot sequence P02769). On the structure, one can see that they are widespread at the surface of the protein. Due to their

homogeneous distribution, they cannot be used as a marker for orientation and most likely give information about the adsorbed quantity of BSA on the surface. From Figure 4.11, one can see that a larger intensities of both peaks corresponding to Pro and Lys ($C_4H_8N^+$ at m/z 70.07 and $C_5H_{10}N^+$ at 84.05) are observed on both $-CH_3$ and $-NH_2$ surfaces while the quantity is lower on the $-COOH$ one as expected from PM-IRRAS or XPS results. Surprisingly, the measured intensity in ToF-SIMS seems higher for the $-NH_2$ surface. This is explained by the fact that the two considered fragments could also originate from the fragmentation of the amine terminated thiol during the sputtering process.

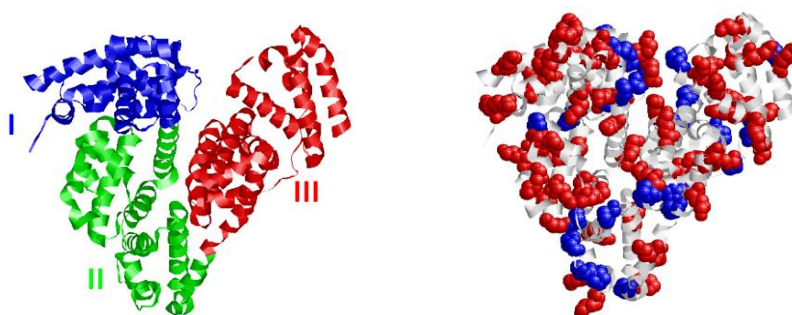


Figure 4.13 Left Panel: Native structure of the BSA protein with its 3 domains highlighted in blue green and red (respectively named I, II and III); Right Panel: localization of the Pro (blue) and Lys (red) a.a. in the BSA protein

In Figure 4.14, the a.a. evidenced for the separation of each surface in PCA (Table 4.2) have been highlighted; possible orientations or defoldings for the adsorption of BSA on the $-COOH$, the $-CH_3$ or the $-NH_2$ SAMs will now be discussed. For the $-COOH$ surface (Figure 4.14 a), one can see that the evidenced a.a. are spread all over the BSA structure. Moreover, positive PC1 loadings (Figure 4.10) allowing this separation and corresponding to His, Phe, Tyr or Glu were smaller in absolute value than the negative ones

(Pro or Lys). It indicates a weaker separation along the PC1 axis compare to $-\text{CH}_3$ or $-\text{NH}_2$ surfaces. Based on the native structure model, no preferential orientation is proposed for BSA adsorption on the $-\text{COOH}$ surface.

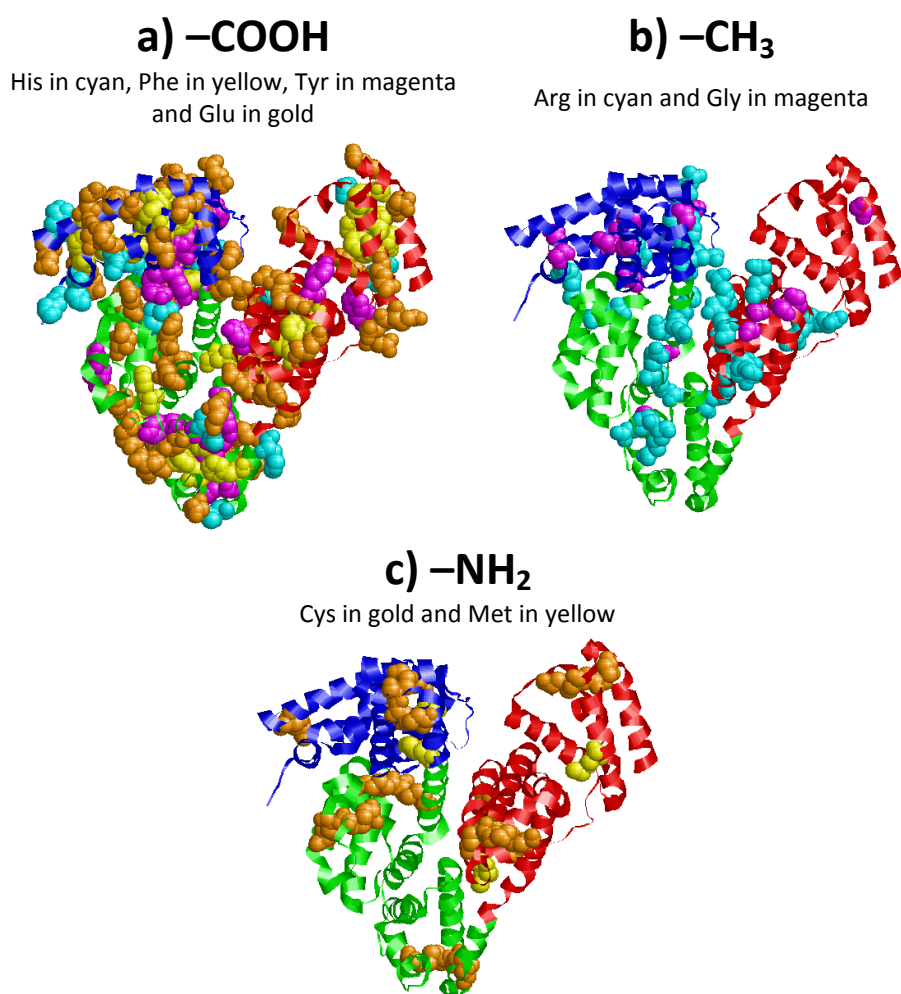


Figure 4.14 Model of the BSA protein with the most important a.a. highlighted for the $-\text{COOH}$ -, $-\text{CH}_3$ - and $-\text{NH}_2$ SAM surfaces as they were determined by PCA calculations on ToF-SIMS results.

In the case of the $-\text{CH}_3$ surface, a.a. evidenced in PCA (Arg mostly and Gly) are localized essentially in the center of the heart-shaped BSA. It is proposed that the protein unfold upon adsorption on the surface. The Arg-rich part in between domain II and III of the native form could consequently be exposed when adsorbed on the hydrophobic surface (see Figure 4.14). The protein would then adopt a state close to the F-Form presented in Figure 4.12 and consistent with its unfolded state in solution at physiological pH.¹⁵⁹ In the literature, BSA is presented as a multidomain protein with both polar or apolar (hydrophobic) patches on its surface.¹⁵⁰ Previous study of adsorption on hydrophobic surfaces showed results consistent with an unfolding of BSA.¹⁶⁰ Moreover, the low level of desorption after rinsing is consistent with a multipoint protein-surface interaction after unfolding.⁴⁴

On the $-\text{NH}_2$ surface, Cys and Met a.a. seems to be localized slightly more on the outside of the protein in all three domains. It is thus proposed a similar unfolding mechanism of the protein (in agreement with the pH conditions) but with an opposed orientation upon adsorption than on the $-\text{CH}_3$ surface. This theory is supported by the fact that Arg residues (evidenced for the $-\text{CH}_3$ surface) bear negative charges at pH 7.1 (unprotonated carboxylic acids at the end of the chain) that could interact with the positive charges on the $-\text{NH}_2$ surface through electrostatic interactions. One should keep in mind that those orientations are only proposed based on the native structure but they still show that ToF-SIMS is a powerful tool for probing the structural properties of adsorbed proteins with a direct link to the a.a. sequence in the protein.

4.4 Conclusion

Adsorption of both β LG and BSA was carried out on $-\text{COOH}$, $-\text{CH}_3$ and $-\text{NH}_2$ terminated SAMs of thiolates on polycrystalline gold. Only the $-\text{CH}_3$ and $-\text{NH}_2$ terminated surfaces showed a clear adsorption of the β LG, with a higher mass uptake on the $-\text{CH}_3$ terminated one. The weak interaction of the protein with $-\text{COOH}$ surfaces is explained by the fact that both the surface and the protein were negatively charged at the pH used for adsorption. For BSA, adsorption was completed on all three surfaces with again a higher amount on the $-\text{CH}_3$ one. It is interesting to see that even if adsorption was not electrostatically favorable on the $-\text{COOH}$ surface with again both the protein and the surface negatively charged, it still took place and an adsorbed protein mass was detected with all applied techniques. This is explained by a restructuring of the labile BSA protein that maximizes the interactions between the surface and the protein.

Regarding the orientation of β LG on both the $-\text{CH}_3$ and $-\text{NH}_2$ SAMs, a clear separation of the samples was obtained from PCA calculations performed on the ToF-SIMS results. Taking into account the physico-chemical condition of adsorption and the molecular structure of this rigid protein, different orientations have been proposed. According to those results, the β LG would preferentially adsorb in a flat lying position with lysine residues pointing upward on the $-\text{NH}_2$ terminated samples, due to electrostatic interactions. As for the $-\text{CH}_3$ -terminated surfaces, two possible orientations are suggested by the ToF-SIMS results, either upright or flat lying, but flipped vertically with respect to the $-\text{NH}_2$ surfaces. This interpretation, in agreement with the complementary information obtained from other

analytical techniques, is also consistent with the idea that adsorption is driven by hydrophobic interactions.

For BSA adsorption, determining an orientation with the same method was difficult because of two main parameters: the lack of a 3D model of the protein in other states than the native one and the extreme lability of the protein that undergo drastic changes in its (secondary or tertiary) structure regarding the external conditions. No orientation could be proposed for the adsorption on the $-\text{COOH}$ surface. However, two opposite orientations of an open form of the protein have been suggested on the $-\text{CH}_3$ and $-\text{NH}_2$ surface. This state of the adsorbed protein would be consistent with the one described in solution at physiological pH.

This study demonstrated, if needed to be, the extreme sensitivity of ToF-SIMS to determine the structural properties of adsorbed proteins. The direct access to fragments corresponding to a.a. in the protein sequence combined with the low sampling depth of the technique makes it a tool of choice for studying adsorption even with only a partial information on the structure of the proteins itself. Even for *soft* proteins such as BSA, information provided by ToF-SIMS and PCA was precious to determine the adsorption state upon interaction with different surfaces. This methodology will be applied in the next chapter to the direct determination of the orientation of antibodies in link with more traditional methods for bio-recognition.

5 Toward a More Realistic System – Antibody Adsorption and Grafting

Results presented in this chapter have been published in 2014 under the title “ToF-SIMS Investigation of the Orientation of Adsorbed Antibodies on SAMs correlated to biorecognition tests” (*J. Phys. Chem. C*, **2014**, *118* (4), 2085-2092).

Based on the work on model proteins presented in the previous chapter, we investigated a more realistic and complex case; the adsorption of a monoclonal mouse IgG1 antibody directed toward glutamate dehydrogenase (Anti-GDH) on –COOH- and –CH₃-terminated SAMs. The studied antibody/antigen (Ab/Ag) couple is used in strip tests, developed by our partner Coris BioConcept (Gembloux, Belgium), for the detection of gastroenteritis of bacterial origin. The orientation of the antibody have been studied in three situations: adsorbed or grafted onto the –COOH

surfaces and adsorbed onto the $-CH_3$ ones. The $-NH_2$ -terminated SAM was not used for this study in order to reduce the quantity of antigen necessary but also because we wanted to probe the differences in adsorption induced by simple adsorption or covalent grafting on the same type of surface. We could have imagined using the $-NH_2$ SAMs in this aim but that would mean heavier chemical modification of the antibodies themselves to activate their $-COOH$ moieties. It was then chosen to keep only the $-COOH$ SAMs for this study in addition to the $-CH_3$ ones that proved to retain greater quantities of proteins in model studies. Adsorption has been investigated using the combination of ToF-SIMS and PCA as described earlier. This methodology gives crucial information on the preferential orientations resulting from each interaction. In a second stage, PM-IRRAS and QCM-D measurements were used to perform biorecognition tests, results were correlated to the orientation in each case.

5.1 Samples

SAMs formation and their characterization have been described earlier (see Chapter 3). Two procedures were used for the deposition of antibodies on the $-COOH$ -terminated surface: adsorption and grafting. To perform a chemical attachment (grafting), the acid layer was activated with a mixture of NHS-EDC as shown in chapter 3. The monoclonal Anti-GDH antibody used is a mouse IgG1 and is directed toward a specific GDH produced in bacteria responsible for certain forms of gastro enteritis (*Clostridium difficile*). Anti-GDH antibodies and the corresponding antigen GDH (Glutamate Dehydrogenase) were kindly provided by Coris BioConcept and they were

both used as received after dilution to $5 \mu\text{g.mL}^{-1}$ in a carbonate buffer (pH 9.5). The carbonate buffer was chosen in accordance with our partner Coris BioConcept. They used a pH of 9.5 when adsorbing antibodies to ensure a global negative charge of the proteins. In our studies, this buffer was kept during all adsorption steps (antibody, milk saturation or antigen) to keep the same media at all time, especially for QCM-D measurements. QCM-D is indeed really sensitive to adsorption media. Changing the buffer in the middle of the experiments would necessitate much longer stabilization steps in between each type of protein adsorption. All experiments described below are performed at room temperature. For QCM-D measurements, the flow cell is maintained at a temperature of 20.0 ± 0.1 °C.

As for model proteins, adsorptions of the Anti-GDH on the different surfaces were achieved by immersing SAM functionalized gold substrates in the $5 \mu\text{g.mL}^{-1}$ protein solution for 90 min in 24-well plates. The concentration and time were determined by performing Anti-GDH adsorption isotherms with concentrations ranging from 0.5 to $10 \mu\text{g.mL}^{-1}$ and time ranging from 15 min to 2h. The $5 \mu\text{g.mL}^{-1}$ / 90 min couple was shown to be the best compromise to reach an adsorption plateau and not use too much product for each experiments (antibodies can cost up to a few thousands euros per mg). Samples were then successively rinsed in a carbonate buffer well for 2 min and in two separate MilliQ water wells for respectively 2 and 10 min. A final drying step is performed under N_2 before ToF-SIMS or PM-IRRAS analysis under UHV or in air respectively.

Commercially available powder milk (Régilait, France) was used to “saturate” the surface and prevent non-specific adsorption of proteins. Régilait is a commercial product whose exact composition is unknown, however it is considered to be mostly composed of proteins of various sizes and isoelectric points. The great variability of proteins will ensure a maximum coverage of the surface. Milk used during all this study was taken from the same box to avoid any reproducibility problems. The antibody-covered surfaces were immersed for 60 min in a powder milk solution at $5 \mu\text{g}\cdot\text{mL}^{-1}$ in carbonate buffer and rinsed, as previously described, in buffer and two times in MilliQ water before drying under N_2 and analyzing with PM-IRRAS. Finally for biorecognition tests, samples were immersed in a buffer solution of GDH at $5 \mu\text{g}\cdot\text{mL}^{-1}$ for 90 min, rinsed in buffer and MilliQ water and dried in N_2 before PM-IRRAS analysis.

For QCM-D measurements the SAM-functionalized crystals were first placed in the flow cell. The successive protein buffer solutions (antibody, milk or antigen) are then flowed at a rate of $50 \mu\text{L}\cdot\text{min}^{-1}$ with buffer rinsing steps in between. In the case of the $-\text{COOH}$ surfaces (before or after activation), the Anti-GDH adsorption was really slow while it was faster on the $-\text{CH}_3$ surfaces. The Anti-GDH solution was then flowed for 90 min on $-\text{COOH}$ surfaces where only 30 min were necessary to obtain a good signal on the $-\text{CH}_3$ ones. Functionalization steps are summed up in Figure 5.1.

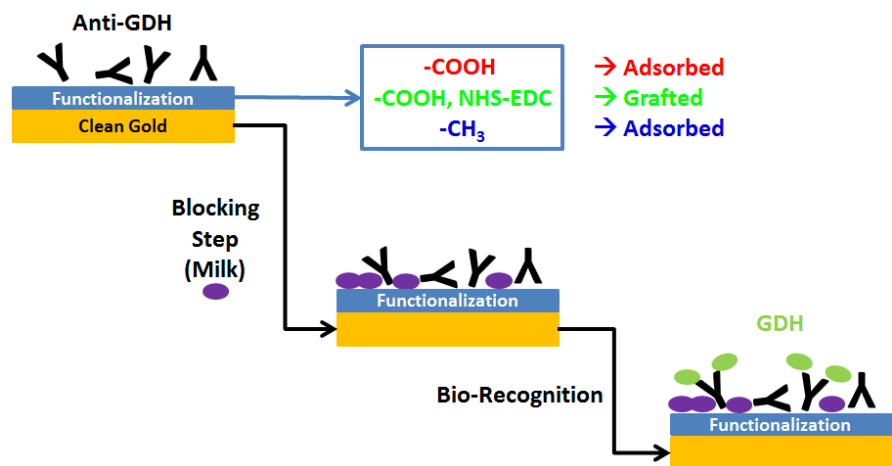


Figure 5.1 Schematic summarizing the different steps after SAMs functionalization of gold samples using Anti-GDH antibodies and milk saturation before testing the bio-recognition of the antigen (GDH)

5.2 Results

5.2.1 Anti-GDH Adsorption on SAMs

Protein adsorption was investigated at each step by PM-IRRAS on a minimum of three samples. The Amide I and II bands at 1660 and 1550 cm^{-1} , evidence the presence of proteins. Moreover, the integrated areas of these bands provide quantitative information on the amounts of adsorbed proteins.⁵⁴ Typical PM-IRRAS spectra after each adsorption step together with integrated Amide I and II band areas are presented in Figure 5.2. Results in Figure 5.2 show that Anti-GDH is adsorbed onto all surfaces. In the case of adsorption on $-COOH$ -terminated SAMs prior or after NHS-EDC activation, the quantity of adsorbed antibodies is similar (2.1 and 2.2 a.u. for the amide I and II band area). Larger quantity is observed in the case of physisorption on the $-CH_3$ -terminated surface with an area of 3.0 a.u.. This

result is in agreement with our previous observations showing that proteins tend to adsorb preferentially on this surface due to strong hydrophobic interactions.

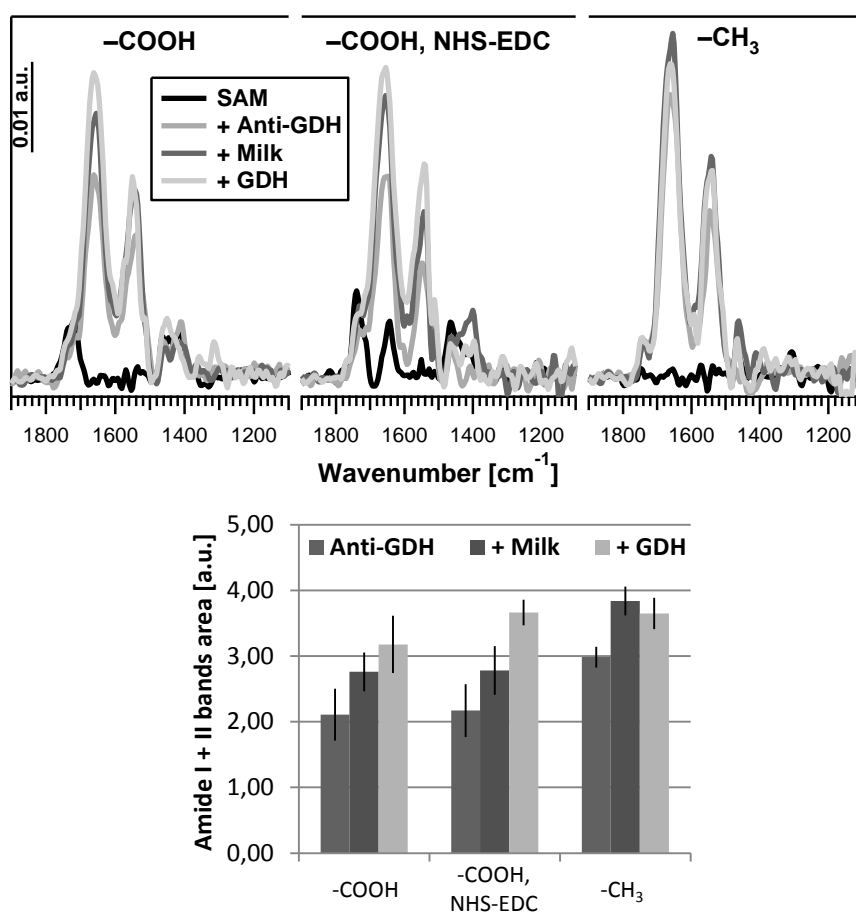


Figure 5.2 Characteristic PM-IRRAS signals are presented for $-\text{COOH}$ SAMs before (adsorption) or after activation (grafting) and for $-\text{CH}_3$ SAMs at each protein adsorption step (bare SAM, Anti-GDH, Milk saturation and GDH recognition). Graph in the bottom panel represents the Amide I and II bands areas variation for each surface at each step

Anti-GDH adsorption on all three surfaces was also monitored *in-situ* (i.e. in the liquid phase) using QCM-D. For both $-\text{COOH}$ -terminated surfaces, 2

experiments were performed with 2 functionalized QCM crystals in parallel giving a total of 4 samples. In the case of the $-\text{CH}_3$ -terminated SAMs, 2 crystals were analyzed the first time and only one the second time, giving a total of 3 samples. The complete dataset is summed-up in Table 5.1 presenting the shifts in frequency for all measurements at each step of the functionalization for the 3rd, 5th, 7th and 9th overtone.

Table 5.1 Frequency shifts (normalized on the considered overtone) measured in QCM-D for all experiments and at each adsorption step (Anti-GDH, Milk, GDH); OT = Overtone

	OT →	$\Delta F_{\text{Anti-GDH}}$				ΔF_{Milk}				ΔF_{GDH}			
		3rd	5th	7th	9th	3rd	5th	7th	9th	3rd	5th	7th	9th
-COOH (4 Samples)	1-1	18.6	18.2	17.2	16.3	12.5	10.7	10.3	9.3	3.5	3.2	2.9	3.5
	1-2	15.3	13.9	13.1	13.3	11.5	11.1	10.3	9.8	3.0	2.6	2.4	2.2
	2-1	12.7	11.5	10.8	10.2	5.9	5.1	4.9	4.6	1.5	1.3	1.2	1.1
	2-2	10.0	9.0	8.4	7.9	4.7	4.2	3.9	3.8	1.0	1.0	0.8	0.7
-COOH, NHS-EDC (4 Samples)	1-1	16.9	15.5	15.3	15.0	14.7	13.5	12.6	12.1	4.9	4.5	4.3	4.0
	1-2	15.3	13.9	13.0	12.5	14.0	12.8	12.1	11.7	5.7	5.1	4.9	4.7
	2-1	10.8	9.8	9.6	8.9	13.5	12.4	11.6	11.3	5.2	4.6	4.5	4.1
	2-2	10.6	9.5	9.2	8.7	12.9	12.0	11.2	10.8	4.8	4.4	4.0	3.8
-CH ₃ (3 Samples)	1-1	29.0	28.3	27.9	27.5	11.7	10.9	10.6	10.1	0.5	0.5	0.5	0.6
	1-2	27.8	26.8	26.3	25.8	11.7	10.8	10.6	10.4	0.4	0.3	0.1	0.0
	2-1	25.5	24.3	23.6	23.2	14.2	12.8	12.4	11.9	-0.2	-0.2	-0.4	-0.2

Figure 5.3 presents typical frequency and dissipation shifts at the 5th overtone recorded upon successive protein injections on the three surfaces. Since dissipation remains lower than $3 \cdot 10^{-6}$, the observed shifts in frequency can be correlated to the quantity of adsorbed proteins on the surface (Sauerbrey model). Upon rinsing with the buffer, there was no desorption of Anti-GDH showing a non-reversible adsorption of antibodies. The quantity of Anti-GDH deposited on the $-\text{COOH}$ (before or after activation by NHS-EDC) surfaces is lower than on $-\text{CH}_3$ -terminated SAMs, in agreement with the PM-IRRAS data. The frequency shift observed after buffer rinsing are 12.9 ± 3.5 , 12.2 ± 2.8 and 26.3 ± 1.9 Hz on $-\text{COOH}$ -, activated $-\text{COOH}$ - and $-\text{CH}_3$ -terminated surfaces respectively. Measured frequency shifts for each surface (3 or 4 samples) and the 3rd, 5th, 7th and 9th

overtones were used to calculate the variability for each type of sample (Table 5.1).

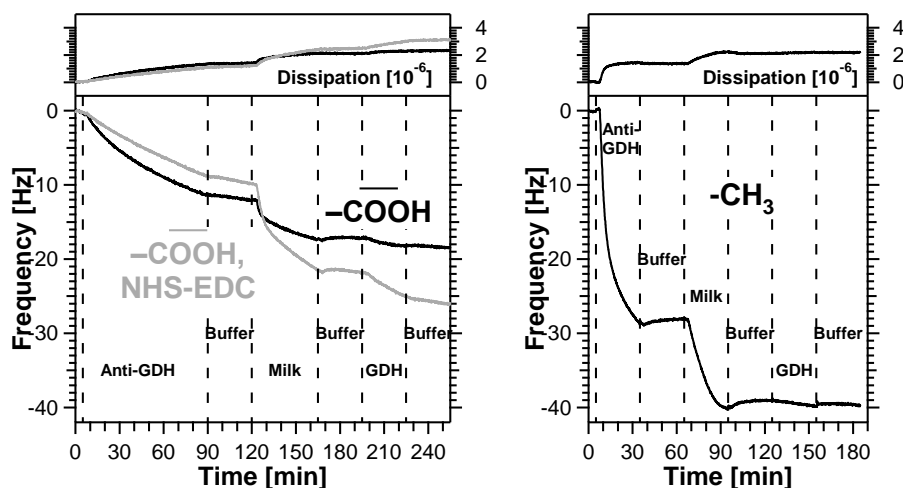


Figure 5.3 Characteristic QCM-D results showing all adsorption steps (Anti-GDH, Milk and GDH) on $-\text{COOH}$ SAMs, $-\text{COOH}$ SAMs after activation, and $-\text{CH}_3$ SAMs; the 5th overtone for one experiment is presented here.

The same trend is observed for both techniques with larger adsorption on $-\text{CH}_3$ surfaces, and Anti-GDH adsorption stable upon rinsing in each case. The relative difference measured in QCM-D between the $-\text{COOH}$ -terminated surfaces (before or after activation) and the $-\text{CH}_3$ one is larger than that measured by PM-IRRAS. The $-\text{COOH}$ to $-\text{CH}_3$ Anti-GDH quantity ratios are 0.7 from PM-IRRAS and 0.4 from QCM-D. Rinsing and drying of the samples prior to analysis for PM-IRRAS could lead to the removal of adsorbed antibodies thus explaining those differences. Influence on GDH recognition will be presented after the characterization of the adsorbed antibody layers on $-\text{COOH}$ -, activated $-\text{COOH}$ - or $-\text{CH}_3$ -terminated SAMs using ToF-SIMS and PCA calculations.

5.2.2 Exploring Anti-GDH Adsorption Using ToF-SIMS and PCA

PM-IRRAS and QCM-D showed differences in the amounts of adsorbed Anti-GDH but no information about the orientation could be retrieved at this point. PCA calculations were then performed on ToF-SIMS measurements to obtain a direct probe of the preferential orientation, if any, on the surfaces. After the first PCA calculations, the main differentiation between samples was obtained on peaks originating directly from the SAM surfaces and not only from the protein layer. In order to detect the proper separation due to differences in the protein orientation, the peaklist presented in Chapter 2 was adapted and several peaks were removed, they can be separated in 3 categories:

CH₂N⁺ and **CH₄N⁺**, respectively at a mass of 28.02 and 30.04 originate from **nearly all a.a.** and therefore did not give any information about the orientation of the adsorbed protein but most likely on the adsorbed quantity of proteins.

C₂H₄N⁺, **C₂H₆N⁺**, **C₃H₈N⁺**, **C₅H₁₀N⁺**, **C₅H₁₂N⁺** and **C₄H₁₀N₃⁺** respectively at 42.03, 44.05, 58.07, 84.09, 86.10 and 100.08 were evidenced to be characteristic of the analysis of the **activated –COOH-terminated SAMs** with NHS and EDC. These peaks showed already really strong intensities on the activated surfaces before Anti-GDH adsorption as it is shown on Figure 5.4. They could result from the fragmentation of residual EDC groups on the surface whom the

chemical formula is $C_8H_{17}N_3^+$ (see Chapter 3 for the exact structure of the molecule).

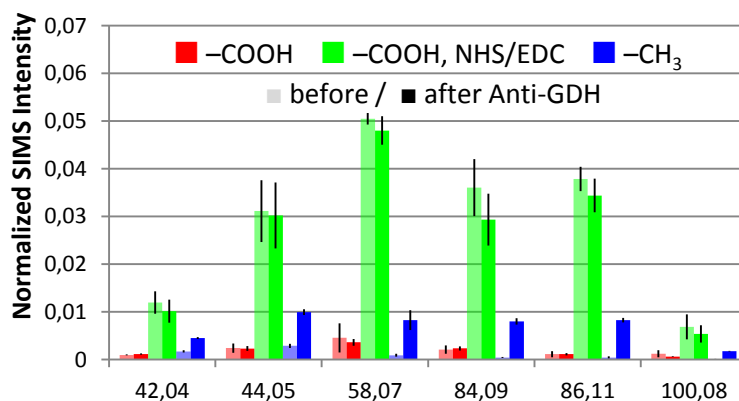


Figure 5.4 SIMS intensity of a.a. fragment peaks perturbed by the activation of the $-COOH$ surfaces as evidenced with PCA calculation

$CH_6N_3^+$ and $C_2H_7N_3^+$ respectively at 60.06 and 73.07 were identified to interfere with the $C_3H_8O^+$, the $C_4H_9O^+$ peaks on the $-COOH$ -terminated SAMs giving a PCA separation not solely based on information coming from the protein itself.

Consequently, a peaklist of 34 fragments was used to perform PCA calculations in this study. In Figure 5.5 are presented the scores for PC1 and PC2; from PC1 (90% of variance) a clear separation of the $-CH_3$ -terminated surfaces is observed with large positive scores. Surfaces bearing $-COOH$ -terminated SAMs give negative scores on PC1 when Anti-GDH is adsorbed without prior activation of the acid functions. When Anti-GDH is grafted, the PC1 scores are still negative but with a shift toward positive values (closer to zero). An additional separation of these two surfaces arises from PC2 (only 9% of variance) where activated surfaces exhibit positive scores

and non-activated surfaces negative ones (together with $-\text{CH}_3$ -terminated surfaces).

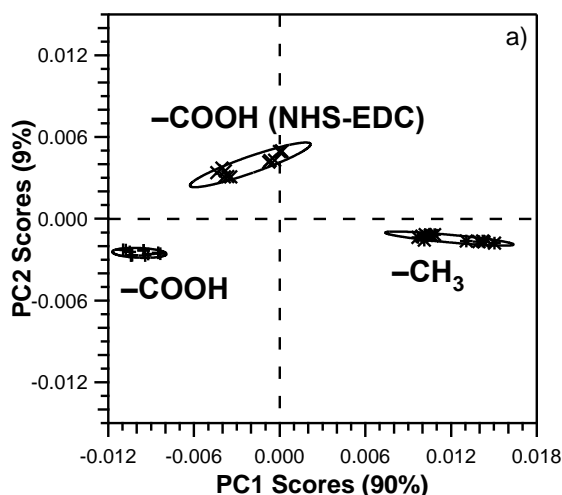


Figure 5.5 PCA calculations results (scores from PC1 and PC2) on $-\text{COOH}$ -, $-\text{COOH}$ -activated with NHS-EDC and $-\text{CH}_3$ -terminated SAMs after Anti-GDH adsorption and adaptation of the a.a. peaklist

The loadings for both PCs are presented in Table 5.2. On PC1, large positive loadings are obtained, indicating a strong separation of the corresponding samples. The positive scores in PC1 are attributed to the $-\text{CH}_3$ -terminated surfaces after adsorption of Anti-GDH. Amino acids (a.a.) corresponding to peaks giving positive PC1 loadings are proline, valine, arginine (or histidine), serine and threonine. These amino acids are the most exposed after adsorption of Anti-GDH on $-\text{CH}_3$ -terminated SAMs. For negative loadings, very small values are observed, indicating a weaker separation of the corresponding samples on the score plot ($-\text{COOH}$ with or without activation). The corresponding a.a. are cysteine, arginine or methionine.

Table 5.2 Most important positive (Pos.) and negative (Neg.) loadings from PC1 and PC2 after PCA calculations performed on ToF-SIMS measurements of the adsorption of Anti-GDH on –COOH, activated –COOH and –CH₃ SAMs.

PC1 (90% of variance) loadings					
Pos.	Mass	a.a.	Neg.	Mass	a.a.
0.83	70.07	Pro	-0.05	46.99	Cys
0.38	72.08	Val	-0.04	43.02	Arg
0.16	110.07	Arg/his	-0.01	127.10	Arg
0.16	60.05	Ser	-0.01	58.99	Cys
0.15	74.06	Thr	-0.01	61.01	Met
PC2 (9% of variance) loadings					
Pos.	Mass	a.a.	Neg.	Mass	a.a.
0.63	72.08	Val	-0.35	46.99	Cys
0.19	81.04	His	-0.27	69.03	Thr
0.14	110.07	Arg/His	-0.26	74.06	Thr
0.13	127.10	Arg	-0.23	70.07	Pro
0.13	56.05	Lys/Phe/Met	-0.18	61.01	Met

PC2, with only 9% of variance, still gives a small separation between Anti-GDH adsorbed onto –COOH- or on –CH₃-terminated SAMs on one hand (negative scores/loadings), and on activated –COOH surfaces on the other hand (positive scores/loadings). Characteristic proline and threonine peaks, already identified for –CH₃ surfaces separation in PC1, are evidenced in the negative PC2 loadings. Cysteine and methionine, which allowed separation of the two –COOH surfaces in PC1 (negative scores), are also observed in negative PC2 loadings. On the other hand, the peak corresponding to valine has positive loadings in PC2 (specific to activated –COOH surfaces), but was previously attributed to the separation of –CH₃ surfaces (positive PC1 loadings). This could explain the shift toward positive values on PC1 scores of samples corresponding to the activated –COOH surfaces (Figure 5.5). The separation of the adsorption of Anti-GDH on the activated –COOH-terminated surface from the non-activated one is characterized by PC1 negative loadings and PC2 positive ones. Arginine together with histidine peaks appears to make most of the separation for these two surfaces. The

determination of possible orientations of the antibody on the different surfaces based on these results will be discussed after presenting the results of biorecognition tests.

5.2.3 Testing Biorecognition of GDH by Anti-GDH

Before testing the biorecognition capabilities of Anti-GDH adsorbed onto the three surfaces, a blocking step was performed using a milk solution to avoid non-specific recognition of the antigen (*i.e.* adsorption on the substrate). Milk was chosen because it is a mixture of different proteins with a variety of molecular weights and electrostatic properties that will maximize adsorption on the gold surfaces. It is considered that after milk adsorption, the entire surface of the substrate is covered with either Anti-GDH or proteins contained in milk. From both PM-IRRAS (Figure 5.2) and QCM-D (Figure 5.3) the signal of adsorbed proteins is increased after milk adsorption. An increase of the IR amide I and II bands area of 30% is observed for all surfaces. In QCM-D, the changes in frequency after milk adsorption on Anti-GDH covered surfaces vary between 40% (for $-\text{CH}_3$ surfaces) and 60% (for activated $-\text{COOH}$ surfaces). Those differences could be explained by the fact that in QCM-D the water trapped in protein layer is also measured.

Upon GDH interaction with $-\text{CH}_3$ -terminated SAMs, PM-IRRAS and QCM-D showed no protein adsorption indicating the absence of molecular recognition. No frequency shifts occur in QCM-D upon flowing antigen solution and even a slight decrease of the amide bands area from 3.8 a.u. to 3.7 a.u., possibly due to the removal of Anti-GDH or milk proteins upon

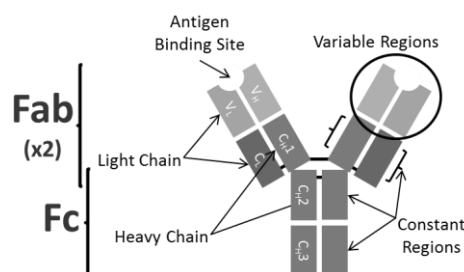
rinsing and drying, is observed in PM-IRRAS. On $-\text{COOH}$ -terminated surfaces, the amide bands area increased from 2.8 to 3.2 a.u. in PM-IRRAS, and a frequency shift of 2.0 ± 1.0 Hz was observed in QCM-D after flowing GDH solution. In the case of activated $-\text{COOH}$ surfaces, the measured amide bands area increased by 0.9 a.u. and the measured frequency shift was 4.6 ± 0.5 Hz after GDH exposure. Biorecognition of GDH by the specific Antibody was thus effective on both $-\text{COOH}$ -terminated SAMs but not on the $-\text{CH}_3$ one. Those results will be further analyzed in the discussion section by comparing these values to the quantity of adsorbed Anti-GDH and by normalizing the results with the mass of the corresponding protein (antibody or antigen). But first, the orientation of Anti-GDH on the different surfaces will be discussed based on ToF-SIMS and PCA results.

5.3 Discussion

5.3.1 Orientation of the Antibody

As pictured in Figure 5.6, antibodies can be described as Y shape proteins with the two Fab fragments at the top side of the Y. Those are both composed of 2 variable parts V_L and V_H and two constant ones C_L and C_H1 (the L and H subscript refer to light and heavy chains in the antibody, see Figure 5.6). On the other side of the antibody, the Fc fragment is composed of the associated C_H2 and C_H3 regions from the two different heavy chains. The antibody used in this study is a monoclonal mouse IgG1 whose exact a.a. sequence of its Fab fragment is not determined. Nevertheless, the sequence of the Fc fragment is the same for all IgG1 and can be retrieved in the UniProt database.¹⁶¹ Most of the amino acids present in the C_H2 and C_H3

regions (forming the Fc fragment) are shown in the table inserted in Figure 5.6. Apart from Arg or His, all the a.a. explaining the separation of Anti-GDH physisorbed on $-CH_3$ -terminated SAMs are amongst the highest concentration a.a. in the Fc. Proline, valine, serine and threonine concentrations in the Fc fragment are 8.9, 9.3, 7.9 and 8.4%, respectively. This strongly indicates that, on the $-CH_3$ surfaces, adsorbed Anti-GDH antibodies mostly expose the Fc region, i.e., they are preferentially attached upside down, the epitopes being in contact with the SAM and not accessible for further Ag recognition. In addition to the suggested orientation, conformational changes of the antibody upon adsorption should be accounted for in the PCA separation. Due to the lack of information about the Anti-GDH exact structure, it will be unfortunately difficult to thoroughly discuss them here.



a. a.	number of a.a.			%age		
	C _{H2}	C _{H3}	Fc	C _{H2}	C _{H3}	Fc
Val	14	6	20	13.1	5.6	9.3
Pro	10	9	19	9.3	8.4	8.9
Lys	9	9	18	8.4	8.4	8.4
Thr	9	9	18	8.4	8.4	8.4
Ser	9	8	17	8.4	7.5	7.9
Glu	8	7	15	7.5	6.5	7.0
Asn	3	9	12	2.8	8.4	5.6
Phe	8	4	12	7.5	3.7	5.6
Gln	5	6	11	4.7	5.6	5.1
Others	32	40	72	29.9	37.4	33.6
Total	107	107	214	100.0	100.0	100.0

Figure 5.6 General representation of an antibody (Mouse IgG1) and table of the most represented a.a. in the constant fragment (Fc)

On the –COOH-terminated surfaces (before or after activation), most of the a.a., responsible for their separation in PCA (Cys, Arg, Met or His), are not present in high concentration in the Fc fragment. One can thus deduce that another part of the antibody is preferentially exposed on those surfaces, *i.e.* the Fab fragments, whose a.a. sequence is not known. Such an orientation is expected to lead to better biorecognition features. Moreover, the separation of the –COOH-terminated surfaces in PC2 (only 9% of variance) suggests slight differences in the preferential orientation of the antibodies on these two surfaces. Results of biorecognition tests on –COOH-terminated surfaces will be interpreted in the light of these suggested preferential orientations in the next section of the discussion.

In a study by Wang *et al.*,⁷⁶ the authors tracked the orientation of an adsorbed IgG using ToF-SIMS and PCA. They compared the mass spectra after adsorption of the whole Anti-hCG antibody to those of the Fab or Fc fragments alone on several SAMs surfaces. They were then able to conclude that the antibodies adopted various orientations, end-on or head-on, on the –COOH- or –NH₂-terminated SAMs. Our approach is a real case study analyzing the adsorption of the whole GDH antibody. However, since the a.a. sequence for the Fc fragments of mouse IgG1 is known, we were able to identify the most likely orientations of the antibodies on the various investigated surfaces.

5.3.2 Influence of Orientation on Biorecognition

Prior to biorecognition tests with anti-GDH, the surface was saturate with milk. During this step, one could wonder if Anti-GDH could not be replaced

with milk protein on the surface following the so-called “Vroman Effect”.¹¹ It was indeed demonstrated by Vroman *et al.* that, in plasma, low molecular weight proteins that adsorb quickly on the surface could be displaced by larger one after a certain adsorption time. In our case, the antibodies have a larger molecular weight (about 150 kDa) than most of milk proteins. Milk proteins have a molecular weight around 20 kDa (for more than 95 % of them) together with some antibodies ($\approx 3\%$).¹⁶² The “Vroman Effect” will then most likely be limited. We will then consider that milk proteins co-adsorb with Anti-GDH on our surfaces and cover the all surfaces. Moreover, in the case of the covalent grafting antibodies could not be easily displaced by other proteins.

No recognition of GDH by adsorbed Anti-GDH was observed on $-\text{CH}_3$ -terminated surfaces. On the basis of previously discussed ToF-SIMS and PCA data, Anti-GDH adsorbed onto this surfaces, is likely oriented preferentially with its Fc fragments facing up. This is consistent with the absence of GDH biorecognition, because Fab fragments are not accessible to target recognition. Let’s add that adsorption on such hydrophobic surface may modify antibody conformation/folding resulting in a loss of bioactivity. Moreover, the structure of GDH shows the presence of both hydrophilic and hydrophobic regions on its surface (see PDB structure 1HRD for an analogue of the GDH used in this study¹⁶³). On a hydrophobic $-\text{CH}_3$ -terminated surface, the anti-GDH likely interacts via its hydrophobic epitopes.

In the case of both –COOH-terminated surfaces, GDH was recognized by the immobilized Anti-GDH as evidenced by PM-IRRAS and QCM-D. In order to quantify this biorecognition, the ratio of the numbers of GDH versus Anti-GDH proteins was calculated (A_g/A_b). The GDH in use for this study is formed of 449 a.a. and has a molecular mass of ≈ 50 kDa (PDB structure 1HRD).¹⁶³ As for Anti-GDH, the exact a.a. composition is unknown but IgG1 antibodies are generally considered to weigh ≈ 150 kDa. In PM-IRRAS the area of amide bands is proportional to the quantity of adsorbed proteins, the ratio GDH/Anti-GDH is then calculated using Eq. 5.1,

$$\frac{N_{GDH}}{N_{Anti-GDH}} = \frac{(A_{GDH} - A_{Milk}) m_{Anti-GDH}}{A_{Anti-GDH} m_{GDH}} \quad (5.1)$$

where N_x is the number of protein x, A_n is the area of the amide I and II bands at the corresponding n step and m_x is the mass of the x protein.

In QCM-D, considering that those measurements remain in the limits of validity of the Sauerbrey model, and assuming that the amount of trapped water molecules is similar for both proteins, Anti-GDH and GDH, the change in frequency at each step can be correlated to the quantity of adsorbed proteins.¹⁶⁴ The GDH/Anti-GDH ratio could thus be calculated using Eq. 5.2,

$$\frac{N_{GDH}}{N_{Anti-GDH}} = \frac{\Delta F_{GDH} m_{Anti-GDH}}{\Delta F_{Anti-GDH} m_{GDH}} \quad (5.2)$$

where N_x is the number of protein x, ΔF_n is the delta in frequency at the corresponding n step and m_x is the mass of the x protein. Results are summed-up in Table 5.3 and show that calculated ratios are in good agreement for the two techniques.

Table 5.3 Calculated ratios of the recognized GDH over the quantity of Anti-GDH on –COOH-terminated SAMs weighed by their respective masses (50 and 150 kDa per unit) obtained from both PM-IRRAS and QCM-D measurements

	PM-IRRAS	QCM-D
–COOH	0.6 ± 0.3	0.4 ± 0.1
–COOH, NHS-EDC	1.3 ± 0.5	1.2 ± 0.2

In the case of the Anti-GDH physisorbed on –COOH surfaces, only one GDH appears to be recognized per two adsorbed antibodies (GDH/Anti-GDH ratio \approx 0.5). When grafting the antibodies to the surface, more than one GDH protein per grafted Anti-GDH is recognized (ratio \approx 1.3). This suggests differences in the orientation of the physisorbed or grafted antibodies as shown earlier by the distinction obtained on PC2 in PCA calculations. In the case of grafted antibodies, a covalent bond is formed between acids on the surface and amines of the Anti-GDH leading to a better biorecognition. In Figure 5.6, one can see that lysine residues, an amine terminated a.a., are largely represented in the Fc fragments (8.4%). They could therefore interact preferentially with activated acid moieties on the surface and force the antibody to adopt an orientation with its Fab fragments up. In the case of physisorbed Anti-GDH, lower biorecognition is observed. Weaker interactions are involved here. The main ones would be electrostatic interactions between acid moieties of the surface and amine from the antibody but H-bond or hydrophobic interactions should also intervene. The antibody is thus prone to adopt various orientations after adsorption (tilted or lying on the surface with no or less access to the Fab fragments for the antigen). Moreover, weaker interactions with the surface could lead to the displacement in the solution of Ab/Ag complexes by competition. Figure 5.7 shows a scheme to sum-up the results obtained in each case.

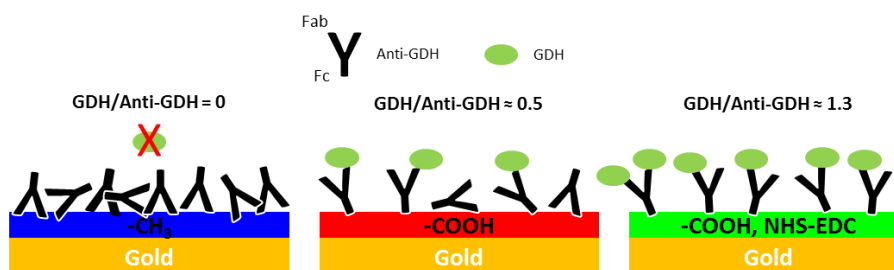


Figure 5.7 Schematic representation of the physisorption or grafting of Anti-GDH on $-CH_3$ - or $-COOH$ -terminated SAMs (before and after activation by NHS-EDC) and consequences on the GDH biorecognition. The milk blocking step is not represented for sake of clarity

5.4 Conclusion

The interaction of a monoclonal antibody Anti-GDH, with three SAMs terminated by $-CH_3$ -, $-COOH$ - and $-COOH$ -activated by NHS-EDC was investigated using PM-IRRAS and QCM-D. The orientation of the so-formed layer was explored by ToF-SIMS and PCA. PM-IRRAS and QCM-D results showed that on $-CH_3$ -terminated SAMs, Anti-GDH adsorbed in greater quantities, possibly due to hydrophobic interactions. However, ToF-SIMS and PCA data suggested that in this case, anti-GDH was oriented upside down. Those results were obtained using the amino acids sequence of the Fc fragment of the antibody but could also come from conformational changes in the structure of the antibody due to the strong hydrophobic interactions. This was later confirmed by biorecognition tests with no recognition of the target, GDH, on this surface.

In both other cases, physisorbed or grafted Anti-GDH on $-COOH$ surfaces, no clear orientation was determined but PCA results suggested an orientation different from the one observed upon adsorption on $-CH_3$ -

terminated SAMs (PC1). Moreover, some differences in orientation between the physisorbed and the grafted antibodies were observed (PC2). Biorecognition measurements showed clearly that GDH recognition mostly takes place when the Anti-GDH is grafted to the –COOH-terminated surface. This was explained by the formation of covalent bonds favoring the preferential heads-up orientation of Anti-GDH. Orientation of Anti-GDH physisorbed on the surface is governed by weaker electrostatic interactions, some of the measured biorecognition could then be in competition with displacement of Ab/Ag complexes in the solution. Covalent bonds are indeed characterized by energies of about 500 kJ.mol^{-1} while the energy stored by electrostatic interactions is about 100 times weaker ranging from 1 to 10 kJ.mol^{-1} .¹⁶⁵

In the perspective of biosensor development, our studies have a fundamental interest by detecting directly the orientation of adsorbed antibodies. PCA calculations allowed the prediction of the orientation before biorecognition tests. Tests with the antigen showed that covalent grafting of mouse IgG1 through their amine function on a –COOH-terminated surface could improve by nearly a factor 3 the detection of the antigen compare to adsorption only driven by electrostatic interactions. Such analysis could be carried out for different types of antibodies to help in the development of template surfaces favoring an end-on orientation suitable for biorecognition. PCA can help screening numerous samples in a small amount of time without testing all of them for the antigen. A review by Trilling *et al.* in 2013,¹⁶⁶ showed the interest of finding easily applicable methods for probing immobilized antibodies orientation on surfaces. ToF-

Chapter 5

SIMS in combination with PCA present a great interest since it provides chemical information on the few top nm of the surface.

6 Conclusion and Perspectives

6.1 Principal Results

During this work, the objective was to explore the adsorption modes (orientation/conformation/folding/bioactivity) of several proteins on chemically well controlled surfaces and to link them to the physico-chemical properties of the surface (hydrophobicity/charge). SAMs of thiolates on gold have been chosen as template surfaces to ensure a homogeneous surface for further adsorption. The combination of different surface sensitive techniques was the key to a successful determination of the structural properties of adsorbed proteins.

First, three different types of surfaces were obtained and characterized: one hydrophobic surface with $-\text{CH}_3$ terminations, and two hydrophilic ones with positive and negative charges ($-\text{NH}_2$ - and $-\text{COOH}$ -terminated SAMs respectively). The covalent grafting of proteins was explored after activation of the acid layer. Together with conventional techniques for characterizing SAMs (PM-IRRAS and XPS) we demonstrate experimentally

the **usefulness of large and slow Ar_n^+ clusters in ToF-SIMS to study organic thin films**. We confirm experimentally theoretical molecular dynamic studies that predicted that the lower the energy per atom is in the cluster, the higher the molecular signal coming from an organic coating is (the thiol SAM in our case). This is most likely due to a double effect: a low perturbation of the subsurface because of the low energy of each atom of the cluster after breaking in addition with a large number of species interacting with the surface (up to 10000 different atoms in the cluster).

The influence of the underlying SAMs was then probed after adsorption of different proteins. The application of a careful study of ToF-SIMS results using PCA calculations allows probing the orientation of different proteins in combination with infra-red, XPS or QCM-D measurements:

For **β LG, a *hard* protein, 3 orientations** were proposed regarding the underlying $-NH_2$ - or $-CH_3$ -terminated SAMs. In the case of $-NH_2$ surfaces, the charge state of both the surface and the proteins favored electrostatic interactions with specific parts of the protein that were identified with PCA and the 3D model of β LG. Hydrophobic interactions mostly intervene in the case of the $-CH_3$ surface together with intermolecular interactions of the protein.

The case of **BSA, a *soft* protein**, was more complicated but, still, **unfolding changes** from a known natural structure were shown. Mechanisms of opening of the proteins were proposed to describe the adsorb state of BSA on the different surfaces.

Finally **several orientations** were proposed for an **adsorbed or grafted antibody**. It was determined that the antibody is most likely in an head-up orientation in the case of adsorption or covalent grafting to a –COOH-terminated surface. These results were correlated to biorecognition measurements that confirmed the proposed orientations.

The study about antibodies showed the possibilities opened by combining adsorbed protein characterization at a molecular level in UHV with biorecognition measurements in air or in the liquid phase. It allows a full interpretation of the role of the underlying surface on the immobilization of the antibody on a biosensor-like surface. These results underline the power of the ToF-SIMS technique applied as a direct probe to determine protein orientation on a surface in order to predict its bioactivity. We will now see how the methodologies developed during this thesis can be applied for further fundamental or experimental developments in the biomedical field.

6.2 What's Next?

Characterizing organic thin films over metal surfaces is of great interest in ToF-SIMS measurements. As shown in chapter 3, the use of Ar_n^+ clusters sources improve greatly the results obtained with other sources (Ga^+ , Bi_n^+ or C_{60}^+) for thiol SAM characterization. It is now possible to retrieve a dominant molecular signal allowing the characterization of the organic films. However we would benefit in understanding better the physical process underlying the sputtering of organic films by large and slow clusters. One way is to run theoretical calculations using molecular

dynamics. Theoretical studies have been done for Ga^+ projectile but none for Ar_n^+ clusters bombardment of thiol SAMs. First attempt of such calculations have been performed in our group but no conclusive results have been obtained yet. These studies are really time-consuming due to the fact that a lot of interaction between atoms should be taken into account. Another way of continuing that work is the simulation of protein adsorption in order to correlate obtained experimental results with theoretical studies. This would help in understanding the exact interactions happening between the surface and the protein during the adsorption process. Moreover, this could lead to the identification of moieties interacting directly and driving conformational/unfolding changes or orientation on the surface. In a further step we could imagine the simulation of primary ion bombardment of adsorbed proteins samples.

On an experimental point of view, the methodology developed during this work based on statistical analysis of ToF-SIMS results open the way for the prediction of performances of antibody-based biosensors. It was shown that ToF-SIMS gives precious information on the orientation of antibodies adsorbed on surfaces even with a partial access to their a.a. sequence. The combination with PCA open the way for fast identification of adsorbed protein properties. We can imagine testing large arrays of samples with different surface properties and different antibodies to identify the best combination surface/antibody. This would benefit to the development of biosensors with a greater sensitivity and using less biological material. Antibodies can be really expensive, a better control of their orientation and

bioactivity upon adsorption is necessary to develop non-expensive diagnostic tests.

Finally the main perspective is the transposition of such adsorption mechanisms to nanoparticles (NPs). The ideal goal would be to design NPs ready for adsorption of antibodies in the right orientation for recognition (Fab fragments facing outside). Several types of NPs could be imagined for the different kind of possible Ab: IgG1, 2, 3 from different organisms (mouse, rabbit, human)... These NPs would be used in diagnostic strip tests (as the actual pregnancy test for example). Getting control over the orientation of Ab on the surface of NPs will improve the sensitivity of such tests and allow wasting less costly Ab for functionalization. The first step, in our case, would be to try to adsorb or graft Ab on $-COOH$ terminated NPs as shown on flat surfaces to check if we can still control the bioactivity. Some experiments have been performed in this way but they remain preliminary. The main questions are how to characterize such system and how to control the bioactivity after functionalization? Our first results in this direction are presented in annex.

A – Nanoparticles Functionalization Using Antibodies

In this annex, we will present recent work where results obtained on flat surfaces were transposed to NPs functionalization. The challenge here was to find the best way to characterize the antibody-functionalized NPs with our equipment (ToF-SIMS and XPS in this case). As mentioned earlier, antibody-functionalized NPs are fundamental in the development of diagnostic tests in strips. Such tests are developed by our partner Coris Bioconcept and the same principle applies for pregnancy tests. They are usually based on the migration of functionalized NPs. The principle is to adsorb/graft antibodies (Ab) on NPs and deposit them on an adsorbent strip (nitrocellulose). A drop of the substance to test (blood, urine...) is added and migrate with the NPs contained in the strip. If the corresponding antigen is in the test solution it will be recognized by the adsorbed Ab on the NPs. On the strip two lines with different properties are prepared. On the first one, which is the test line, a second Ab recognizing the antigen is

fixed. It will stop NPs that caught antigens. The second, i.e. the control line, is prepared with an anti-antibody catching all the other NPs. Due to the color of NPs, the lines will be revealed upon migration in the test. Two colored lines are synonym of a positive test and only one (the control line) of a negative one. In the development of such tests, NPs functionalization with Ab is usually empirical. It is then essential to develop new ways of functionalizing the NPs to improve the sensitivity of the tests and established protocols favoring the orientation of Ab on the NPs.

However, the focus of this annex is to show the solutions developed to characterize such functionalized NPs and the difficulties encountered in such studies. ToF-SIMS and XPS being surface analysis techniques, it was necessary to attach the NPs on a surface before characterization.¹⁶⁷ The substrate of choice was silicon wafers that are easily handled in both techniques and that are different from gold to ensure a better detection of the NPs. Two approaches were explored: the first one is to directly let drops of NPs dry on the silicon surface and the second one is to functionalize the wafers with the antigen to recognized the NPs in solution and immobilized them on the surface.

A.1 Samples

Nanoparticles used during this study are kindly provided by our partner (Coris Bioconcept), they are in an aqueous solution and stabilized by citrates. Their diameter is of about 40 nm which gives a maximum of adsorbance in UV/Vis spectroscopy at a 529 nm wavelength, they have an optical density (OD) of ± 4.65 . The OD measures the ratio between

transmitted light through a solution and the incident one. It is directly correlated to the concentration of NPs in the solution (Beer-Lambert law). It was established by Coris that an OD of 1 represents about 2×10^{11} NP.mL⁻¹. The exact protocol for functionalizing the NPs cannot be disclosed here. It was established with our partner Coris Bioconcept and is part of their industrial secret. Nevertheless, the steps are the same as on the flat surfaces. NPs are first functionalized with a –COOH-terminated alkyl thiols and then the antibody is simply adsorbed, or grafted using NHS-EDC. At the end of the functionalization process, three successive steps of washing in a pH 8 buffer solutions and centrifugation before re-suspension are performed. To ensure that the functionalization took place, the wavelength of the maximum of absorbance was monitored. Results are presented in Figure A.1.

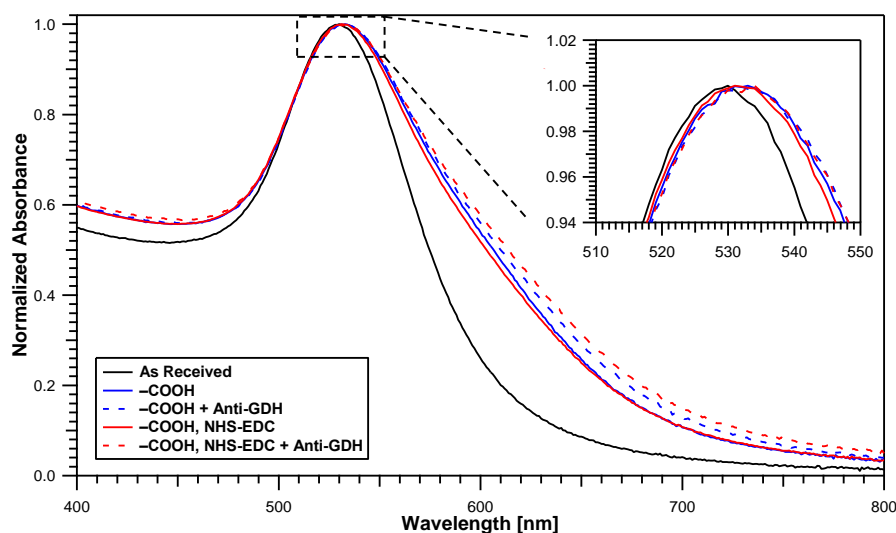


Figure A.1 Typical absorbance spectrum obtained after NPs functionalization with the –COOH thiol and Anti-GDH before and after activation with NHS-EDC. All spectra are re-normalized to their maximum to better see their shape and get rid of differences in height due to concentration only.

The maximum of absorbance is due to plasmon resonance in the NPs. This corresponds to localized states of the electromagnetic light wave in the NPs. Visible light with a wavelength of a few hundred nm interact with nano-objects (a few to a few tens of nm) as a uniform oscillating electric field. Electrons, excited by this field, then acquire a common oscillation in the NPs which is disturbed by boundary conditions. An important absorption is consequently observed for wavelength in the green region (around 500 nm) for gold NPs which explain their purple color.¹⁶⁸ The plasmon absorbance of gold NPs in solution can vary with their diameters, their shape, the nature of their terminal groups or the solvent.^{168,169} In our case (see Figure A.1); we observe a broadening of the absorbance peak and a slight shift toward higher maximum absorbance wavelength with the successive functionalization steps. A first observation here is that this increase is higher when the antibody is added in the case of the activated layer compare to Anti-GDH only adsorbed on the $-COOH$. This could suggest a better adsorption of Anti-GDH on NPs after grafting compare to simple adsorption. Further characterization will be performed using ToF-SIMS and XPS.

To perform such characterizations, two approaches were explored: drying drops of NPs on a clean silicon wafer or trying to recognize the functionalized NPs with surfaces bearing the antigen. In both cases, silicon samples are cleaned in absolute ethanol for 10 min, agitated in ultrasonic bath for 2 min, rinsed with MilliQ water and dried in N_2 before air plasma at 50 W for 5 min. The functionalization of NPs ends with successive steps of centrifugation and re-suspension. In the first approach, after the last

centrifugation, only the pellet of the tubes which is highly concentrated in NPs (OD \approx 20) is kept after removing the supernatant. This pellet is deposited in successive drops of 5 to 10 μ L and left to dry on the clean silicon samples. This approach was mostly performed to find a good methodology for studying such systems in SIMS. The literature on the subject shows the lack of standards for such analysis in ToF-SIMS.^{167,170,171} Nevertheless, XPS measurements were also performed on those systems.

In the second approach, further functionalization of the silicon surface is necessary. Clean silicon samples are first functionalized with (3-Aminopropyl)triethoxysilane (APTES) which is forming an amine terminated film on the silicon wafers. Silanization is performed by placing clean silicon samples in a clean petri dish containing 10 mL of a 1:100 APTES:toluene solution for 1h, followed by rinsing under flowing toluene and ultrasonic agitation in 10 mL of fresh toluene for 10 min. To reduce moisture ingress that could cause polymerization of APTES in solution during silanization, petri dishes used for functionalization were wrapped in aluminum foil for this step.¹⁷¹ Finally, samples are rinsed abundantly in ethanol and MilliQ water and dried under N_2 . To complete the formation of the Si-O bonds, samples are placed in a clean oven at 120 °C for 30 min. We want to achieve a covalent grafting of the antigen (GDH), thus a crosslinker is used to form the bond between the amine terminated surface and the proteins. The chosen cross-linker is PDITC (p-Phenylene Diisothiocyanate) which was already shown to be suitable for such grafting.⁵³ Samples are immersed in 10 mL of a 200 mg.mL⁻¹ solution of PDITC in 1:9 pyridine:DMF for 30 min

and subsequently rinsed in ethanol and dried under N_2 . The chemistry of the obtained surface is depicted in Figure A.2.

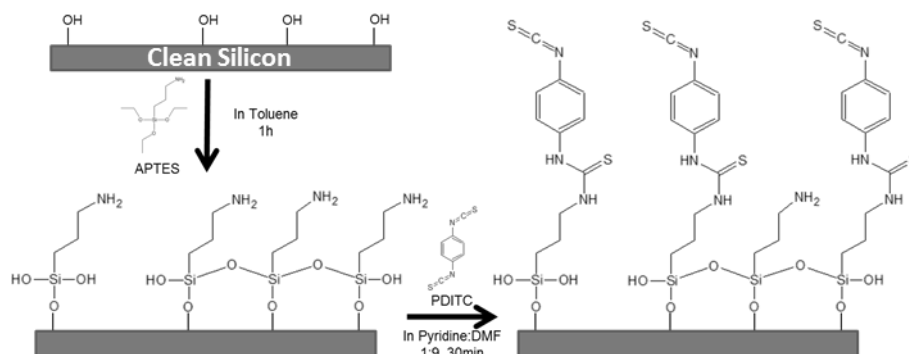


Figure A.2 Silanization and activation of the APTES layer by PDITC

The PDITC activated samples are then placed in $5 \mu\text{g.mL}^{-1}$ GDH solution in a phosphate buffer (pH 7.1) for 90 min. After rinsing in buffer and MilliQ water, a further saturation step using $100 \mu\text{g.mL}^{-1}$ BSA solution in phosphate buffer is performed. Samples are finally rinsed with the buffer and MilliQ water before drying under N_2 . These surfaces are used to quantify the biorecognition by solutions of Anti-GDH (controls) or by the functionalized NPs. To perform the recognition, NPs are diluted to an OD of 1 in phosphate buffer and the Anti-GDH is in phosphate buffer solution at a concentration of $5 \mu\text{g.mL}^{-1}$. Results obtained by ToF-SIMS and XPS measurements at each successive step are detailed below. Figure A.3 sums up the three types of samples obtained after all functionalization's performed here.

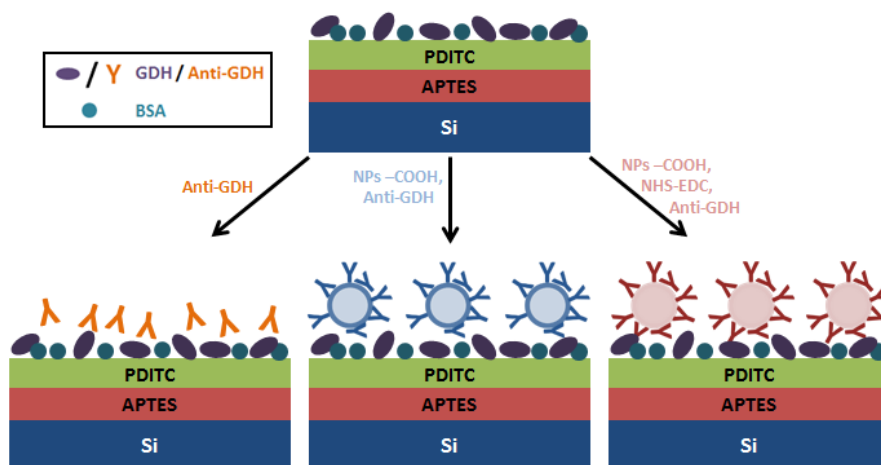


Figure A.3 Schematic representation of the samples obtained after functionalization of the silicon surfaces with GDH

A.2 Dried-Drops Samples Study

Letting drops of functionalized NPs dry on silicon surfaces turned out to be difficult to reproduce. From XPS, the quantity of gold detected was varying significantly for all 4 types of NPs ($-\text{COOH}$ -NPs activated or not, before and after Anti-GDH adsorption) and for samples prepared in separate experiments within the same type of NPs (see the Au 4f signal variation in Table A.1). This is explained by the sample preparation protocol. The amount of gold NPs in the pellet of the centrifugation tubes at the end of each functionalization step can vary significantly. The dried drops will then contained a different amount of NPs between all samples. Since the Au 4f signal only depends on the quantity of NPs deposited on the surface, it will be used as a normalization parameter to study the organic layer around the NPs.

Annex

On the survey spectrum, signal from C, O, N, Au and Si were identified. The atomic % resulting from the C, O, N and Au signal have been renormalized to 100% to only take into account the signal coming from the NPs by excluding the Si signal. Finally, the signal from the organic part (C, O and N) is normalized to the gold signal in order to compare the different samples studied even if the quantity of dried gold NPs vary between them. In Table A.1, the mean of XPS measurements for three different samples made in two separate experiments is presented at each functionalization step. In this study, the O 1s peaks were not decomposed and are not taken into account in the analysis since most of the oxygen signal comes from atoms involved in a Si-O bond. Results of oxygen measurements were therefore difficult to interpret.

Table A.1 XPS results for dried-drop samples. Results are presented for both types of –COOH-terminated NPs (*i.e.* without or with NHS-EDC activation) before (a) or after (b) Anti-GDH adsorption^a

	C 1s				O 1s	N 1s	Au 4f
	C-(C,H)	C-(O,N)	COO- C=O Amide	(C=O)-OH			
(eV)	284.8	286.3	287.5	288.9	Total		
	NPs –COOH						
(a)	9.69	1.13		0.49	11.31	4.97	7.62
+/-	4.98	0.67		0.22	5.87	4.30	5.00
(b)	6.33	0.78	0.18	0.33	7.62	2.10	0.12
+/-	2.50	0.33	0.05	0.13	2.99	1.43	0.04
	NPs –COOH, NHS-EDC						
(a)	6.70	0.82		0.37	7.88	3.01	9.36
+/-	2.77	0.35		0.12	3.25	2.13	4.23
(b)	7.61	1.15	0.35	0.44	9.55	3.29	0.30
+/-	0.20	0.06	0.08	0.02	0.23	1.84	0.10

^a The C, O, N, Au atomic % are renormalized to 100% to exclude the signal coming from Si and the organic part (C, N and O) is renormalized to the Au atomic % presented in the last column

In addition to the variation of the XPS gold signal revealing different quantities of NPs fixed on the surface, one can observe that even after renormalization of the organic part to the gold signal, a large variability is observed in the carbon signal. This is most likely due to the contamination by adventitious carbon during the drying process. Before Anti-GDH adsorption in both cases, no signal was detected for the characteristic amide bonds components in the C 1s peaks, and no nitrogen was detected. After Anti-GDH adsorption or grafting, we can see that the component corresponding to carbon in an amide bond is in good correlation with the nitrogen signal (0.18 vs 0.12 when adsorbing the antibodies on NPs compare to 0.35 vs 0.30 when grafting them). Most of the nitrogen atoms in the system are brought in by the protein. This indicates that the functionalization of NPs tends to be more efficient when grafting the Anti-GDH than when simply adsorbing it.

Results deduced from XPS measurements were difficult to interpret and, at this step, no information about the influence on biorecognition by the NPs could be deduced. Due to small quantities of NPs on the surfaces, XPS was proved not to be the best technique for such characterizations. As mentioned earlier, these studies with the dried drop samples were mostly performed to find a suitable NPs characterization way in ToF-SIMS. The results obtained with SIMS are presented below before testing biorecognition with the second type of samples.

In ToF-SIMS, as in XPS measurements, three different samples made at two different occasions are studied. On each sample, three spectra were

acquired in the positive and negative polarity making a total of 9 spectra for each functionalization step in each polarity. In a first attempt to determine the differences in adsorption mode of the antibody on NPs, PCA calculations were performed with different pre-treatments. Spectra were first either normalized on the total counts in each spectrum or on the gold signal to take into account differences in adsorbed quantities. Several peaklists were also tested: all the peaks between the mass over charge ratio 0 to 200 in the negative or positive polarity, and the a.a. fragments peaklist already used during this work and characteristic of proteins in positive polarity. Moreover, PCA calculations with all four types of samples (NPs –COOH, NPs –COOH-activated with or without Anti-GDH) or only with the samples containing Anti-GDH were carried out.

None of the above mentioned PCA calculations showed a clear separation between samples. All spectra were scattered over the score plots and no conclusion could be drawn. Nevertheless, by coming back to peak intensities in the spectra we can retrieve the information already obtained in XPS. In panels a and c from Figure A.4, intensities relative to a.a. fragments in proteins are presented. In the negative (CN^- or CNO^-) or positive (CH_2N^+ and CH_4N^+) polarities, presented peaks were already identified as characteristic of all a.a. and not to specific ones, they are thus not specific of one orientation of the adsorbed or grafted antibodies. However, they give an indication about the quantity of proteins deposited on each type of NPs since their intensity is normalized to the gold signal. For all these peaks, a larger increase of the signal is observed when grafting the Anti-GDH than when only adsorbing it on the –COOH-terminated NPs.

Peaks most likely coming from the NP functionalization with the -COOH terminated thiol, or by the activation with NHS-EDC are also presented (see Figure A.4 b and d). In the negative polarity, peaks with a general formula as $\text{C}_n\text{H}_n\text{O}_2^-$ are identified as characteristics of the -COOH thiol, a decrease in their intensity is observed when the thiol layer is activated and when the antibody is adsorbed or grafted. In positive polarity, the $\text{C}_3\text{H}_8\text{N}^+$ was identified in Chapter 5 as characteristic of the activation (and most likely to residual EDC groups after activation). It shows a large intensity on the activated NPs which decreases when grafting the antibody. The $\text{C}_5\text{H}_7\text{O}^+$ is an a.a. fragment characteristic of valine but it could also be characteristic of the -COOH thiol, and presents the same behavior as negative peaks identified in Figure A.4 b.

This first part of the functionalized NPs study, using the dried-drops approach, allows detecting a larger quantity of Anti-GDH on NPs when the antibody is grafted (NHS-EDC activation) than when it is simply adsorbed on the -COOH -terminated NPs. However, no differences could be detected in the adsorption modes of antibodies on such NPs. PCA did not allow the separation of samples most likely because of the drying process that would favor contamination in air and also because of the small amount of NPs fixed on the surface. In order to retrieve information about the biorecognition efficiency of the NPs, they were further tested on surfaces where the antigen (GDH) was immobilized. Results are presented below.

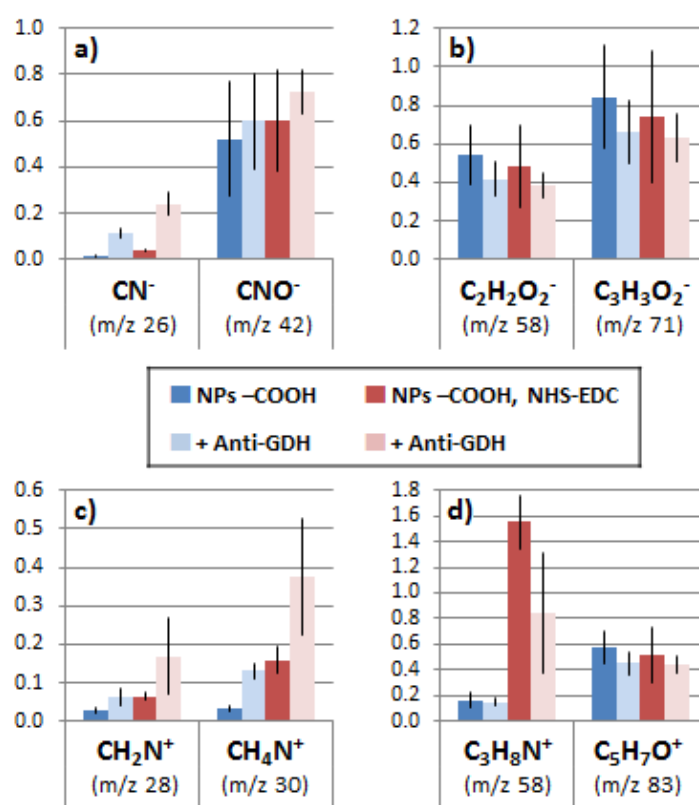


Figure A.4 Relevant peaks in ToF-SIMS analysis of the dried-drops samples. Presented intensities are normalized to the gold one.

A.3 Antigen Immobilization on Si for Biorecognition with NPs

In this approach, the functionalized NPs will be tested against a surface bearing the antigen. Immobilization of Anti-GDH on the surface of the NPs could lead to their denaturation and to the loss of their biorecognition ability. In Chapter 5 it was shown that antibodies grafted on the –COOH-terminated SAMs after activation with NHS-EDC adopted a better orientation leading to better biorecognition of the free antigen in solution than when only adsorbed. The goals of the following study are, first, to show the interest of ToF-SIMS in studying such complex systems, and, second, to see if we can demonstrate different biorecognition performances of both types of NPs in XPS or ToF-SIMS measurements.

A.3.1 Grafting of GDH on Silicon

The first step here was to graft GDH on the surface and to see if it was still recognized by the free Anti-GDH antibodies in solution. XPS and ToF-SIMS measurements were performed and results are presented respectively in Table A.2 and in Figure A.5. On XPS survey spectra, peaks from C, O, N, Au (when the NPs were adsorbed) and Si were detected. To follow the evolution of the atomic % coming from the different elements at each functionalization step, results are presented after renormalization of the organic part (+ Au in the case of NPs) to 100%. The last column of the table shows the evolution of the Si 2s atomic % before renormalization to analyze the attenuation of the Si signal during functionalization. For ToF-SIMS

measurements, peaks presented in Figure A.5 are normalized to the total counts in each considered spectra to limit variations between samples due to the analysis. Presented peaks are characteristic of the substrate or of proteins in negative or positive polarities.

Both XPS and ToF-SIMS gave characteristic results for the silanization with APTES and its activation using PDITC. In XPS, the silanization is followed by the attenuation of the Si 2s peak from 55.6 to 45.7% and by the increase of the N 1s signal (0.5 to 4.1%) indicating the formation of the amine terminated layer on the surface. ToF-SIMS results showed an increase of the CN^- peak (also characteristic of the proteins) after APTES functionalization consistent with the presence of amine at the extreme surface. Moreover, an attenuation of the Si^- and the SiOH^- peaks is observed compatible with the screening of the silicon surface by APTES (see Figure A.5). The activation of the silane layer with PDITC was more difficult to characterize by XPS, only a slight increase of the N 1s signal is observed (from 4.1 to 4.7%) but no more attenuation of the Si 2s signal. However in ToF-SIMS, the activation was clearly evidenced by the large peak at m/z 58 corresponding to a CSN^- ion which was not present before the PDITC activation. This fragment is characteristic of PDITC and is at the extreme surface after grafting of the cross-linker (see Figure A.3). This shows, if need be, the power of ToF-SIMS for extreme surface characterization. In the literature, no mention of a clear characterization of this cross-linker grafting was found.

Table A.2 XPS results of biorecognition performance of NPs on GDH functionalized surfaces^a

(eV)	C 1s				Total	O 1s	N 1s	Au 4f	Si 2s
	C-(C,H)	C-(O,N)	COO- C=O Amide	(C=O)-OH					
	284.8	286.3	287.5	288.9					
(1) Si	23.6	9.6		0.3	33.4	66.1	0.5		55.6
+/-	1.6	0.9		0.4	3.0	3.0	0.1		3.7
(2) 1 + APTES	35.3	10.0	1.7	1.6	48.6	47.3	4.1		45.7
+/-	7.7	1.6	0.9	0.9	9.3	10.3	0.9		8.2
(3) 2 + PDITC	33.1	10.4	1.8	1.9	47.1	48.2	4.7		45.7
+/-	4.4	1.5	0.6	0.4	6.1	7.4	1.3		7.9
(4) 3 + GDH	35.4	11.7	3.9	1.7	52.8	40.8	6.5		39.3
+/-	3.9	0.4	1.0	0.5	4.3	5.1	0.9		7.0
(5) 4 + BSA	34.2	14.7	8.6	0.8	58.3	31.6	10.1		31.9
+/-	5.8	0.4	0.7	0.1	4.6	4.1	0.5		6.1
(6) 5 + Anti-GDH	35.8	15.1	8.9	0.7	60.6	29.0	10.4		28.5
+/-	4.8	0.6	1.0	0.3	3.3	2.6	0.7		3.9
(7) 5 + NPs Adsorbed	34.3	14.7	8.3	1.0	58.3	31.1	9.6	1.1	31.2
+/-	4.3	0.3	0.9	0.2	3.4	3.4	0.7	1.1	4.9
(8) 5 + NPs Grafted	34.1	14.7	8.6	0.9	58.3	30.3	10.1	1.3	30.1
+/-	4.6	0.2	0.6	0.1	4.1	4.6	0.3	1.1	6.5

^a The C, O, N, Au atomic % are renormalized to 100% to exclude the signal coming from Si. The Si atomic % before renormalization are presented in the last column

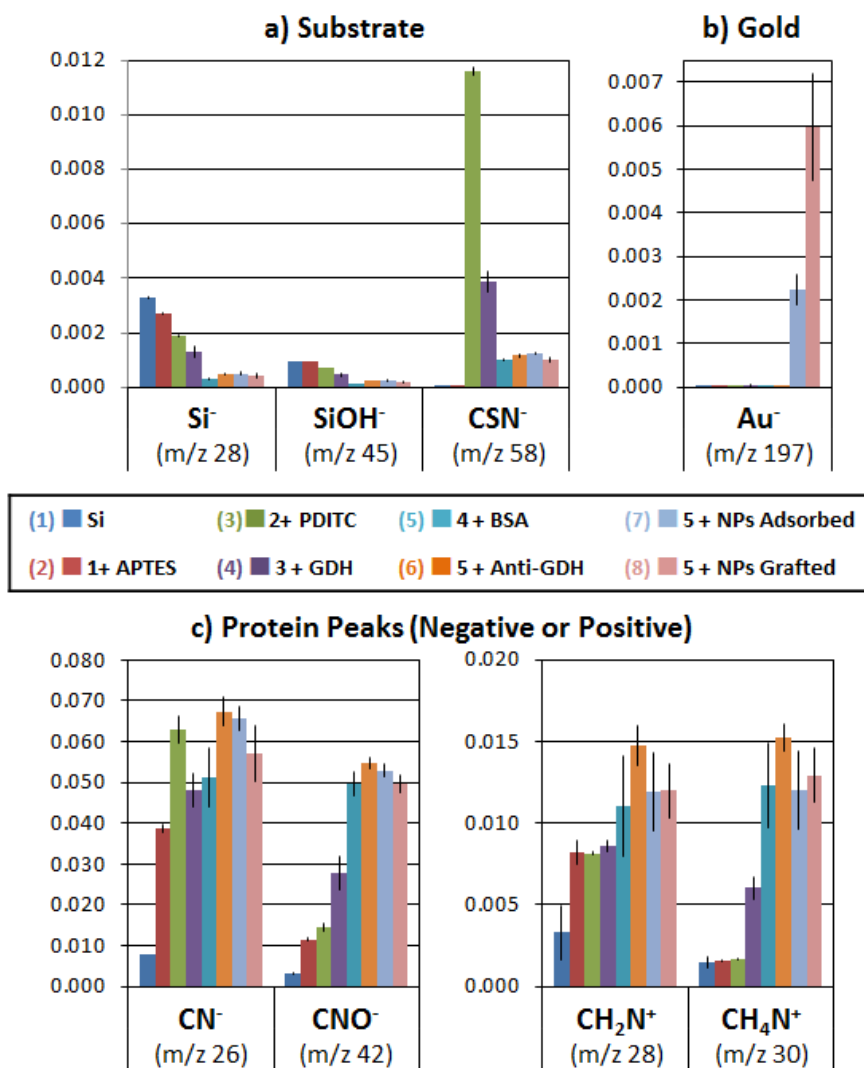


Figure A.5 Relevant peaks in ToF-SIMS analysis of the biorecognition samples. Presented intensities are normalized to the total counts.

The next step of the functionalization was to expose the surface to the GDH protein in order to cover the surface and prepare a biorecognition template for Anti-GDH functionalized NPs. Further saturation with BSA was also performed to avoid nonspecific recognition by the antibody. Both the GDH grafting using the cross-linker and the saturation with BSA are evidenced by the attenuation of the Si 2p peak atomic % in XPS that are decreasing respectively from 45.7% (PDITC surface) to 39.3 % after GDH and finally 31.9 % after BSA. The grafting of proteins is also characterized by the increase of the N 1s peak from 4.7 % to 6.5% (GDH) and 10.1% (BSA), and of the amide component in the C 1s peak (1.8% to 3.9% and 8.6% respectively for GDH and BSA grafting).

In ToF-SIMS, the adsorption of the GDH and BSA was followed with protein fragments characteristic of most a.a. in the positive mode (CH_2N^+ and CH_4N^+) and by the CN^- and CNO^- ions in the negative mode. The CN^- ions were already largely detected for the PDITC-activated samples, however an increase of the intensity is observed between the GDH and BSA steps. The adsorption is mostly evidenced by the large increase observed in the intensity of the CNO^- and CH_4N^+ peaks. The goal here is not to quantify precisely the quantity grafted on the surface but mostly to show that the GDH is successfully grafted on the surface. In the next paragraph, the ability of the Anti-GDH antibody to recognize the immobilized GDH will be tested either with free antibodies in solution or with the functionalized NPs presented earlier.

A.3.2 Biorecognition Tests

A first observation here, based on XPS results, is that after BSA saturation the renormalized signal corresponding to protein adsorption (amide in C 1s and N 1s signal) is nearly constant after each step. It could be explained by the fact that even if the total protein quantity increases on the sample (Anti-GDH or functionalized NPs adsorption), the proportion of the XPS signal coming from proteins will remain more or less constant due to the large quantity of BSA adsorbed. Most of the discussion of XPS results will then be based on the attenuation of the Si 2s signal.

The GDH-surface (saturated with BSA) was first tested with free antibodies in solution. XPS results showed a higher attenuation of the silicon signal which goes from 31.9 to 28.9% after biorecognition by Anti-GDH. The increase in intensity for protein related peaks is also evidenced in ToF-SIMS (see Figure A.5 c) confirming XPS measurements. This indicates that even after rinsing and drying the surface, Anti-GDH proteins are attached to the surface most likely by interacting with the GDH since the surfaces were saturated with BSA. It means that the epitopes are still accessible for Ab/Ag interaction in the described setup. These GDH-surfaces have then been tested with the NPs adsorbed or grafted with Anti-GDH to see if differences in their recognition efficiency could be observed.

Looking at XPS results in Table A.2, the percentage of gold on the surface after NPs biorecognition is higher for the NPs where Anti-GDH are grafted (1.3%) compare to when they are adsorbed (1.1%). Moreover, the attenuation of silicon seems higher in the grafted case than in the adsorbed

one; from 31.9% (after BSA adsorption) to 30.1% or 31.2% respectively. Differences are not really important in XPS but they seem to be comforted by ToF-SIMS measurements where the intensity of the Au⁻ peak is about two to three times higher in the case of the grafted NPs than in the adsorbed ones. Those results showed a similar effect than on the flat surface where grafting the antibody lead to twice more antigen recognized compared to the adsorbed Anti-GDH.

A.4 Conclusions

This study showed first that a larger quantity of antibodies is grafted on the NPs when the –COOH thiol layer is activated with NHS-EDC than when the Anti-GDH is simply adsorbed. However, despite several PCA calculations performed with different pre-treatments, no clear separation of the functionalized NPs was demonstrated. We could not conclude on the most likely orientation of the antibodies on the NPs in both studied cases. This could come from the fact that antibodies are in similar orientations on both types of NPs but also from the experimental procedures. The drying process of the NPs on the silicon wafers is difficult to control. In our case, samples were generally dried in air or by creating a rough vacuum in a desiccator before transferring into UHV. The drying could lead to the contamination of the extreme surface of samples from the environment that will disturb XPS or ToF-SIMS measurements. Moreover, after centrifugation with the different functionalization steps it is difficult to control the exact amount of NPs deposited on the surface and thus to compare samples.

The second idea in this study was to test the biorecognition properties of the NPs. Results tend to show similar results as in the flat surface case: grafting of Anti-GDH on the NPs is more efficient than adsorption for recognition of the GDH. However, these results are preliminary and were only obtained after drying of samples and measurements under UHV by XPS and ToF-SIMS. It was shown that a really small amount of the surface is covered with gold NPs in all cases. It would be interesting to test the biorecognition with other techniques and especially QCM-D. Building the bio-sensing template (silicon wafer with immobilized GDH) in the liquid phase to perform directly biorecognition tests with the NPs would avoid a lot of manipulations of the samples and allow a direct interpretation of the results. Moreover, we could also gain from SEM analysis to determine the morphology of adsorbed NPs (scattered on the surface, aggregates...).

Unfortunately, we were limited in the amount of Anti-GDH or GDH provided by our partner and also by time constraint; it was then difficult to push this study further. These first results are nevertheless promising and would need more investigation. It is proposed to switch to less costly couples of Ab/Ag (Anti-BSA/BSA for example) to finely tune the best functionalization protocol of the NPs. Moreover, it could lead to the creation of templates NPs for several types of antibodies allowing the rapid development of diagnostic tests. Nevertheless, this study also showed that ToF-SIMS could be used as tool to probe the surface characteristics of complex systems including NPs with an organic coating.

Bibliography

- (1) Kasemo, B. Biological Surface Science. *Surf. Sci.* **2002**, *500*, 656–677.
- (2) Thévenot, D.; Toth, K.; Durst, R.; Wilson, G. Electrochemical Biosensors: Recommended Definitions and Classification. *Pure Appl. Chem.* **2001**, *71*, 2333–2348.
- (3) Gruhl, F. J.; Rapp, B. E.; Länge, K. Biosensors for Diagnostic Applications. In *Molecular Diagnostics*; Seitz, H.; Schumacher, S., Eds.; Springer Berlin Heidelberg: Berlin, 2013; pp. 115–148.
- (4) Jonkheijm, P.; Weinrich, D.; Schröder, H.; Niemeyer, C. M.; Waldmann, H. Chemical Strategies for Generating Protein Biochips. *Angew. Chem. Int. Ed. Engl.* **2008**, *47*, 9618–47.
- (5) Lin, P.-C.; Weinrich, D.; Waldmann, H. Protein Biochips: Oriented Surface Immobilization of Proteins. *Macromol. Chem. Phys.* **2010**, *211*, 136–144.
- (6) Norde, W.; Buijs, J.; Lyklema, J. Adsorption of Globular Protein. In *Fundamentals of Interface and Colloid Science, Volume V: Soft Colloids*; Lyklema, J., Ed.; Elsevier Inc., 2005; p. 844.
- (7) Rabe, M.; Verdes, D.; Seeger, S. Understanding Protein Adsorption Phenomena at Solid Surfaces. *Adv. Colloids Interface Sci.* **2011**, *162*, 87–106.
- (8) Norde, W.; Horbett, T. A.; Brash, J. L. Proteins at Interfaces III: Introductory Overview. In *Proteins at Interfaces III State of the Art*; Horbett, T. A.; Brash, J. L.; Norde, W., Eds.; American Chemical Society: Washington, DC, 2012; pp. 1–34.
- (9) Norde, W. My Voyage of Discovery to Proteins in Flatland ...and Beyond. *Colloids Surf. B* **2008**, *61*, 1–9.

-
- (10) Tsapikouni, T. S.; Missirlis, Y. F. Protein–material Interactions: From Micro-to-Nano Scale. *Mater. Sci. Eng. B* **2008**, *152*, 2–7.
- (11) Vroman, L.; Adams, A. L.; Fischer, G. C.; Munoz, P. C. Interaction of High Molecular Weight Kininogen, Factor XII, and Fibrinogen in Plasma at Interfaces. *Blood* **1980**, *5*, 156–159.
- (12) Gray, J. J. The Interaction of Proteins with Solid Surfaces. *Curr. Opin. Struct. Biol.* **2004**, *14*, 110–115.
- (13) Brash, J. L. Protein Surface Interactions and Biocompatibility: A Forty Year Perspective. In *Proteins at Interfaces III State of the Art*; Horbett, T. A.; Brash, J. L.; Norde, W., Eds.; American Chemical Society: Washington, DC, 2012; pp. 277–300.
- (14) Li, D.; Chen, H. Regulation of Protein / Surface Interactions by Surface Chemical Modification and Topographic Design. In *Proteins at Interfaces III State of the Art*; Horbett, T. A.; Brash, J. L.; Norde, W., Eds.; American Chemical Society: Washington, DC, 2012; pp. 301–319.
- (15) Castner, D. G.; Ratner, B. D. Biomedical Surface Science: Foundations to Frontiers. *Surf. Sci.* **2002**, *500*, 28–60.
- (16) Chen, S.; Li, L.; Zhao, C.; Zheng, J. Surface Hydration: Principles and Applications toward Low-Fouling/nonfouling Biomaterials. *Polymer (Guildf)*. **2010**, *51*, 5283–5293.
- (17) Jiang, S.; Cao, Z. Ultralow-Fouling, Functionalizable, and Hydrolyzable Zwitterionic Materials and Their Derivatives for Biological Applications. *Adv. Mater.* **2010**, *22*, 920–32.
- (18) Ulman, A. Formation and Structure of Self-Assembled Monolayers. *Chem. Rev.* **1996**, *96*, 1533–1554.
- (19) Schreiber, F. Structure and Growth of Self-Assembling Monolayers. *Prog. Surf. Sci.* **2000**, *65*, 151–257.

-
- (20) Love, J. C.; Estroff, L. A.; Kriebel, J. K.; Nuzzo, R. G.; Whitesides, G. M. Self-Assembled Monolayers of Thiolates on Metals as a Form of Nanotechnology. *Chem. Rev.* **2005**, *105*, 1103–69.
- (21) Schreiber, F. Self-Assembled Monolayers: From “Simple” Model Systems to Biofunctionalized Interfaces. *J. Phys. Condens. Matter* **2004**, *16*, R881–R900.
- (22) Prime, K. L.; Whitesides, G. M. Self-Assembled Organic Monolayers: Model Systems for Studying Adsorption of Proteins at Surfaces. *Science (80-.)*. **1991**, *252*, 1164–1167.
- (23) Elwing, H. Protein Adsorption and Ellipsometry in Biomaterial Research. *Biomaterials* **1998**, *19*, 397–406.
- (24) Arwin, H. Application of Ellipsometry Techniques to Biological Materials. *Thin Solid Films* **2011**, *519*, 2589–2592.
- (25) Chittur, K. K. FTIR/ATR for Protein Adsorption to Biomaterial Surfaces. *Biomaterials* **1998**, *19*, 357–69.
- (26) Tengvall, P.; Lundström, I.; Liedberg, B. Protein Adsorption Studies on Model Organic Surfaces: An Ellipsometric and Infrared Spectroscopic Approach. *Biomaterials* **1998**, *19*, 407–22.
- (27) Genet, M. J.; Dupont-Gillain, C. C.; Rouxhet, P. G. XPS Analysis of Biosystems and Biomaterials. In *Medical Applications of Colloids*; Matijevic, E., Ed.; Springer: New York, NY, 2008.
- (28) Graham, D. J.; Castner, D. G. Multivariate Analysis of ToF-SIMS Data from Multicomponent Systems: The Why, When, and How. *Biointerphases* **2012**, *7*, 49.
- (29) Vogler, E. A. Protein Adsorption in Three Dimensions. *Biomaterials* **2012**, *33*, 1201–37.

-
- (30) Sethuraman, A.; Han, M.; Kane, R. S.; Belfort, G. Effect of Surface Wettability on the Adhesion of Proteins. *Langmuir* **2004**, *20*, 7779–88.
- (31) Jandt, K. D. Atomic Force Microscopy of Biomaterials Surfaces and Interfaces. *Surf. Sci.* **2001**, *491*, 303–332.
- (32) Siedlecki, C. A.; Marchant, R. E. Atomic Force Microscopy for Characterization of the Biomaterial Interface. *Biomaterials* **1998**, *19*, 441–54.
- (33) Konradi, R.; Textor, M.; Reimhult, E. Using Complementary Acoustic and Optical Techniques for Quantitative Monitoring of Biomolecular Adsorption at Interfaces. *Biosensors* **2012**, *2*, 341–376.
- (34) Marx, K. A. Quartz Crystal Microbalance: A Useful Tool for Studying Thin Polymer Films and Complex Biomolecular Systems at the Solution-Surface Interface. *Biomacromolecules* **2003**, *4*, 1099–1120.
- (35) Yano, Y. F. Kinetics of Protein Unfolding at Interfaces. *J. Phys. Condens. matter* **2012**, *24*, 503101.
- (36) Bulheller, B. M.; Rodger, A.; Hirst, J. D. Circular and Linear Dichroism of Proteins. *Phys. Chem. Chem. Phys.* **2007**, *9*, 2020–35.
- (37) Prime, K. L.; Whitesides, G. M. Adsorption of Proteins onto Surfaces Containing End-Attached Oligo(ethylene Oxide): A Model System Using Self-Assembled Monolayers. *J. Am. Chem. Soc.* **1993**, *115*, 10714–10721.
- (38) Saito, N.; Matsuda, T. Protein Adsorption on Self-Assembled Monolayers with Water-Soluble Non-Ionic Oligomers Using Quartz-Crystal Microbalance. *Mater. Sci. Eng. C* **1998**, *6*, 261–266.
- (39) Ostuni, E.; Chapman, R. G.; Holmlin, R. E.; Takayama, S.; Whitesides, G. M. A Survey of Structure–Property Relationships of Surfaces That Resist the Adsorption of Protein. *Langmuir* **2001**, *17*, 5605–5620.

-
- (40) Chapman, R. G.; Ostuni, E.; Yan, L.; Whitesides, G. M. Preparation of Mixed Self-Assembled Monolayers (SAMs) That Resist Adsorption of Proteins Using the Reaction of Amines with a SAM That Presents Interchain Carboxylic Anhydride Groups. *Langmuir* **2000**, *16*, 6927–6936.
- (41) Ostuni, E.; Yan, L.; Whitesides, G. M. The Interaction of Proteins and Cells with Self-Assembled Monolayers of Alkanethiolates on Gold and Silver. *Colloids Surf. B* **1999**, *15*, 3–30.
- (42) Ostuni, E.; Grzybowski, B. A.; Mrksich, M.; Roberts, C. S.; Whitesides, G. M. Adsorption of Proteins to Hydrophobic Sites on Mixed Self-Assembled Monolayers. *Langmuir* **2003**, *19*, 1861–1872.
- (43) Nelson, K. E.; Gamble, L. J.; Jung, L. S.; Boeckl, M. S.; Naeemi, E.; Golledge, S. L.; Sasaki, T.; Castner, D. G.; Campbell, C. T.; Stayton, P. S. Surface Characterization of Mixed Self-Assembled Monolayers Designed for Streptavidin Immobilization. *Langmuir* **2001**, *17*, 2807–2816.
- (44) Silin, V.; Weetall, H.; Vanderah, D. J. SPR Studies of the Nonspecific Adsorption Kinetics of Human IgG and BSA on Gold Surfaces Modified by Self-Assembled Monolayers (SAMs). *J. Colloid Interface Sci.* **1997**, *185*, 94–103.
- (45) Martins, M. C. L.; Fonseca, C.; Barbosa, M. A.; Ratner, B. D. Albumin Adsorption on Alkanethiols Self-Assembled Monolayers on Gold Electrodes Studied by Chronopotentiometry. *Biomaterials* **2003**, *24*, 3697–3706.
- (46) Martins, M. C. L.; Ratner, B. D.; Barbosa, M. A. Protein Adsorption on Mixtures of Hydroxyl- and Methyl-Terminated Alkanethiols Self-Assembled Monolayers. *J. Biomed. Mater. Res. Part A* **2003**, *67*, 158–71.
- (47) Gonçalves, I. C.; Martins, M. C. L.; Barbosa, M. A.; Ratner, B. D. Protein Adsorption on 18-Alkyl Chains Immobilized on Hydroxyl-

Terminated Self-Assembled Monolayers. *Biomaterials* **2005**, *26*, 3891–3899.

- (48) Briand, E.; Salmain, M.; Compère, C.; Pradier, C.-M. Immobilization of Protein A on SAMs for the Elaboration of Immunosensors. *Colloids Surf. B* **2006**, *53*, 215–24.
- (49) Patel, N.; Davies, M. C.; Hartshorne, M.; Heaton, R. J.; Roberts, C. J.; Tandler, S. J. B.; Williams, P. M. Immobilization of Protein Molecules onto Homogeneous and Mixed Carboxylate-Terminated Self-Assembled Monolayers. *Langmuir* **1997**, *13*, 6485–6490.
- (50) Wiseman, M. E.; Frank, C. W. Antibody Adsorption and Orientation on Hydrophobic Surfaces. *Langmuir* **2012**, *28*, 1765–74.
- (51) Dupont-gillain, C. C. Orientation of Adsorbed Antibodies : In Situ Monitoring by QCM and Random Sequential Adsorption Modeling. In *Proteins at Interfaces III State of the Art*; Horbett, T.; Brash, J. L.; Norde, W., Eds.; American Chemical Society: Washington, DC, 2012; pp. 453–469.
- (52) Salmain, M.; Ghasemi, M.; Boujday, S.; Pradier, C. Elaboration of a Reusable Immunosensor for the Detection of Staphylococcal Enterotoxin A (SEA) in Milk with a Quartz Crystal Microbalance. *Sensors Actuators B* **2012**, *173*, 148–156.
- (53) Salmain, M.; Ghasemi, M.; Boujday, S.; Spadavecchia, J.; Técher, C.; Val, F.; Le Moigne, V.; Gautier, M.; Briandet, R.; Pradier, C.-M. Piezoelectric Immunosensor for Direct and Rapid Detection of Staphylococcal Enterotoxin A (SEA) at the Ng Level. *Biosens. Bioelectron.* **2011**, *29*, 140–4.
- (54) Boujday, S.; Bantegnie, A.; Briand, E.; Marnet, P.-G.; Salmain, M.; Pradier, C.-M. In-Depth Investigation of Protein Adsorption on Gold Surfaces: Correlating the Structure and Density to the Efficiency of the Sensing Layer. *J. Phys. Chem. B* **2008**, *112*, 6708–15.

- (55) Delcorte, A.; Leblanc, C.; Poleunis, C.; Hamraoui, K. Computer Simulations of the Sputtering of Metallic, Organic, and Metal–Organic Surfaces with Bi N and C 60 Projectiles. *J. Phys. Chem. C* **2013**, *117*, 2740–2752.
- (56) Mantus, D. S.; Ratner, B. D.; Carlson, B. A.; Moulder, J. F. Static Secondary Ion Mass Spectrometry of Adsorbed Proteins. *Anal. Chem.* **1993**, *65*, 1431–8.
- (57) Bartiaux, S. Etude de Poly(acides Aminés) Par ToF-SIMS et XPS - Application À L'analyse D'une Protéine. Undergraduate Thesis, Université catholique de Louvain, 1995.
- (58) Baugh, L.; Weidner, T.; Baio, J. E.; Nguyen, P.-C. T.; Gamble, L. J.; Stayton, P. S.; Castner, D. G. Probing the Orientation of Surface-Immobilized Protein G B1 Using ToF-SIMS, Sum Frequency Generation, and NEXAFS Spectroscopy. *Langmuir* **2010**, *26*, 16434–41.
- (59) Baio, J. E.; Cheng, F.; Ratner, D. M.; Stayton, P. S.; Castner, D. G. Probing Orientation of Immobilized Humanized Anti-Lysozyme Variable Fragment by Time-of-Flight Secondary-Ion Mass Spectrometry. *J. Biomed. Mater. Res. Part A* **2011**, *97A*, 1–7.
- (60) Baio, J. E.; Weidner, T.; Baugh, L.; Gamble, L. J.; Stayton, P. S.; Castner, D. G. Probing the Orientation of Electrostatically Immobilized Protein G B1 by Time-of-Flight Secondary Ion Spectrometry, Sum Frequency Generation, and Near-Edge X-Ray Adsorption Fine Structure Spectroscopy. *Langmuir* **2012**, *28*, 2107–12.
- (61) Baio, J. E.; Weidner, T.; Ramey, D.; Pruzinsky, L.; Castner, D. G. Probing the Orientation of Electrostatically Immobilized Cytochrome C by Time of Flight Secondary Ion Mass Spectrometry and Sum Frequency Generation Spectroscopy. *Biointerphases* **2013**, *8*, 18.
- (62) Lhoest, J.-B.; Detrait, E.; van den Bosch de Aguilar, P.; Bertrand, P. Fibronectin Adsorption, Conformation, and Orientation on

Polystyrene Substrates Studied by Radiolabeling, XPS, and ToF SIMS. *J. Biomed. Mater. Res.* **1998**, *41*, 95–103.

- (63) Wagner, M. S.; Horbett, T. A.; Castner, D. G. Characterization of the Structure of Binary and Ternary Adsorbed Protein Films Using Electron Spectroscopy for Chemical Analysis, Time-of-Flight Secondary Ion Mass Spectrometry, and Radiolabeling. *Langmuir* **2003**, 1708–1715.
- (64) Tidwell, C. D.; Castner, D. G.; Golledge, S. L.; Ratner, B. D.; Meyer, K.; Hagenhoff, B.; Benninghoven, A. Static Time-of-Flight Secondary Ion Mass Spectrometry and X-Ray Photoelectron Spectroscopy Characterization of Adsorbed Albumin and Fibronectin Films. *Surf. Interface Anal.* **2001**, *31*, 724–733.
- (65) Lhoest, J.-B.; Wagner, M. S.; Tidwell, C. D.; Castner, D. G. Characterization of Adsorbed Protein Films by Time of Flight Secondary Ion Mass Spectrometry. *J. Biomed. Mater. Res.* **2001**, *57*, 432–40.
- (66) Wagner, M. S.; Castner, D. G. Characterization of Adsorbed Protein Films by Time-of-Flight Secondary Ion Mass Spectrometry with Principal Component Analysis. *Langmuir* **2001**, *17*, 4649–4660.
- (67) Aoyagi, S.; Oiw, Y.; Kudo, M. Detection of Protein Immobilization on Biosensor Surfaces by TOF-SIMS. *Appl. Surf. Sci.* **2004**, *231-232*, 432–436.
- (68) Henry, M.; Bertrand, P. Influence of Polymer Surface Hydrophilicity on Albumin Adsorption. *Surf. Interface Anal.* **2004**, *36*, 729–732.
- (69) Canavan, H. E.; Graham, D. J.; Cheng, X.; Ratner, B. D.; Castner, D. G. Comparison of Native Extracellular Matrix with Adsorbed Protein Films Using Secondary Ion Mass Spectrometry. *Langmuir* **2007**, *23*, 50–56.
- (70) Henry, M.; Dupont-Gillain, C. C.; Bertrand, P. Characterization of Insulin Adsorption in the Presence of Albumin by Time-of-Flight

Secondary Ion Mass Spectrometry and X-Ray Photoelectron Spectroscopy. *Langmuir* **2008**, *24*, 458–464.

- (71) Henry, M.; Bertrand, P. Surface Composition of Insulin and Albumin Adsorbed on Polymer Substrates as Revealed by Multivariate Analysis of ToF-SIMS Data. *Surf. Interface Anal.* **2009**, *41*, 105–113.
- (72) Brüning, C.; Hellweg, S.; Dambach, S.; Lipinsky, D.; Arlinghaus, H. F. Improving the Interpretation of ToF-SIMS Measurements on Adsorbed Proteins Using PCA. *Surf. Interface Anal.* **2006**, *38*, 191–193.
- (73) Xia, N.; May, C. J.; McArthur, S. L.; Castner, D. G. Time-of-Flight Secondary Ion Mass Spectrometry Analysis of Conformational Changes in Adsorbed Protein Films. *Langmuir* **2002**, *18*, 4090–4097.
- (74) Xia, N.; Castner, D. G. Preserving the Structure of Adsorbed Protein Films for Time-of-Flight Secondary Ion Mass Spectrometry Analysis. *J. Biomed. Mater. Res. Part A* **2003**, *67*, 179–90.
- (75) Henry, M.; Dupont-Gillain, C. C.; Bertrand, P. Conformation Change of Albumin Adsorbed on Polycarbonate Membranes as Revealed by ToF-SIMS. *Langmuir* **2003**, *19*, 6271–6276.
- (76) Wang, H.; Castner, D. G.; Ratner, B. D.; Jiang, S. Probing the Orientation of Surface-Immobilized Immunoglobulin G by Time-of-Flight Secondary Ion Mass Spectrometry. *Langmuir* **2004**, *20*, 1877–87.
- (77) Liu, F.; Dubey, M.; Takahashi, H.; Castner, D. G.; Grainger, D. W. Immobilized Antibody Orientation Analysis Using Secondary Ion Mass Spectrometry and Fluorescence Imaging of Affinity-Generated Patterns. *Anal. Chem.* **2010**, *82*, 2947–58.
- (78) Park, J.-W.; Cho, I.-H.; Moon, D. W.; Paek, S.-H.; Lee, T. G. ToF-SIMS and PCA of Surface-Immobilized Antibodies with Different Orientations. *Surf. Interface Anal.* **2011**, *43*, 285–289.

-
- (79) Giambianco, N.; Zhavnerko, G.; Tuccitto, N.; Licciardello, A.; Marletta, G. Coadsorption-Dependent Orientation of Fibronectin Epitopes at Hydrophilic Gold Surfaces. *Soft Matter* **2012**, *8*, 8370.
- (80) Vickerman, J. C. Prologue: ToF-SIMS - An Evolving Mass Spectrometry of Materials. In *ToF-SIMS: Materials Analysis by Mass Spectrometry*; Vickerman, J. C.; Briggs, D., Eds.; Chichester & Manchester (UK), 2013; pp. 1–37.
- (81) Wucher, A. Laser Post-Ionisation - Fundamentals. In *ToF-SIMS: Materials Analysis by Mass Spectrometry*; Vickerman, J. C.; Briggs, D., Eds.; Chichester & Manchester (UK), 2013; pp. 217–246.
- (82) McPhail, D.; Dowset, M. Dynamic SIMS. In *Surface Analysis - The Principal Techniques (2nd Edition)*; Vickerman, J. C.; Gilmore, I. S., Eds.; Chichester (UK), 2009; pp. 207–268.
- (83) Benninghoven, A. The Analysis of Monomolecular Layers of Solids by Secondary Ion Emission. *Zeitschrift für Phys.* **1970**, *230*, 403–417.
- (84) Benninghoven, A. Surface Investigation of Solids by the Statical Method of Secondary Ion Mass Spectroscopy (SIMS). *Surf. Sci.* **1973**, *35*, 427–457.
- (85) Benninghoven, A. Developments in Secondary Ion Mass Spectroscopy and Applications to Surface Studies. *Surf. Sci.* **1975**, *53*, 596–625.
- (86) Vickerman, J. C. Molecular Surface Mass Spectrometry by SIMS. In *Surface Analysis - The Principal Techniques (2nd Edition)*; Vickerman, J. C.; Gilmore, I. S., Eds.; Chichester (UK), 2009; pp. 113–205.
- (87) *TOF-SIMS: Materials Analysis by Mass Spectrometry (2nd Edition)*; Vickerman, J. C.; Briggs, D., Eds.; IM Publica.; Chichester & Manchester (UK), 2013; p. 732.
- (88) *Surface Analysis: The Principal Techniques*; Vickerman, J. C.; Gilmore, I. S., Eds.; John Wiley.; Chichester (UK), 2009; p. 666.

- (89) Mahoney, C. M.; Gillen, G. An Introduction to Cluster Secondary Ion Mass Spectrometry. In *Cluster Secondary Ion Mass Spectrometry: Principles and Applications*; Mahoney, C. M., Ed.; Hoboken, NJ, USA, 2013; pp. 1–12.
- (90) Arlinghaus, H. F. Laser-SNMS. In *Surface and Thin Film Analysis: A Compendium of Principles, Instrumentation, and Applications*; Bubert, H.; Jenett, H., Eds.; Wiley-VCH Verlag GmbH: Weinheim (Germany), 2002; pp. 132–140.
- (91) Jenett, H. Electron-Impact (EI) Secondary Neutral Mass Spectrometry (SNMS). In *Surface and Thin Film Analysis: A Compendium of Principles, Instrumentation, and Applications*; Bubert, H.; Jenett, H., Eds.; Wiley-VCH Verlag GmbH: Weinheim (Germany), 2002; pp. 122–131.
- (92) Mouhib, T.; Delcorte, A.; Poleunis, C.; Bertrand, P. Organic Secondary Ion Mass Spectrometry: Signal Enhancement by Water Vapor Injection. *J. Am. Soc. Mass Spectrom.* **2010**, *21*, 2005–10.
- (93) Schueler, B. M. Time-of-Flight Mass Analysers. In *ToF-SIMS: Materials Analysis by Mass Spectrometry*; Vickerman, J. C.; Briggs, D., Eds.; Chichester & Manchester (UK), 2013; pp. 247–270.
- (94) Belu, A. M.; Graham, D. J.; Castner, D. G. Time-of-Flight Secondary Ion Mass Spectrometry: Techniques and Applications for the Characterization of Biomaterial Surfaces. *Biomaterials* **2003**, *24*, 3635–3653.
- (95) Tuccitto, N.; Torrisi, V.; Delfanti, I.; Licciardello, A. Monoatomic and Cluster Beam Effect on ToF-SIMS Spectra of Self-Assembled Monolayers on Gold. *Appl. Surf. Sci.* **2008**, *255*, 874–876.
- (96) Vickerman, J. C. Introduction. In *Surface Analysis - The Principal Techniques (2nd Edition)*; Vickerman, J. C.; Gilmore, I. S., Eds.; Chichester (UK), 2009; pp. 1–8.

-
- (97) Michel, R.; Castner, D. G. Advances in Time-of-Flight Secondary Ion Mass Spectrometry Analysis of Protein Films. *Surf. Interface Anal.* **2006**, *38*, 1386–1392.
- (98) Henry, M. Development of Biocompatible Polymeric Membranes for Bioartificial Pancreas, Université catholique de Louvain, 2008, p. 205.
- (99) Graham, D. J.; Wagner, M. S.; Castner, D. G. Information from Complexity: Challenges of TOF-SIMS Data Interpretation. *Appl. Surf. Sci.* **2006**, *252*, 6860–6868.
- (100) Jackson, J. E. *A User's Guide to Principal Components*; John Wiley & Sons: New York, 1991; Vol. 43.
- (101) Wold, S.; Esbensen, K.; Geladi, P. Principal Component Analysis. *Chemom. Intell. Lab. Syst.* **1987**, *2*, 37–52.
- (102) Wagner, M. S.; Graham, D. J.; Ratner, B. D.; Castner, D. G. Maximizing Information Obtained from Secondary Ion Mass Spectra of Organic Thin Films Using Multivariate Analysis. *Surf. Sci.* **2004**, *570*, 78–97.
- (103) Siegbahn, K.; Nordling, C.; Fahlman, A.; Ragnar, N.; Hamrin, K.; Hedman, J.; Johansson, G.; Bergmark, T.; Karlsson, S.-E.; Lindgren, I.; et al. *ESCA: Atomic, Molecular and Solid State Structure Studied by Means of Electron Spectroscopy*; Almqvist &. Uppsala, Sweden, 1967; p. 282.
- (104) Hertz, H. Ueber Einen Einfluss Des Ultravioletten Lichtes Auf Die Electriche Entladung. *Ann. Phys.* **1887**, *267*, 983–1000.
- (105) Einstein, A. Uber Einen Die Erzeugung Und Verwandlung Des Lichtes Betreffenden Heuristischen Gesichtspunkt. *Ann. Phys.* **1905**, *322*, 132–148.

-
- (106) Briggs, D.; Grant, J. T. *Surface Analysis by Auger and X-Ray Photoelectron Spectroscopy*; IM Publication & Surface Spectra Limited, 2003; p. 899.
- (107) Wagner, C. D.; Davis, L. E.; Zeller, M. V.; Taylor, J. A.; Raymond, R. H.; Gale, L. H. Empirical Atomic Sensitivity Factors for Quantitative Analysis by Electron Spectroscopy for Chemical Analysis. *Surf. Interface Anal.* **1981**, *3*, 211–225.
- (108) Baio, J. E.; Weidner, T.; Brison, J.; Graham, D. J.; Gamble, L. J.; Castner, D. G. Amine Terminated SAMs: Investigating Why Oxygen Is Present in These Films. *J. Electron Spectros. Relat. Phenomena* **2009**, *172*, 2–8.
- (109) NIST X-ray Photoelectron Spectroscopy Database, Version 4.1 (National Institute of Standards and Technology, Gaithersburg, 2012) <http://srdata.nist.gov/xps/>.
- (110) Francis, S. A.; Ellison, A. H. Infrared Spectra of Monolayers on Metal Mirrors. *J. Opt. Soc. Am.* **1959**, *49*, 131.
- (111) Greenler, R. G. Reflection Method for Obtaining the Infra Red Spectrum of a Thin Layer on a Metal Surface. *J. Chem. Phys.* **1969**, *50*, 1963.
- (112) Greenler, R. G. Infrared Study of Adsorbed Molecules on Metal Surfaces by Reflection Techniques. *J. Chem. Phys.* **1966**, *44*, 310.
- (113) Greenler, R. G. Design of a Reflection-Adsorption Experiment for Studying the Ir Spectrum of Molecules Adsorbed on a Metal Surface. *J. Vac. Sci. Technol.* **1975**, *12*, 1410.
- (114) Hoffmann, F. M. Infrared Reflection-Absorption Spectroscopy of Adsorbed Molecules. *Surf. Sci. Rep.* **1983**, *3*, 107–192.
- (115) Socrates, G. *Infrared and Raman Characteristic Group Frequencies : Tables and Charts (Third Edition)*; John Wiley & Sons, Inc.: New York, NY, 2001.

-
- (116) Bouhekka, A.; Bürgi, T. In Situ ATR-IR Spectroscopy Study of Adsorbed Protein: Visible Light Denaturation of Bovine Serum Albumin on TiO₂. *Appl. Surf. Sci.* **2012**, *261*, 369–374.
- (117) Curie, J.; Curie, P. Développement Par Compression de L'électricité Polaire Dans Les Cristaux Hémihédres À Faces Inclinaées. *Bull. la Société Minéralogique Fr.* **1880**, *3*, 90–93.
- (118) Sauerbrey, G. Use of Quartz Vibrator for Weighing Thin Films on a Microbalance. *Zeitschrift für Phys.* **1959**, *155*, 206–222.
- (119) Lu, C.-S.; Lewis, O. Investigation of Film Thickness Determination by Oscillating Quartz Resonators with Large Mass Load. *J. Appl. Phys.* **1972**, *43*, 4385.
- (120) King, W. H. Piezoelectric Sorption Detector. *Anal. Chem.* **1964**, *36*, 1735–1739.
- (121) Grate, J. W. Acoustic Wave Microsensor Arrays for Vapor Sensing. *Chem. Rev.* **2000**, *100*, 2627–48.
- (122) Janshoff, A.; Galla, H.-J.; Steinem, C. Piezoelectric Mass-Sensing Devices as Biosensors - An Alternative to Optical Biosensors? *Angew. Chemie Int. Ed.* **2000**, *39*, 4004–4032.
- (123) Rodahl, M.; Kasemo, B. A Simple Setup to Simultaneously Measure the Resonant Frequency and the Absolute Dissipation Factor of a Quartz Crystal Microbalance. *Rev. Sci. Instrum.* **1996**, *67*, 3238.
- (124) Höök, F.; Rodahl, M.; Brzezinski, P.; Kasemo, B. Energy Dissipation Kinetics for Protein and Antibody - Antigen Adsorption under Shear Oscillation on a Quartz Crystal Microbalance. *Langmuir* **1998**, *14*, 729–734.
- (125) Reviakine, I.; Johannsmann, D.; Richter, R. P. Hearing What You Cannot See and Visualizing What You Hear: Interpreting Quartz Crystal Microbalance Data from Solvated Interfaces. *Anal. Chem.* **2011**, *83*, 8838–8848.

- (126) Voinova, M. V.; Rodahl, M.; Jonson, M.; Kasemo, B. Viscoelastic Acoustic Response of Layered Polymer Films at Fluid-Solid Interfaces : Continuum Mechanics Approach. *Phys. Scr.* **1999**, *59*, 391–396.
- (127) Höök, F.; Kasemo, B.; Nylander, T.; Fant, C.; Sott, K.; Elwing, H. Variations in Coupled Water, Viscoelastic Properties, and Film Thickness of a Mefp-1 Protein Film During Adsorption and Cross-Linking: A Quartz Crystal Microbalance With Dissipation Monitoring, Ellipsometry, and Surface Plasmon Resonance Study. *Anal. Chem.* **2001**, *73*, 5796–804.
- (128) Höök, F.; Vörös, J.; Rodahl, M.; Kurrat, R.; Böni, P.; Ramsden, J. J.; Textor, M.; Spencer, N. D.; Tengvall, P.; Gold, J.; et al. A Comparative Study of Protein Adsorption on Titanium Oxide Surfaces Using In Situ Ellipsometry , Optical Waveguide Lightmode Spectroscopy , and Quartz Crystal Microbalance / Dissipation. *Colloids Surf. B* **2002**, *24*, 155–170.
- (129) Ferreira, G. N. M.; Da-Silva, A.-C.; Tomé, B. Acoustic Wave Biosensors: Physical Models and Biological Applications of Quartz Crystal Microbalance. *Trends Biotechnol.* **2009**, *27*, 689–697.
- (130) Bain, C. D.; Troughton, B. E.; Tao, Y. T.; Evall, J.; Whitesides, G. M.; Nuzzo, R. G. Formation of Monolayer Films by the Spontaneous Assembly of Organic Thiols from Solution onto Gold. *J. Am. Chem. Soc.* **1989**, *111*, 321–335.
- (131) Azioune, A.; Pireaux, J.-J.; Houssiau, L. ToF-SIMS Surface and Interface Characterization of the Immobilized Camel Antibody (cAb) onto SAMs-COOH/Au Substrates. *Appl. Surf. Sci.* **2004**, *231-232*, 402–405.
- (132) Thébault, P.; Boujday, S.; Sénéchal, H.; Pradier, C.-M. Investigation of an Allergen Adsorption on Amine- and Acid-Terminated Thiol Layers. *J. Phys. Chem. B* **2010**, *114*, 10612–10619.

-
- (133) Nuzzo, R. G.; Dubois, L. H.; Allara, D. L. Fundamental Studies of Microscopic Wetting on Organic Surfaces. 1. Formation and Structural Characterization of a Self-Consistent Series of Polyfunctional Organic Monolayers. *J. Am. Chem. Soc.* **1990**, *112*, 558–569.
- (134) Porter, M. D.; Bright, T. B.; Allara, D. L.; Chidsey, C. E. D. Spontaneously Organized Molecular Assemblies. 4. Structural Characterization of N-Alkyl Thiol Monolayers on Gold by Optical Ellipsometry, Infrared Spectroscopy, and Electrochemistry. *J. Am. Chem. Soc.* **1987**, *109*, 3559–3568.
- (135) Apte, J. S.; Collier, G.; Latour, R. A.; Gamble, L. J.; Castner, D. G. XPS and ToF-SIMS Investigation of Alpha-Helical and Beta-Strand Peptide Adsorption Onto SAMs. *Langmuir* **2010**, *26*, 3423–32.
- (136) Wang, H.; Chen, S.; Li, L.; Jiang, S. Improved Method for the Preparation of Carboxylic Acid and Amine Terminated Self-Assembled Monolayers of Alkanethiolates. *Langmuir* **2005**, *21*, 2633–6.
- (137) Chuang, W.; Lin, J. Surface Characterization and Platelet Adhesion Studies for the Mixed Self-Assembled Monolayers with Amine and Carboxylic Acid Terminated Functionalities. *J. Biomed. Mater. Res. Part A* **2007**, *82A*, 820–830.
- (138) *Bioconjugates Techniques*; Hermanson, G., Ed.; Academic P.; 2008; p. 1323.
- (139) Cheng, F.; Gamble, L. J.; Grainger, D. W.; Castner, D. G. Secondary Ion Mass Spectrometry, and Principal Component Analysis of the Hydrolysis, Regeneration, and Reactivity of N-Hydroxysuccinimide-Containing Organic Thin Films. *Anal. Chem.* **2007**, *79*, 8781–8788.
- (140) Arezki, B.; Delcorte, A.; Bertrand, P. Kinetic Energy Distributions of Molecular and Cluster Ions Sputtered from Self-Assembled Monolayers of Octanethiol on Gold. *Nucl. Instruments Methods Phys. Res. B* **2002**, *193*, 755–761.

- (141) Arezki, B.; Delcorte, A.; Chami, A. C.; Garrison, B. J.; Bertrand, P. Gold-Thiolate Cluster Emission from SAMs under keV Ion Bombardment: Experiments and Molecular Dynamics Simulations. *Nucl. Instruments Methods Phys. Res. B* **2003**, *212*, 369–375.
- (142) Arezki, B.; Delcorte, A.; Bertrand, P. Emission Processes of Molecule – Metal Cluster Ions from Self-Assembled Monolayers of Octanethiols on Gold and Silver. *Appl. Surf. Sci.* **2004**, *231-232*, 122–126.
- (143) Arezki, B.; Delcorte, A.; Garrison, B. J.; Bertrand, P. Understanding Gold-Thiolate Cluster Emission from Self-Assembled Monolayers upon Kiloelectronvolt Ion Bombardment. *J. Phys. Chem. B* **2006**, *110*, 6832–40.
- (144) Rzeznik, L.; Czerwinski, B.; Garrison, B. J.; Winograd, N.; Postawa, Z. Microscopic Insight into the Sputtering of Thin Polystyrene Films on Ag{111} Induced by Large and Slow Ar Clusters. *J. Phys. Chem. C* **2008**, *112*, 521–531.
- (145) Walstra, P.; Jenness, R.; Badings, H. T. *Dairy Chemistry and Physics*; John Wiley.; New York, 1984; p. 467.
- (146) Wong, D. W. S.; Camirand, W. M.; Pavlath, A. E. Structures and Functionalities of Milk Proteins. *Crit. Rev. Food Sci. Nutr.* **1996**, *36*, 807 – 844.
- (147) Brownlow, S.; Cabral, J. H. M.; Cooper, R.; Flower, D. R.; Yewdall, S. J.; Polikarpov, I.; North, A. C. T.; Sawyer, L. Bovine B-Lactoglobulin at 1.8 Å Resolution — Still an Enigmatic Lipocalin. *Structure* **1997**, *64*, 481–495.
- (148) Briand, E.; Salmain, M.; Compère, C.; Pradier, C.-M. Anti-Rabbit Immunoglobulin G Detection in Complex Medium by PM-RAIRS and QCM Influence of the Antibody Immobilisation Method. *Biosens. Bioelectron.* **2007**, *22*, 2884–90.

-
- (149) Wahlgren, M.; Elofsson, U. Simple Models for Adsorption Kinetics and Their Correlation to the Adsorption of B -Lactoglobulin A and B. *J. Colloid Interface Sci.* **1997**, *188*, 121–129.
- (150) Carter, D. C.; Ho, J. X. Structure of Serum Albumin. *Adv. Protein Chem.* **1994**, *45*, 153–203.
- (151) Engvall, E.; Perlmann, P. Enzyme-Linked Immunosorbent Assay , Elisa : III . Quantitation of Specific Antibodies by Anti-Immunoglobulin in Antigen-Coated Tubes. *J. Immunol.* **1972**, *109*, 129–135.
- (152) Roach, P.; Farrar, D.; Perry, C. C. Interpretation of Protein Adsorption: Surface-Induced Conformational Changes. *J. Am. Chem. Soc.* **2005**, *127*, 8168–73.
- (153) Wilhelmi, M.; Müller, C.; Ziegler, C.; Kopnarski, M. BSA Adsorption on Titanium: ToF-SIMS Investigation of the Surface Coverage as a Function of Protein Concentration and pH-Value. *Anal. Bioanal. Chem.* **2011**, *400*, 697–701.
- (154) Vallée, A.; Humblot, V.; Al Housseiny, R.; Boujday, S.; Pradier, C.-M. BSA Adsorption on Aliphatic and Aromatic Acid SAMs: Investigating the Effect of Residual Surface Charge and Sublayer Nature. *Colloids Surfaces B* **2013**, *109*, 136–42.
- (155) Thourson, S. B.; Marsh, C. A.; Doyle, B. J.; Timpe, S. J. Quartz Crystal Microbalance Study of Bovine Serum Albumin Adsorption onto Self-Assembled Monolayer-Functionalized Gold with Subsequent Ligand Binding. *Colloids Surfaces B* **2013**, *111*, 707–712.
- (156) Beilis, E.; Belgorodsky, B.; Fadeev, L.; Cohen, H.; Richter, S. Surface-Induced Conformational Changes in Doped Bovine Serum Albumin Self-Assembled Monolayers. *J. Am. Chem. Soc.* **2014**, *In Press*.
- (157) Mücksch, C.; Urbassek, H. M. Molecular Dynamics Simulation of Free and Forced BSA Adsorption on a Hydrophobic Graphite Surface. *Langmuir* **2011**, *27*, 12938–43.

-
- (158) Jachimska, B.; Pajor, A. Physico-Chemical Characterization of Bovine Serum Albumin in Solution and as Deposited on Surfaces. *Bioelectrochemistry* **2012**, *87*, 138–46.
- (159) Curvale, R.; Masuelli, M.; Padilla, A. P. Intrinsic Viscosity of Bovine Serum Albumin Conformers. *Int. J. Biol. Macromol.* **2008**, *42*, 133–7.
- (160) Wertz, C. F.; Santore, M. M. Effect of Surface Hydrophobicity on Adsorption and Relaxation Kinetics of Albumin and Fibrinogen : Single-Species and Competitive Behavior. *Langmuir* **2001**, *17*, 3006–3016.
- (161) Ig gamma-1 chain C region secreted form
<http://www.uniprot.org/uniprot/P01868>.
- (162) Caira, S.; Pizzano, R.; Picariello, G.; Pinto, G.; Cuollo, M.; Chianese, F.; Addeo, F. Allergenicity of Milk Proteins. In *Milk Protein*; Hurley, W., Ed.; 2012.
- (163) Yip, K. S. P.; Stillman, T. J.; Britton, K. L.; Artymiuk, P. J.; Baker, P. J.; Sedelnikova, S. E.; Engel, P. C.; Pasquo, A.; Chiaraluce, R.; Consalvi, V.; et al. The Structure of Pyrococcus Furiosus Glutamate Dehydrogenase Reveals a Key Role for Ion-Pair Networks in Maintaining Enzyme Stability at Extreme Temperatures. *Structure* **1995**, *3*, 1147–58.
- (164) Dupont-gillain, C. C. Orientation of Adsorbed Antibodies : In Situ Monitoring by QCM and Random Sequential Adsorption Modeling. In *Proteins at Interfaces III State of the Art*; Horbett, T.; Brash, J. L.; Norde, W., Eds.; 2012; pp. 453–469.
- (165) Berg, J. M.; Tymoczko, J. L.; Stryer, L. Section 1.3, Chemical Bonds in Biochemistry. In *Biochemistry. 5th Edition*; New York, 2002.
- (166) Trilling, A. K.; Beekwilder, J.; Zuilhof, H. Antibody Orientation on Biosensor Surfaces: A Minireview. *Analyst* **2013**, *138*, 1619–27.

-
- (167) Baer, D. R.; Gaspar, D. J.; Nachimuthu, P.; Techane, S. D.; Castner, D. G. Application of Surface Chemical Analysis Tools for Characterization of Nanoparticles. *Anal. Bioanal. Chem.* **2010**, *396*, 983–1002.
- (168) Pluchery, O.; Carriere, M. Nanoparticules D 'or. *Tech. l'ingénieur* **2011**.
- (169) Link, S.; El-Sayed, M. A. Size and Temperature Dependence of the Plasmon Absorption of Colloidal Gold Nanoparticles. *J. Phys. Chem. B* **1999**, *103*, 4212–4217.
- (170) Neunzehn, J.; Draude, F.; Golla-Schindler, U.; Arlinghaus, H. F.; Wiesmann, H.-P. Detection of Protein Coatings on Nanoparticles Surfaces by ToF-SIMS and Advanced Electron Microscopy. *Surf. Interface Anal.* **2013**, *45*, 1340–1346.
- (171) Yang, L.; Seah, M. P.; Anstis, E. H.; Gilmore, I. S.; Lee, J. L. S. Sputtering Yields of Gold Nanoparticles by C 60 Ions. *J. Phys. Chem. C* **2012**, *116*, 9311–9318.

Dissemination

Publications

Probing the Orientation of β -Lactoglobulin on Gold Surfaces Modified by Alkyl Thiols Self-Assembled Monolayers

Lebec V., Landoulsi J., Boujday S., Poleunis C., Pradier C.-M., Delcorte A. D.
Journal of Physical Chemistry C, **2013**, 117 (22), 11569-11577

ToF-SIMS Investigation of the Orientation of Adsorbed Antibodies on SAMs Correlated to Biorecognition Tests

Lebec V., Boujday S., Poleunis C., Pradier C.-M., Delcorte A. D.
Journal of Physical Chemistry C, **2014**, 118 (4), 2085-2092

Communications

Multitechnique study of the adsorption modes of β -Lactoglobulin on -COOH, -NH₂ and -CH₃-terminated SAMs

Lebec V., Landoulsi J., Boujday S., Poleunis C., Pradier C.-M., Delcorte A. D.
Oral, ECASIA'11 (Cardiff, Wales, UK, 2011)

ToF-SIMS study of alkyl thiol self-assembled monolayers using large argon cluster projectiles

Lebec V., Poleunis C., Delcorte A. D.
Oral, SIMS Europe 2012 (Münster, Germany, 2012)

Linking proteins bio-recognition to their orientation on different substrates by means of surface analysis

Lebec V., Boujday S., Poleunis C., Pradier C.-M., Delcorte A. D.
Oral, 19th International Vacuum Congress (Paris, France, 2013)

Determination of Antibody Orientations on Different Surfaces and Nanoparticles Using ToF-SIMS

Lebec V., Boujday S., Poleunis C., Pradier C.-M., Delcorte A. D.
Oral, SIMS19 (Jeju, South Korea, 2013)

Posters

Determination of Antibody Orientations on Different Surfaces and Nanoparticles Using ToF-SIMS

Léonard C., Lebec V., Mertens P., Dupont-Gillain C., Delcorte A. D.
Poster, SIMS19 (Jeju, South Korea, 2013)

Direct determination of the orientation of adsorbed anti-GDH antibodies by ToF-SIMS

Lebec V., Boujday S., Poleunis C., Pradier C.-M., Delcorte A. D.
Poster, Desorption 2014 (Montreal, Quebec, Canada, 2014)

ToF-SIMS investigation of Adsorbed Anti-GDH antibodies orientation correlated to biosensing efficiency

Lebec V., Boujday S., Poleunis C., Pradier C.-M., Delcorte A. D.
Poster, Biosensors 2014 (Melbourne, Australia, 2014)